STUDIES OF $HG_{(1-x)}CD_xTe$ (MCT) FORMATION BY ELECTROCHEMICAL ATOMIC LAYER DEPOSITION (ALD), AND INVESTIGATIONS INTO BANDGAP ENGINEERING

by

VENKATRAM VENKATASAMY

(Under the Direction of John L. Stickney)

ABSTRACT

HgCdTe or Mer-Cad-Tel is the most widely used Infrared material. The present study describes the growth of MCT via Electrochemical ALD, using an automated electrochemical flow cell deposition system. Deposits were characterized using X-ray diffraction (XRD), electron probe microanalysis (EPMA) and reflection absorption Fourier transform Infrared spectroscopy (FTIR). As deposited films showed a strong (111) preferred orientation. Changes in deposit composition showed the expected trend in band gaps: the more Hg the lower the band gap, but with some significant deviations. Electrochemical quartz crystal microbalance (EQCM) studies, using an automated flow cell, indicated that some deposited Cd was stripping at potentials used to deposit Hg. In addition, redox replacement of deposited Cd for Hg was evident, a function of the greater stability of Hg than Cd.

INDEX WORDS: MCT, Bandgap engineering, ALD, EC-ALE, upd, Electrodeposition, XRD, FTIR, EPMA

STUDIES OF $HG_{(1-x)}CD_xTe$ (MCT) FORMATION BY ELECTROCHEMICAL ATOMIC LAYER DEPOSITION (ALD), AND INVESTIGATIONS INTO BANDGAP ENGINEERING

by

VENKATRAM VENKATASAMY

B.Tech., Madurai Kamaraj University, India, 2003

A Dissertation Submitted to the Graduate Faculty of The University of Georgia in Partial Fulfillment of the Requirements for the Degree

DOCTOR OF PHILOSOPHY

ATHENS, GEORGIA

2007

STUDIES OF $HG_{(1-x)}CD_xTe$ (MCT) FORMATION BY ELECTROCHEMICAL ATOMIC LAYER DEPOSITION (ALD), AND INVESTIGATIONS INTO BANDGAP ENGINEERING

by

VENKATRAM VENKATASAMY

Major Professor: John L. Stickney

Committee: Jonathan I. Amster
Uwe Happek

Electronic Version Approved:

Maureen Grasso
Dean of the Graduate School
The University of Georgia
May 2007

DEDICATION

I would like to dedicate my phD to my parents, Mr. N. Venkatasamy and Mrs. V. Shantha. Without your unconditional love and support, I could not have reached this position. I would like to thank you from the bottom of my heart. I would also like to thank my sister, Mrs. Sudha Prakash, for being there for me all the time. You have always been a source of encouragement for me.

ACKNOWLEDGEMENTS

I consider myself very fortunate to have a mentor like John Stickney. He has not only been a good teacher, but more than that, he has been like a father figure for me. He has taught me everything from being a good scientist to being a good person. I cannot thank him enough for all the advice and support he has given me throughout the years that I have worked with him.

I would like to thank Dr. Jonathan Amster and Dr. Uwe Happek for being in my committee and guiding me through my research.

I would also like to thank Dr. Youn-Geun Kim for all his advice about life and research. I would like to thank all group members, past and present, who made my stay in "Stickney Lab" a memorable one: Dr. Raman Vaidyanathan, Dr. Ken Mathe, Dr. Madhivanan Muthuvel, Nagarajan jayaraju, Jay Kim, Dhego Banga, Chandru Thambidurai, Deepa Vairavapandiyan.

Last but not the least, I would like to thank Jeejaji and also my lovely nephews, Gujji and Kari. You guys have given me lots of joy in my life.

TABLE OF CONTENTS

Page

LIST OF TABLES

Page

LIST OF FIGURES

Page

CHAPTER 1

INTRODUCTION

HgCdTe or Mer-Cad-Tel is the most widely used Infrared material[1]. It is considered to be the third semiconductor of technological importance behind Si and GaAs. Since its first synthesis, HgCdTe based IR detectors have been intensively developed and studied.

HgCdTe was first synthesized in 1958 by a research group led by Lawson[2] at the Royal Radar Establishment in England. This work was the successful outcome of a deliberate effort to engineer a direct-bandgap, intrinsic semiconductor for the long wavelength infrared (LWIR) spectral region (8-14 μm).The importance of HgCdTe lies in the fact that it is an alloy of HgTe and CdTe, where HgTe is a zero bandgap semimetal and CdTe, a high bandap semicondictor. With a change in alloy composition, the bandgap of MCT can be tuned anywhere between 0 to 1.5 eV. This coupled with some other important properties like direct bandgap with high absorption coefficient, moderate dielectric constant, moderate thermal coefficient of expansion and presence of lattice matched substrates, make it very attractive for IR detection.

Properties

Excitation of an electron from the valence band into the conduction band is the basis for Infrared detection. The minimum photon energy required to achieve this phenomenon, is equal to the bandgap, *Eg*. The bandgap of $Hg_{(1-x)}Cd_xTe$ is a function of the alloy composition ratio "*x*" of CdTe to HgTe, and the temperature of the material. A number of equations have been developed to summarize this relationship. One such, developed by Hansen *et al.* [3] is given by the expression:

$$E_g = -0.302 + 1.93\ x - 0.81\ x^2 + 0.832\ x^3 + 5.35\ (1-2\ x)\ 10^{-4}\ T$$

The dependence of the bandgap to the alloy composition, obtained by the Hansen expression, is given by the following: when x = 0.2, 0.3, and 0.4, medium-to-long wavelength spectral regions, 3–14 μm, are covered. With higher values of *x* the bandgap can be tailored to

wavelengths as short as 0.7 μm, corresponding to the bandgap of CdTe. Since the bandgap of HgTe is negative, the alloy can also be grown to achieve small bandgaps. In practice, HgCdTe has not been used much beyond 25 μm.

HgCdTe is a direct bandgap semiconductor. Hence, it has a sharp onset of optical absorption as the photon energy increases above *Eg*. The optical absorption coefficient for HgCdTe has been measured by Scott[4] . Strong optical absorption allows HgCdTe detector structures to be thin, on the order of 10–20 μm, while absorbing a very high percentage of the signal. Minimizing the detector thickness helps to minimize the volume of material which can generate noise and thermal excess carriers, in the diffusion-limited operating mode.

Epitaxial growth is very common for HgCdTe detector array production. It was found earlier that the crystal perfection and surface morphology of the epitaxial layers were significantly influenced by the substrate-epitaxial layer lattice constant mismatch. At present, the substrates used are obtained by adding about 4% ZnTe to CdTe, to tune the substrate lattice constant to match that of HgCdTe.

Detector timeline

The HgCdTe detectors became popular due to their flexibility in spectral response over a wide range of the infrared regions of interest. Three generations of HgCdTe devices have been successively developed since its first development [1].

The first generation of HgCdTe detectors consists mainly of linear arrays of photoconductive devices. Good quality photoconductors are fabricated by applying metal electrodes to pure n-type material, thinned to about 10 μm. Low impedance and low noise are the reasons why the photoconductors have not been deployed with focal plane readouts operating at 80 K. This reason has limited the scope of first generation devices to linear arrays with typically fewer than

200 elements. Within this limitation, the industry has produced tens of thousands of thermal imaging systems using photoconductive arrays.

Second-generation HgCdTe devices are generally, two-dimensional arrays of photodiodes. Photodiodes having modest impedance of 10 Ω cm^2 can be attached to silicon readout arrays with indium bumps at the pixel level. The signal-to-noise ratio of a sensor, generally improves with the square root of the number of detector elements in an array. At present, millions of pixels are connected to millions of amplifiers in a unit cell of readout circuits. The key technology that was needed to make photovoltaic devices possible was surface passivation. Silicon oxide was first employed for passivation of HgCdTe detectors, based upon low-temperature deposition using a photochemical reaction. SiO_2 can be deposited with low surface state densities and hence, excellent PV device properties were demonstrated. However, the excellent surface properties could not be maintained when the devices were heated in vacuum for extended periods of time for good vacuum packaging integrity.

ZnS, a common antireflection coating for photoconductive HgCdTe, was used next with some success, but lacked stability during vacuum baking. Many other materials like oxides, sulfides, and fluorides, were also tried with varying success. With the advent of CdTe passivation, HgCdTe photodiodes were finally passivated reliably. CdTe passivation is stable during vacuum packaging bake cycles and shows little effect from the radiation found in space applications. This development has made possible the full-scale production of second-generation devices. Second-generation photovoltaic HgCdTe technology is now capable of being produced for a variety of low-background strategic applications as well higher-background flux tactical applications. Work is still being done to push the performance of long wavelength detectors for critical applications such as monitoring the earth's atmosphere from a spacecraft.

The definition of third-generation devices is not well established at present. It is usually taken to mean device structures that have substantially enhanced capabilities over an ordinary photodiode. The technical advancements key to the development of third -generation devices include: dry etching, vapour-phase epitaxy, optical coatings, and advanced readout concepts. The following are three examples for third generation HgCdTe devices:

- Two colour detectors.
- Avalanche photodiodes.
- Hyperspectral arrays.

Growth

The growth of HgCdTe has evolved along with other semiconductor materials technologies over the past decades. The following are the most widely used techniques to grow HgCdTe commercially:

- Bulk.
- Liquid phase epitaxy – LPE.
- Vapour phase epitaxy – VPE.
    - Metalorganic chemical vapour deposition – MOCVD.
    - Molecular beam epitaxy – MBE.

Bulk crystal growth

The growth of HgCdTe by Bulk crystal method has proved to be very difficult due to the high vapor pressure of Hg at the crystal melting point, about 950 C. Early experiments and a significant fraction of early production was done using a quench-anneal or solid-state recrystallization process. In this method the alloy is reacted from purified starting materials and then rapidly quenched [5]. Rapid quenching is needed to prevent segregation of HgTe from

CdTe which have significantly different melting temperatures. The result of quenching is a highly polycrystalline solid. Annealing near the melting point is used to grow larger grains.

Bridgeman growth performed at high pressure was attempted for several years to overcome the problem with the Hg pressure [6]. During the same time solvent growth methods were also initiated, which could be carried out at reduced temperature. Solvent growth also provided an additional purification step through zone refining. Bulk growth produced thin rods of HgCdTe material, generally 8-12 mm in diameter and about 20 cm in length. This material could be used for linear array production, but the vision of larger two-dimensional arrays could not be realized with this method. Another drawback to bulk material was the need to thin the bulk wafers from about 500 μm thick down to the final device thickness of about 10 μm. On the whole, the process of polishing the wafers, mounting them on suitable substrates, and cutting them to the final device thickness is labor intensive.

Liquid phase epitaxy

Liquid phase epitaxy (LPE) is the most well developed technology to grow HgCdTe epilayers for IR sensors [7, 8]. Te solution with dissolved Cd and saturated with Hg vapor is used efficiently to grow HgCdTe layers with thickness suitable for direct device fabrication. Cd has limited solubility in Hg melts, so the volume of the Hg melts had to be much larger than Te melts in order to minimize melt depletion during the layer growth. Hg-melt epitaxy was developed using large dipping vessels. One of the important lessons that was learnt to reduce surface morphology defects and achieve uniform, smooth epitaxial layers was the importance of having precise substrate orientation and the need for lattice- matched substrates.

Diodes fabricated on early LPE materials were made by ion implantation into p-type layers which had to be annealed to generate Hg-vacancy acceptors. LPE growth technology is

now very mature for production of both first and second-generation tactical detectors. Even then, LPE technology is limited for a variety of advanced HgCdTe structures that are of interest at present. The gradient in *x*-value, a consequence of the partial depletion of Cd during the operation, can generate a barrier to carrier transport in certain cases. LPE also melts off a thin layer of the underlying material each time an additional layer is grown. These limitations have provided an opportunity for vapor-phase growth to replace LPE technology for growing advanced device structures.

Vapor phase epitaxy

Vapor phase epitaxy is a method based on an evaporation – interdiffusion mechanism and is a relatively simple and inexpensive method to grow HgCdTe layers with good morphological and electrical properties. The modern vapour phase era began in the early 80s with parallel efforts using metalorganic chemical vapour deposition (MOCVD) and molecular beam epitaxy (MBE) [1].

Advancement in the MOCVD front involved a wide variety of metalorganic compounds being developed along with a number of reaction chamber designs [9, 10]. MBE technology, in parallel, had to address specially designed Hg-source ovens to overcome the low sticking coefficient of Hg at the growth temperature. A few attempts were also made using hybrid systems like MOMBE [11], where metalorganic sources were used in an MBE chamber.

At present, MBE has become the dominant vapour phase growth method for HgCdTe [12-14]. Although the quality of MBE material is not yet on a par with LPE, it has made tremendous progress in the past decade to the point where a variety of high-background device formats have been successfully demonstrated using this growth technique. Keys to its success

have been the ability to dope layers both p and n-type, and the reduction of etch pit densities by an order of magnitude or more from a range of 10^7 cm^{-2} to below 10^6 cm^{-2}.

Some work on the growth of MCT by electrodeposition has also been done, mostly using the co-deposition methodology, where a single solution contains precursors for all constituent elements, and a single potential or current density is used to form the deposit [15-21]. Most such studies were performed in aqueous solutions, though some non aqueous solutions have also been studied [22, 23]. Only moderate success has been obtained in the electrodeposition of MCT. In nearly all cases low crystallinity was observed for as formed deposits, requiring post deposition annealing to display a reasonable XRD pattern.

Electrochemical ALD is one of the electrochemical techniques that has the potential to grow high quality HgCdTe thin films. It is the electrochemical analog of both atomic layer epitaxy (ALE)[24-26] and atomic layer deposition (ALD) [27-30]. All three methods are based on the use of surface limited reactions to form nanofilm deposits with atomic layer control. These methods break the deposition process into a sequence of individually controllable steps, which are then used in a cycle, to form deposits of a thickness determined by the number of cycles performed. Use of such cycles greatly improves the ability to optimize a deposition process, though it tends to increases the complexity of the deposition hardware, and can increase the deposition time. In the formation of nanofilms, however, deposition time is seldom the primary concern, as the number of cycle needed is limited.

In electrochemistry, underpotential deposition (UPD) is the prominent surface limited reaction. UPD [31-35] refers to a phenomenon where an atomic layer of one element electrodeposits on another at a potential prior to (under) the potential at which the element deposits on to itself, limiting UPD to the formation of an atomic layer. Electrochemical ALD is

the application of UPD, or other electrochemical surface limited reactions, to the sequential deposition of atomic layers of elements for the growth of nanofilms of materials[36-39]. In some systems ALD can promote epitaxy, in which case the method has been referred to at times as atomic layer epitaxy (ALE). There are a number of such electrochemical cases, and they have previously been referred to as electrochemical atomic layer epitaxy (EC-ALE).

Most previous work with electrochemical ALD has involved formation of nanofilms of compound semiconductors, including: II-VI compounds such as CdTe, CdS, ZnSe and HgSe [40-43] as well as some III-V compounds such as GaAs, InAs, and InSb [44-46]. PbSe [47], PbTe [48], Bi_2Te_3 [49-51] and Sb_2Te_3 [52] have also been grown using electrochemical ALD. Recently, this work has been extended to the formation of metal nanofilms, such as Cu, Ag and Pt [53-57].

Experimental

The electrochemical flow deposition system [58-60] consists of pump heads, valves and tubing, confined inside a nitrogen purged Plexiglas box to limit oxygen concentration (Figure 1). The electrochemical cell consists of a thin-layer design to promote laminar flow. The auxiliary electrode was an ITO glass slide (Delta Technologies, Ltd., Stillwater MN), and the reference electrode was Ag/AgCl (3 M NaCl) (Bioanalytical Systems, Inc., West Lafayette, IN). Substrates used in all experiments were 300 nm thick gold films on glass slides. The substrates were annealed at 400^{o}C for 12 hours under a vacuum of 10^{-6} Torr, after Au vapor deposition, resulting in a perdominant (111) habit. The working and auxiliary electrodes are held apart by a 2 mm thick silicon rubber gasket, which defines a 1x3 cm^2 rectangular opening where deposition take place. The ITO auxiliary is transparent, allowing deposition to be followed visually. The reference electrode, Ag/AgCl (3M NaCl) is positioned at the cavity outlet.

The solutions used are usually made with high purity salts of the constituent elements. The water used to make solutions are supplied from a Nanopure water filtration system (Barnstead, Dubuque, IA) attached to the house DI water system. The blank solution used in all the experiments contained 0.5 M Na_2SO_4, at pH 4. Solution pH is adjusted using H_2SO_4..

Deposit thickness is monitored using a single wavelength ellipsometer (Sentech SE 400). A Scintag PAD-V diffractometer with CuKα radiation (λ= 1.5418 A), is used to obtain glancing angle X-ray diffraction patterns. Electron probe microanalysis (EPMA) is run on a Joel 8600 wavelength dispersive scanning electron microprobe. Glancing angle absorption measurements are performed, using an FTIR spectrophotometer (Bruker FTS-66v, Bruker optics, Inc.).

Optimal deposition conditions are then studied using a flow cell based electrochemical quartz crystal microbalance (EQCM). A 9 MHz AT-cut quartz crystal (Seiko EG&G) is used, where both sides are coated with circular Au electrodes (ca. 0.2 cm^2, 5 mm in diameter). The electrodes are formed with 50 nm of Ti, followed by 300 nm of sputtered Au. Calibration of the EQCM is carried out using Ag electrodeposition coulometry.

The optimization of deposition conditions for HgSe compound semiconductor, was the first project of my graduate research. In Chapter 2, I will discuss about the experiments done to find out the ideal deposition conditions for putting down Hg and Se. After HgSe, I devoted my attention to the deposition of HgCdTe. To achieve an ideal deposition condition for HgCdTe, I needed to develop an ideal deposition condition for growing HgTe and CdTe. Hence, I next worked on the optimization of CdTe and HgTe deposition, which are discussed in chapters 3 and 4 respectively. Chapter 5 talks about the work done to grow HgCdTe and the problems encountered, when trying to grow a superlattice of HgTe and CdTe. The work done on bandgap engineering of HgCdTe is also discussed in detail.

References

1. Norton, P., Opto-Electronics Review, 2002. **10**(3): p. 159-174.
2. Lawson, W.D., et al., J. Phys. Chem. Solids, 1959. **9**: p. 325–329.
3. Hansen, G.L. and J.L. Schmit, J. Appl. Phys., 1983. **54**(3): p. 1639-1640
4. Scott, M.W., J. Appl. Phys., 1969. **40**: p. 4077–4081.
5. Honga, K.J., et al., Journal of Crystal Growth, 2002. **240**: p. 135–141.
6. Watring, D.A. and S.L. Lehoczky, Journal of Crystal Growth, 1996. **167**: p. 478-487.
7. Radhakrishnan, J.K., S. Sitharaman, and S.C. Gupta, J. Crystal Growth, 2003. **252**: p. 79-86.
8. Radhakrishnan, J.K., S. Seetharaman, and S.C. Gupta, Appl. Surf. Sci. , 2003. **207**: p. 33-39.
9. Matsushita, K. and A. Kamata, Journal of Crystal Growth, 1998. **184-185**: p. 1228-1231.
10. Shigenaka, K., et al., Journal of Crystal Growth, 1992. **117**((1-4)): p. 37-43.
11. Parikh, A., et al., Journal of Crystal Growth, 1996. **159**: p. 1152-1156.
12. Wu, O.K. and G.S. Kamath, Semicond. Sci. Technol., 1991. **6**: p. C6-C9.
13. Wijewarnasuriya, P.S., et al., Journal of Crystal Growth, 1997. **175-176**: p. 647-652.
14. He, L., et al., Journal of Crystal Growth, 2001. **227–228**: p. 677–682.
15. Basol, B.M., Solar Cells, 1988. **23**: p. 69-88.
16. Rakhshani, A.E., Semicond. Sci. Technol., 2002. **17**(9): p. 924-930.
17. Sahu, S.N., M.J. Antonio, and C. Sanchez, Solar Energy Materials and Solar Cells, 1996. **43**(3): p. 223-235.
18. Jun, L., T. Zheng, and M. Tian-Ying, Sci. China (series B), 1990. **33**: p. 1153.
19. Ramiro, J. and E.G. Camarero, Journal of Materials Science, 1996. **31**(8): p. 2047-2050.

20. Sahu, S.N. and C. Sanchez, Solid State Communications 1990. **73**(9): p. 597-600.

21. Basol, B.M., et al. *Cd(1-x)ZnxTe thin films prepared by a two-stage process utilizing electrodeposition*. in *IEEE Photovoltaic specialists conference*. 1988: IEEE.

22. Colyer, C.L. and M. Cocivera, J. Electrochem. Soc., 1992. **139**: p. 406.

23. Nair, J.P., et al., Journal of Physics and Chemistry of Solids, 1999. **60**(10): p. 1693-1703.

24. Bedair, S., ed. *Atomic Layer Epitaxy*. 1993, Elsevier: Amsterdam. 304.

25. Kuech, T.F., P.D. Dapkus, and Y. Aoyagi, eds. *Atomic Layer Growth and Processing*. Vol. 222. 1991, Materials Research Society: Pittsburgh. 360.

26. Goodman, C.H.L. and M.V. Pessa, JAP, 1986. **60**: p. R65.

27. Leskela, M. and M. Ritala, Thin Solid Films, 2002. **409**(1): p. 138-146.

28. Yousfi, E.B., et al., Thin Solid Films, 2001. **387**(1-2): p. 29-32.

29. Sammelselg, V., et al., Applied Surface Science, 1998. **134**(1-4): p. 78-86.

30. Ylilammi, M., Thin Solid Films, 1996. **279**(1-2): p. 124-130.

31. Kolb, D.M., Przasnys.M, and Gerische.H, Journal of Electroanalytical Chemistry, 1974. **54**(1): p. 25-38.

32. Kolb, D.M., *Physical and Electrochemical Properties of Metal Monolayers on Metallic Substrates*, in *Advances in Electrochemistry and Electrochemical Engineering*, H. Gerischer and C.W. Tobias, Editors. 1978, John Wiley: New York. p. 125.

33. Juttner, K. and W.J. Lorenz, Z. Phys. Chem. N. F., 1980. **122**: p. 163.

34. Hubbard, A.T., et al., *Electrochemical surface characterization*, in *New Dimensions in Chemical Analysis*, B.L. Shapiro, Editor. 1985, Texas A & M University Press: College Station, Texas. p. 135.

35. Gewirth, A.A. and B.K. Niece, Chem. Rev., 1997. **97**: p. 1129-1162.

36. B.W. Gregory, D.W.S., J.L. Stickney, J. Electrochem. Soc., 1991. **138**: p. 1279.

37. Stickney, J.L., *Electrochemical Atomic Layer Epitaxy*, in *Electroanalytical Chemistry*, A.J. Bard and I. Rubenstein, Editors. 1997, Marcel Dekker: New York. p. in press.

38. Stickney, J.L., et al., *Compound semiconductor formation by electrochemical atomic layer eptiaxy (EC-ALE): Surface Chemistry*, in *Encyclopedia of Surface and Colloid Science*, A.T. Hubbard, Editor. 2002, Marcel Dekker, Inc.: New York.

39. Stickney, J.L., *Electrochemical atomic layer epitaxy (EC-ALE): Nanoscale control in the electrodeposition of compound semiconductors*, in *Advances in Electrochemical Science and Engineering*, D.M. Kolb and R. Alkire, Editors. 2002, Wiley-VCH: Weinheim. p. 1-107.

40. Colletti, L.P., B.H. Flowers Jr., and J.L. Stickney, Journal of the Electrochemical Society, 1998. **145**(5): p. 1442-1449.

41. Flowers, J., Billy H., et al., Journal of Electroanalytical Chemistry, 2002. **524-525**: p. 273-285.

42. Wade, T.L., et al. *Formation of II-VI and III-V compound semiconductors by electrochemical ALE*. in *National Meeting of the Electrochemical Society, Spring*. 1999. Seattle, Washington: The Electrochemical Society.

43. Venkatasamy, V., et al., Journal of Applied Electrochemistry, 2006. **36**(11): p. 1223-1229

44. Wade, T.L., et al. *Electrochemical Atomic Layer Eptitaxy: Electrodeposition of III-V and II-VI Compounds,*. in *Materials Research Society*. 2000: Materials Research Society.

45. Wade, T.L., et al., Electrochemical and Solid State Letters, 1999. **2**(12): p. 616.

46. Wade, T.L., et al., JEC, 2001. **500**: p. 322-332.

47. Vaidyanathan, R., U. Happek, and J.L. Stickney, Electrochimica Acta, 2004. **49**(8): p. 1321-1326.

48. Vaidyanathan, R., et al., Langmuir 2006. **22**(25): p. 10590-10595

49. Zhu, W., et al., Electrochimica Acta, 2005. **50**(20): p. 4041-4047.

50. Zhu, W., et al., J. Electroanal. Chem., 2005. **585**(1): p. 83-88.

51. Yang, J.Y., et al., J. Electroanal. Chem., 2005. **577**(1): p. 117-123.

52. Yang, J.Y., et al., J. Phys. Chem. B, 2006. **110**(10): p. 4599-4604.

53. Vasilic, R. and N. Dimitrov, Electrochem. Solid State Lett., 2005. **8**(11): p. C173-C176.

54. Vasilic, R., L. Viyannalage, and N. Dimitrov, J. Electrochem. Soc., 2006. **153**(9): p. C648-C655.

55. Brankovic, S.R., J.X. Wang, and R.R. Adzic, Surface Science, 2001. **474**: p. L173-L179.

56. Mrozek, M.F., Y. Xie, and M.J. Weaver, Analytical Chemistry, 2001. **73**(24): p. 5953-5960.

57. Kim, J.Y., Y.G. Kim, and J.L. Stickney, ECS Transactions, 2006. **1**(30): p. 41-48.

58. Stickney, J.L., *Electrochemical atomic layer epitaxy*, in *Electroanalytical Chemistry*, A.J. Bard and I. Rubenstein, Editors. 1999, Marcel Dekker: New York. p. 75-211.

59. Wade, T.L., T. Sorenson, A., and J.L. Stickney, *Epitaxial Compound Electrodeposition*, in *Interfacial Electrochemistry*, A. Wieckowski, Editor. 1999, Marcel Dekker: New York. p. 757-768.

60. Venkatasamy, V., et al., Electrochimica Acta, 2006. **51**(21): p. 4347-4351.

Figure 1.1: Automated flow cell deposition system.

CHAPTER 2

OPTIMIZATION STUDIES OF HGSE THIN FILM DEPOSITION BY ELECTROCHEMICAL ATOMIC LAYER EPITAXY (EC-ALE)[1]

[1] Venkatasamy, V., et al., Electrochimica Acta, 2006. **51**(21): p. 4347-4351 (Used by permission).

Abstract

Studies of the optimization of HgSe thin film deposition using electrochemical atomic layer epitaxy (EC-ALE) are reported. Cyclic voltammetry was used to obtain approximate deposition potentials for each element. These potentials were then coupled with their respective solutions to deposit atomic layers of the elements, in a cycle. The cycle, used with an automated flow deposition system, was then repeated to form thin films, the number of cycles performed determining the thickness of the deposit. In the formation of HgSe, the effect of Hg and Se deposition potentials, and a Se stripping potential, were adjusted to optimize the deposition program. Electron probe microanalysis (EPMA) of 100 cycle deposits, grown using the optimized program, showed a Se/Hg ratio of 1.08. Ellipsometric measurements of the deposit indicated a thickness of 19 nm, where 35 nm was expected. X-ray diffraction displayed a pattern consistent with the formation of a zinc blende structure, with a strong (111) preferred orientation. Glancing angle fourier transform infrared spectroscopy (FTIR) absorption measurements of the deposit suggested a negative gap of 0.60 eV.

Keywords: HgSe, EC-ALE, UPD, Electrodeposition, XRD, EPMA, FTIR, ALE, ALD

Introduction

Mercury selenide, HgSe, is a II-VI compound semiconductor. Based on its electrical properties, it is classified as a semimetal or degenerate semiconductor [1-3]. It is of special interest for fundamental studies because of its inverted band structure [4]. Some of the possible applications for mercury selenide lie in optoelectronics. Molecular beam epitaxy (MBE) [5, 6], chemical bath deposition [7-9] and the cold traveling heater method (CTHM) [10] are some of the methods previously used to deposit HgSe.

Recently, this group reported the first deposits of mercury selenide formed via. electrochemical atomic layer epitaxy (EC-ALE) [11]. EC-ALE is the electrochemical analog of atomic layer epitaxy (ALE) [12-17], and atomic layer deposition (ALD) [18-21]. All are methods for which the deposits are grown layer by layer, using surface limited reactions, under potential deposition (UPD) in the case of EC-ALE. UPD refers to the electrodeposition of an atomic layer of a first element on a second, at a potential prior to, under, that needed to deposit the element on itself [22-26]. A number of II-VI compounds such as CdTe, CdS and ZnSe have been successfully grown using EC-ALE [27-30], as well as some III-V compounds such as GaAs, InAs, and InSb [28, 29, 31-33]. Recently PbSe [34], PbTe and Bi_2Te_3 [35] have also been grown using EC-ALE.

This paper is an extension of previous work on HgSe deposition by this group [11]. Attempts have been made to optimize the deposition cycle HgSe by adjusting the potentials for Se and Hg used in the EC-ALE cycle.

Experimental

Depositions were performed using a thin layer flow electrodeposition system [16, 36, 37], which consisted of pumps, valves, a flow cell and a potentiostat. All components were computer controlled using a LABVIEW program.

The flow cell has been previously described [38], with minor design changes to the reference compartment. A Teflon tube fitting was changed to a simple O-ring, which provided a better seal. The auxiliary electrode was an ITO glass slide, and the reference electrode was Ag/AgCl (3 M NaCl) (Bioanalytical Systems, Inc., West Lafayette, IN). Substrates consisted of 300 nm thick gold films on glass. The substrates were annealed at 400^{o}C for 12 hours under a vacuum of 10^{-6} Torr, after Au vapor deposition, resulting in a (111) habit.

The solutions used were 0.2 mM HgO, pH 2 and 0.5 mM SeO_2, pH 3. Both solutions contained 0.5 M Na_2SO_4 as a supporting electrolyte. The blank solution contained only the 0.5 M Na_2SO_4, at pH 4. Solution pH was adjusted using H_2SO_4. The water used to make solutions was supplied from a Nanopure water filtration system (Barnstead, Dubuque, IA) attached to the house DI water system. Chemicals were reagent grade or better.

The EC-ALE cycle used to deposit HgSe was performed as follows: the Se solution was flushed into the cell for 2 s (40 mL/min), and then held quiescent for 15 s, all at the chosen Se deposition potential. Blank solution was then flushed through the cell for 3 s. This was followed by filling the cell with the Hg solution for 2 s, and holding quiescent for 15 s for deposition. The cycle was then completed by flushing with blank solution for 3 s. This cycle was repeated 100 times for each experiment.

Deposit thickness was monitored using a single wavelength ellipsometer (Sentech SE 400). A Scintag, PAD-V diffractometer with CuKα radiation (λ= 1.5418 A), was used to obtain the glancing angle X-ray diffraction patterns. Electron probe Microanalysis (EPMA) was run on a Joel 8600 wavelength dispersive scanning electron microprobe.

Glancing angle absorption measurements were performed, using an FTIR spectrophotometer (Bruker FTS-66v, Bruker optics, Inc.).

Results and Discussions

Cyclic voltammetry was used to determine approximate starting deposition potentials for the EC-ALE cycle. The voltammetric behaviors of $HSeO_3^-$ and Hg^{2+} with gold on glass substrates are shown in Figures 1 and 2. Potentials of 0.20 V for Se and 0.45 V for Hg were identified as reasonable initial potentials for the EC-ALE cycle. Thus, the initial program went as follows: the cell was filled with the Se solution, pumped for 2 s at 0.20 V, no flow (static) for 15 s for deposition, then blank solution was flushed for 3 s at 0.2 V. The Hg solution flush in, pumped for 2 s at 0.45 V, static for 15 s, and blank solution flush for 3 s at 0.45 V. The intent was that this cycle would ideally result in the deposition of one compound monolayer.

Using these conditions, no deposition was observed by visual inspection after 100 cycles. Evidently the potentials chosen were insufficiently negative to drive the deposition of HgSe, even though UPD of these elements on Au looked promising.

A series of experiments were then performed where the deposition potentials for Se were varied from 0.20 V to -0.20 V, while keeping the same deposition potential for Hg at 0.45 V (Figure 3). No deposits were evident until the potential for Se deposition was -0.10 V or below. Optical microscopy and EPMA were performed on each deposit to determine homogeneity and

stoichiometry, respectively. Based on deposit homogeneity, -0.15 V was selected as a good Se deposition potential. The resulting deposits appeared homogeneous and stoichiometric, however, ellipsometric data suggested the deposits were close to 100 nm thick, significantly thicker than expected for a simple model of one compound monolayer per cycle, where a 100 cycle deposit was expected to result in a 37.4 nm thick film. This model assumes one Hg-Se bi-layer grows each cycle, with the (111) orientation [38].

Previous studies of Se deposition [39-41] have shown that Se does not result in a classic underpotential deposition process. On the contrary, Se deposition requires an over potential, but bulk deposition of Se is so slow that a surface limited feature is still visible. The result is that along with the surface limited reaction, formation of an atomic layer of Se, a small amount of bulk Se is deposited as well. This can be seen from the current time profile, during Se deposition (Figure 4). The current for Se deposition does not drop down to zero after the surface is covered, that suggests that it is not a surface limited process and the amount of bulk Se deposited depends on the deposition time. The surface limited process is fast, reaching completion quickly, while the bulk deposition is slow, resulting in a small steady state current [42]. Thus, one explanation for the excess deposit thicknesses is the formation of some bulk Se on the surface. Deposition of bulk Se can be minimized by using a short deposition time, just long enough for the majority of the surface limited deposition to complete. Alternatively, bulk Se can be removed by introduction of an extra step designed to reduce excess bulk Se to a soluble selenide species [27]. This second methodology was selected for the present study. After 15 s of Se deposition, the cell was rinsed with blank solution for 3 s, at which point the potential was shifted negatively, such that bulk Se was reduced to HSe^-. HSe^- is a soluble species, which diffuses away, leaving only upd Se on the surface. A set of experiments were performed by varying this reductive stripping

potential for Se from -0.55 V to -0.65 V, while keeping all the other parameters constant (Figure 5). Based on the resulting deposit stoichiometry data from EPMA, and optical microscopy observations of the deposit thickness and homogeneity, -0.63 V was picked as the reductive stripping potential for the cycle.

To optimize the deposition potential for Hg, another series of experiments were conducted, where only the deposition potential for Hg (Figure 6) was varied. The best Hg deposition potential appeared to be 0.48 V, based on stoichiometry and optical microscopy. However, it is of note that the coulometry for Hg, at this potential, suggested a coverage of only 0.10 ML, instead of the 0.44 ML ideally expected. Previous results have suggested that the formation of one bi-layer of Cd and Se from the (111) plane of zinc blende CdSe would require 0.44 ML of Cd and 0.44 ML of Se. It is not clear why the coulometry for Hg was so low, 0.10 ML vs. 0.44 ML. One possibility is that some of the deposited Se was oxidized at the positive potentials required for surface limited Hg deposition. The coulometry observed was thus the net charge for Hg^{2+} reduction and Se oxidation. In addition, the resulting films were about half as thick as ideally expected, where deposition of a compound monolayer is expected with each cycle, see below.

Overall, the optimal EC-ALE cycle for HgSe deposition appeared to be as follows: Se solution was rinsed into the cell for 2 s at -0.15 V. The solution was held static for 15 s for deposition. The cell was then flushed with blank solution for 3 s at -0.15 V, at which point, the potential was changed to -0.63 V for 5 s. After this, the Hg solution was filled for 2 s, and deposited for 15 s at 0.48 V. This was followed by another blank rinse at 0.48 V for 3 s (Figure 7).

Ellipsometric measurements of the resulting deposit indicated that the film was 19 nm thick. EPMA of the deposit indicated a Se/Hg atomic ratio of 1.08. Figure 8, shows the X-ray diffraction pattern for the deposit. Peaks corresponding to (111), (220) and (311) planes of HgSe (JCPDS 8-469) were evident, and no elemental peaks for Hg and Se were observed. The deposit showed a predominant (111) orientation as the ratio of the intensity between the (111) and (220) peak came out to be 10.2, which is considerably higher than the literature value of 2.

Room temperature IR absorption studies of HgSe were performed using a glancing angle of 85^{o} from the surface normal. Figure 9 shows a plot of the square of the absorption data vs. energy for a 100 cycle deposit of HgSe. An absorption edge was found at - 0.60 eV. This value corresponds to the $\Gamma_6^{VB} \rightarrow \Gamma_8^{CB}$ transition of the inverted band structure of HgSe, reported to be -0.51 eV from theoretical calculations [43] and -0.46 eV experimentally [4].

Conclusion

The influence of the deposition potentials for Hg and Se, as well as that for a reductive Se stripping step, has been reported. The optimal deposition cycle devised includes deposition of Se at -0.15 V, stripping of excess Se at -0.63 V, and deposition of Hg at 0.48 V. The resulting deposit was a little over half of that expected from the ideal model of one compound monolayer for each cycle, but the deposit was stoichometric, and showed strong preferential (111) deposition. The absorption spectrum for this deposit appears consistent with the literature: an inverted band structure and a negative gap of 0.6 eV.

Acknowledgements

The authors would like to acknowledge the support of NSF divisions of Chemistry and Material science.

References

1. Harman, T.C. and A.J. Strauss, Journal of Applied Physics, 1961. 32: p. 2265-&.
2. Blue.M.D, K.P.W., J. Phys. Chem. Solids, 1963. 23: p. 577.
3. Gawlik, K.U., et al., Physical Review Letters, 1997. 78(16): p. 3165-3168.
4. Einfeldt, S., et al., Physical Review B, 1995. 51(8): p. 4915-4925.
5. Einfeldt, S., et al., Journal of Crystal Growth, 1994. 138(1-4): p. 471-476.
6. Becker, C.R., et al., Journal of Crystal Growth, 1993. 127(1-4): p. 331-334.
7. Hankare, P.P., et al., Materials Chemistry and Physics, 2001. 71(1): p. 53-57.
8. Pramanik, P. and S. Bhattacharya, Materials Research Bulletin, 1989. 24(8): p. 945-952.
9. Li, Y., et al., Journal of Physics and Chemistry of Solids, 1999. 60(7): p. 965-968.
10. Reig, C., Y.S. Paranchych, and V. Munoz-Sanjose, Crystal Growth & Design, 2002. 2(2): p. 91-92.
11. Mkhulu K. Mathe, S.M.C., Venkatram Venkatasamy, Uwe Happek and John L. Stickney*, Journal of Electrochemical society, 2005. accepted.
12. Bedair, S., *Atomic Layer Epitaxy*. 1993, Amsterdam: Elsevier. 304.
13. Kuech, T.F., P.D. Dapkus, and Y. Aoyagi, *Atomic Layer Growth and Processing*. Vol. 222. 1991, Pittsburgh: Materials Research Society. 360.
14. Goodman, C.H.L. and M.V. Pessa, JAP, 1986. 60: p. R65.
15. Faschinger, W., Physica Scripta, 1993. T49B: p. 492.
16. Stickney, J.L., *Electrochemical atomic layer epitaxy*, in *Electroanalytical Chemistry*, A.J. Bard and I. Rubenstein, Editors. 1999, Marcel Dekker: New York. p. 75-211.
17. B.W. Gregory, D.W.S., J.L. Stickney, J. Electrochem. Soc., 1991. 138: p. 1279.
18. Leskela, M. and M. Ritala, Thin Solid Films, 2002. 409(1): p. 138-146.

19. Yousfi, E.B., et al., Thin Solid Films, 2001. 387(1-2): p. 29-32.

20. Sammelselg, V., et al., Applied Surface Science, 1998. 134(1-4): p. 78-86.

21. Ylilammi, M., Thin Solid Films, 1996. 279(1-2): p. 124-130.

22. Kolb, D.M., Przasnys.M, and Gerische.H, Journal of Electroanalytical Chemistry, 1974. 54(1): p. 25-38.

23. Kolb, D.M., *Physical and Electrochemical Properties of Metal Monolayers on Metallic Substrates*, in *Advances in Electrochemistry and Electrochemical Engineering*, H. Gerischer and C.W. Tobias, Editors. 1978, John Wiley: New York. p. 125.

24. Juttner, K. and W.J. Lorenz, Z. Phys. Chem. N. F., 1980. 122: p. 163.

25. Hubbard, A.T., et al., *Electrochemical surface characterization*, in *New Dimensions in Chemical Analysis*, B.L. Shapiro, Editor. 1985, Texas A & M University Press: College Station, Texas. p. 135.

26. Gewirth, A.A. and B.K. Niece, Chem. Rev., 1997. 97: p. 1129-1162.

27. Colletti, L.P., B.H. Flowers Jr., and J.L. Stickney, Journal of the Electrochemical Society, 1998. 145(5): p. 1442-1449.

28. Wade, T.L., et al. *Formation of II-VI and III-V compound semiconductors by electrochemical ALE*. in *National Meeting of the Electrochemical Society, Spring*. 1999. Seattle, Washington: The Electrochemical Society.

29. Wade, T.L., et al. *Electrochemical Atomic Layer Eptitaxy: Electrodeposition of III-V and II-VI Compounds,*. in *Materials Research Society*. 2000: Materials Research Society.

30. Stickney, J.L., *Electrochemical atomic layer epitaxy (EC-ALE): Nanoscale control in the electrodeposition of compound semiconductors*, in *Advances in Electrochemical Science*

and Engineering, D.M. Kolb and R. Alkire, Editors. 2002, Wiley-VCH: Weinheim. p. 1-107.

31. Wade, T.L., et al., Electrochemical and Solid State Letters, 1999. 2(12): p. 616.
32. Wade, T.L., et al., JEC, 2001. 500: p. 322-332.
33. Vaidyanathan, R., J.L. Stickney, and U. Happek, J. Electroanal. Chem., 2003. 559: p. 55-61.
34. Vaidyanathan, R., J.L. Stickney, and U. Happek, Electrochimica Acta, 2004. 49(8): p. 1321-1326.
35. Zhu.W, Y.J.Y., Zhang.T.J, J. Electroanal. Chem. , 2005. 585(1): p. 83-88.
36. Wade, T.L., T. Sorenson, A., and J.L. Stickney, *Epitaxial Compound Electrodeposition*, in *Interfacial Electrochemistry*, A. Wieckowski, Editor. 1999, Marcel Dekker: New York. p. 757-768.
37. Wade, T.L., et al. *Morphology control in the formation of compound semiconductors using electrochemical atomic layer epitaxy (EC-ALE)*. in *Electrochemical Society National Meeting*. 2001. Washington D.C.: Electrochemcial Society.
38. Flowers, J., Billy H., et al., Journal of Electroanalytical Chemistry, 2002. 524-525: p. 273-285.
39. Huang, B.M., T.E. Lister, and J.L. Stickney, Surface Science, 1997. 392(1-3): p. 27.
40. Greenwood, N.N. and A. Earnshaw, *Chemistry of the Elements*. 1984, Oxford: Pergamon Press.
41. Mathe, K., et al., J of Crystal Growth, 2004. 271(1-2): p. 55-64.
42. Lister, T.E. and J.L. Stickney, Applied Surface Science, 1996. 107: p. 153.
43. Rohlfing, M. and S.G. Louie, Physical Review B, 1998. 57(16): p. R9392-R9395.

Figure 2.1: Cyclic voltammogram of Au electrode in 0.5 mM $HSeO_3^-$, pH 3.

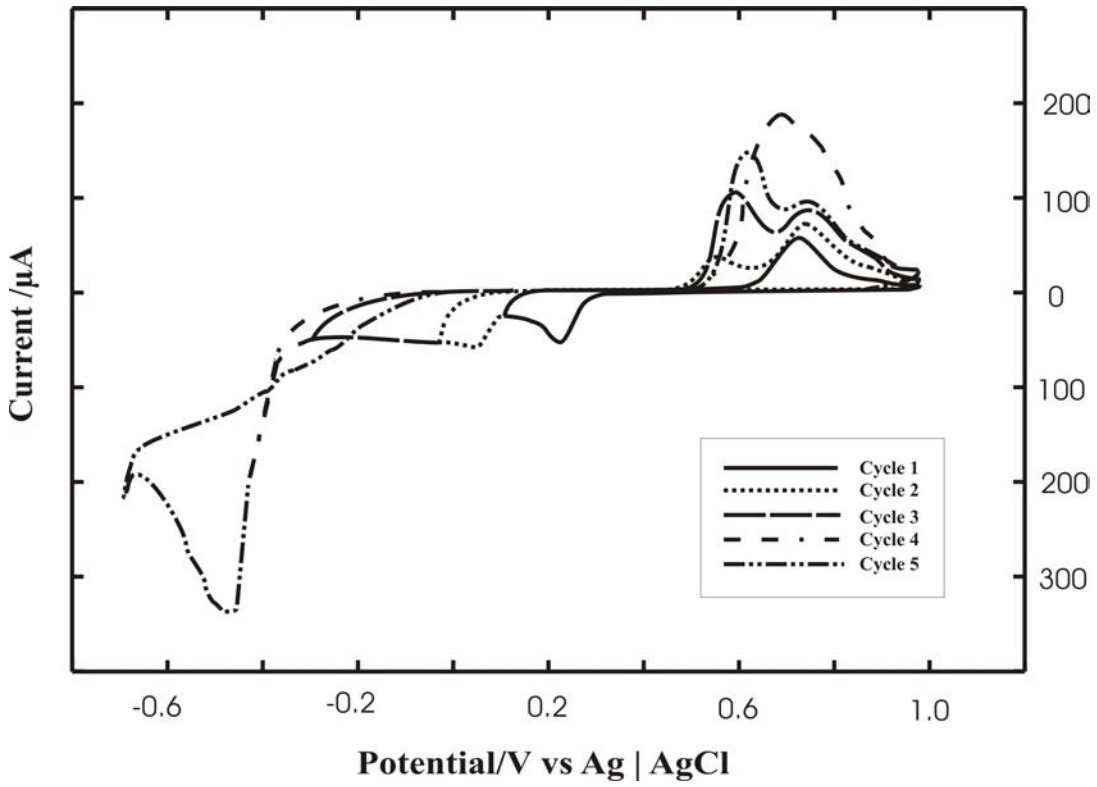

Figure 2.2: Cyclic voltammogram of Au electrode in 0.2 mM Hg^{2+}, pH 2.

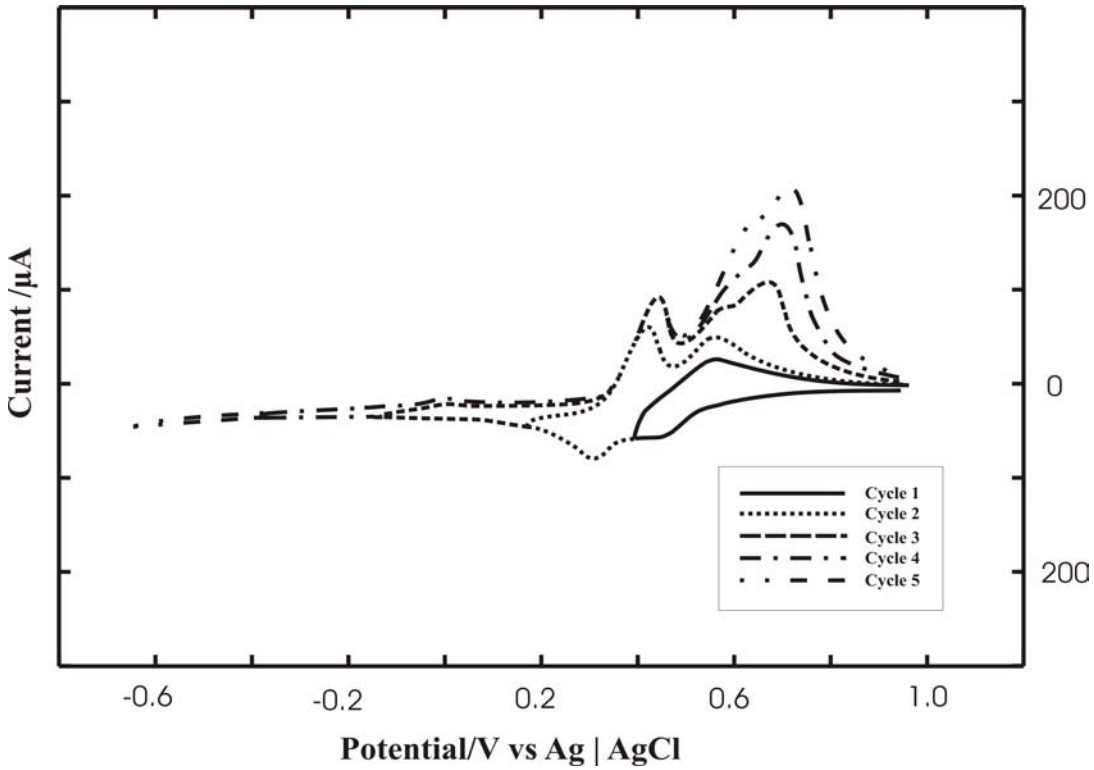

Figure 2.3: Effect of Se deposition potential on HgSe deposition.

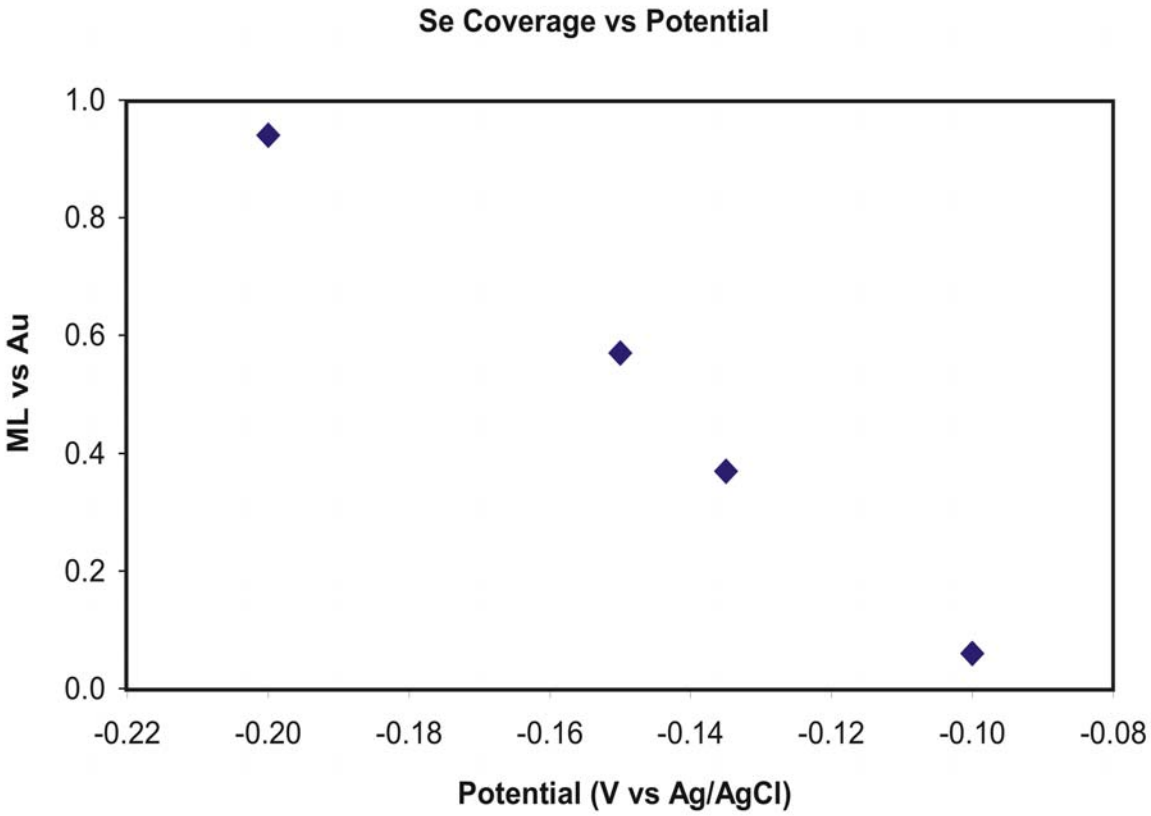

Figure 2.4: Current-time profile during one cycle of HgSe deposition.

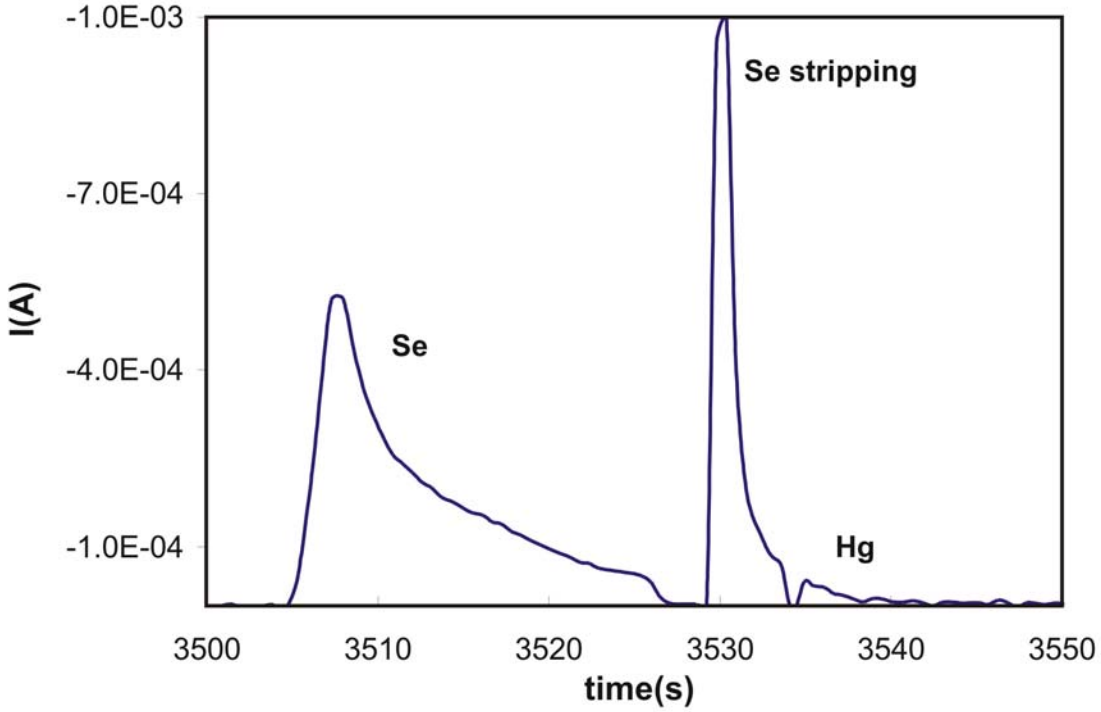

Figure 2.5: Effect of Se stripping potential on deposit thickness.

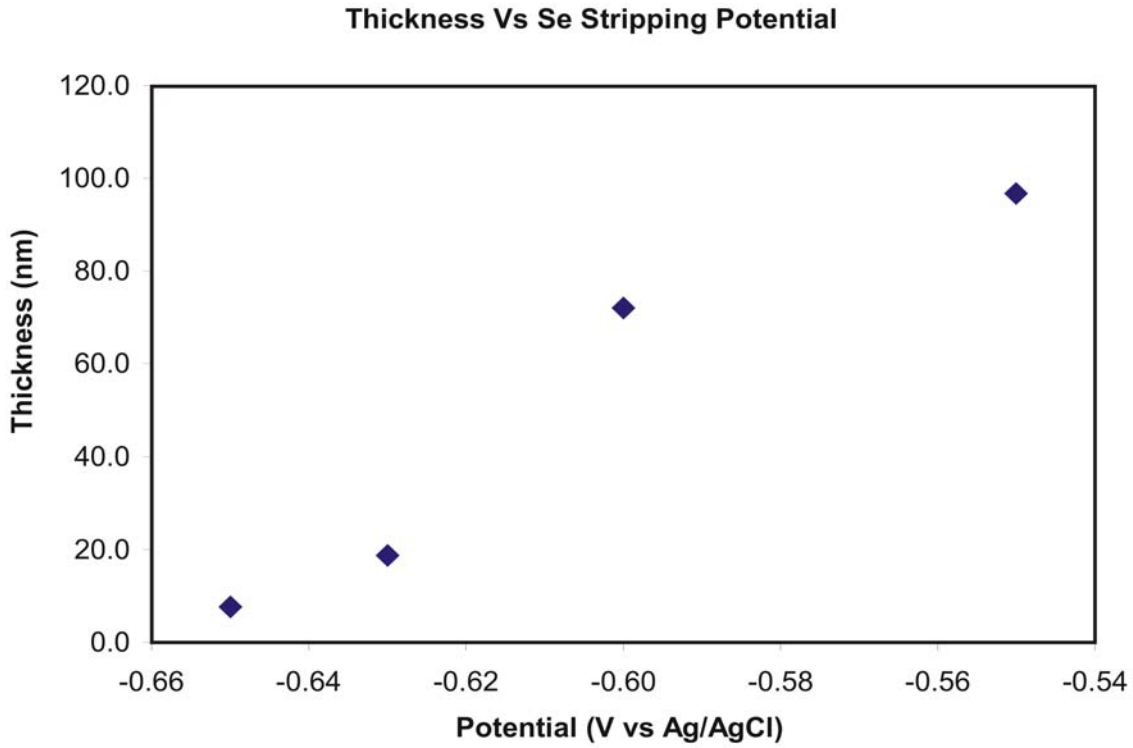

Figure 2.6: Effect of Hg deposition potential on HgSe deposition.

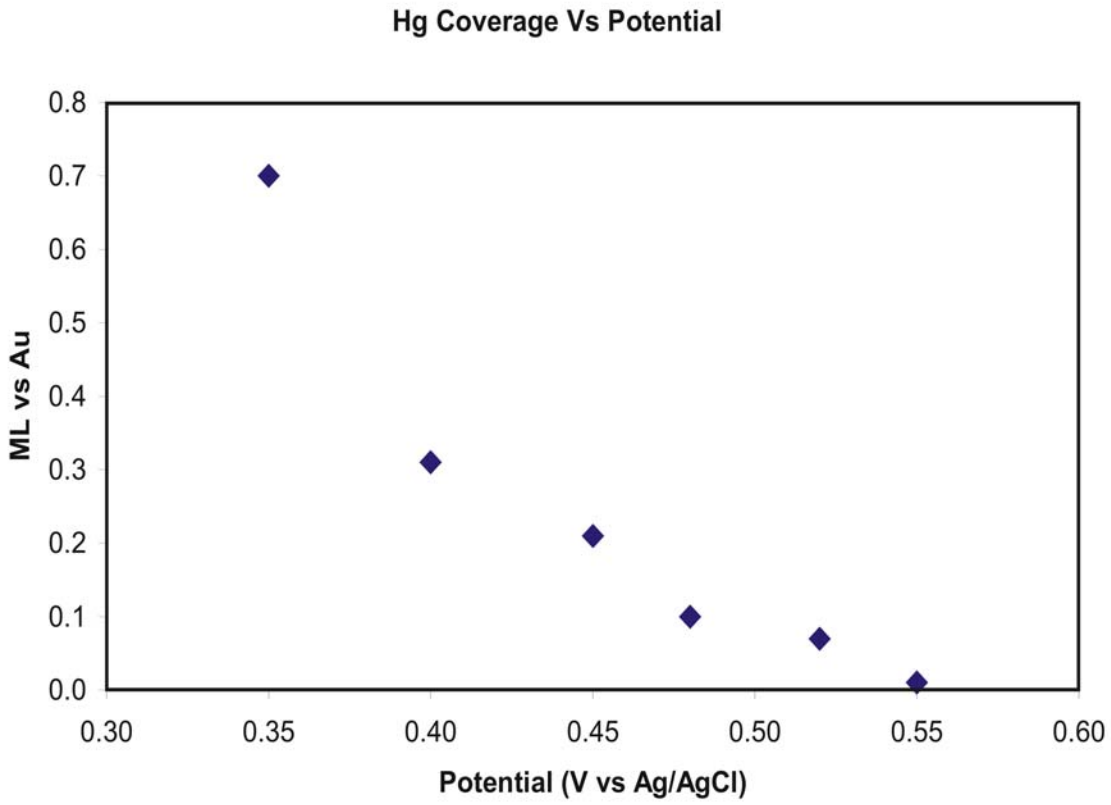

Figure 2.7: Optimal deposition program.

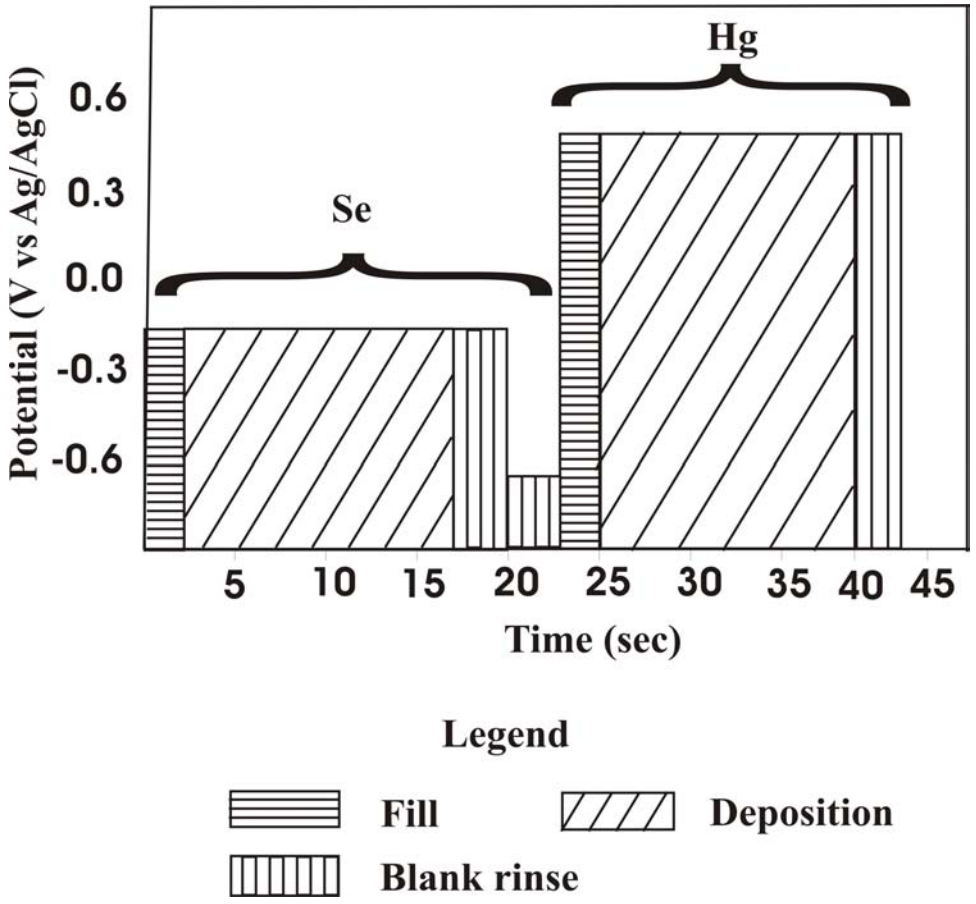

Figure 2.8: XRD diffraction pattern of 100 cycle HgSe thin film.

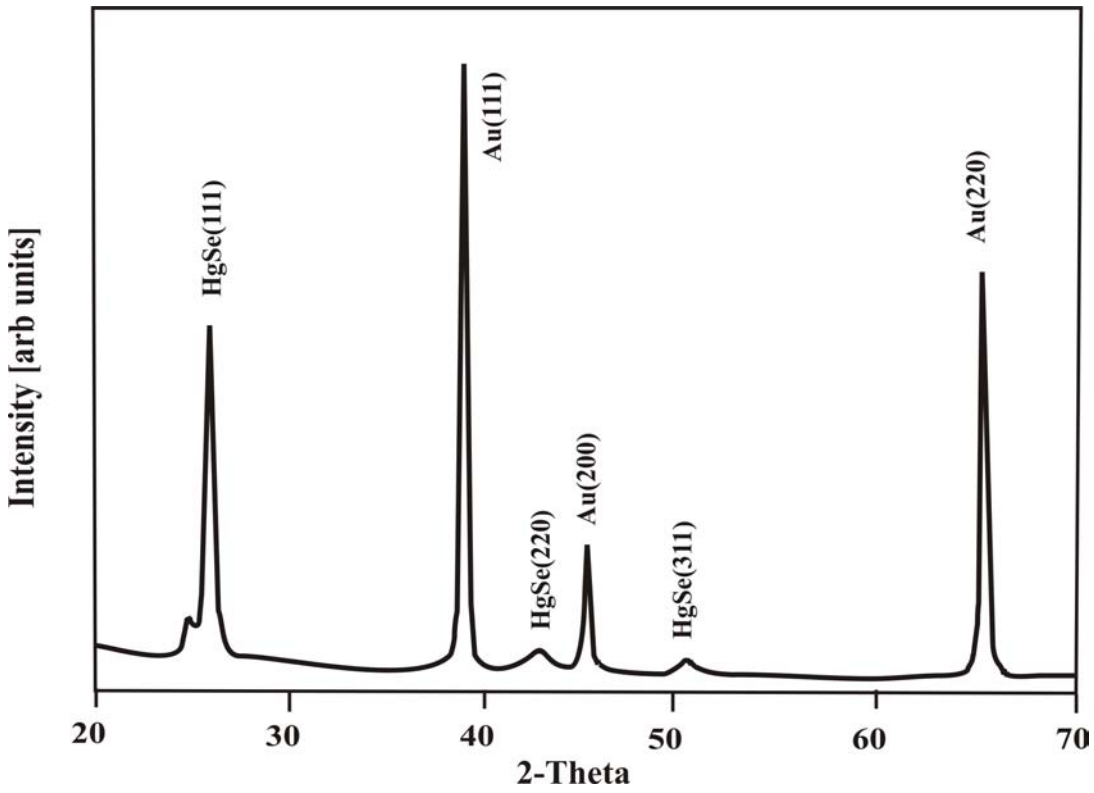

Figure 2.9: Absorption spectrum of 100 cycle HgSe thin film.

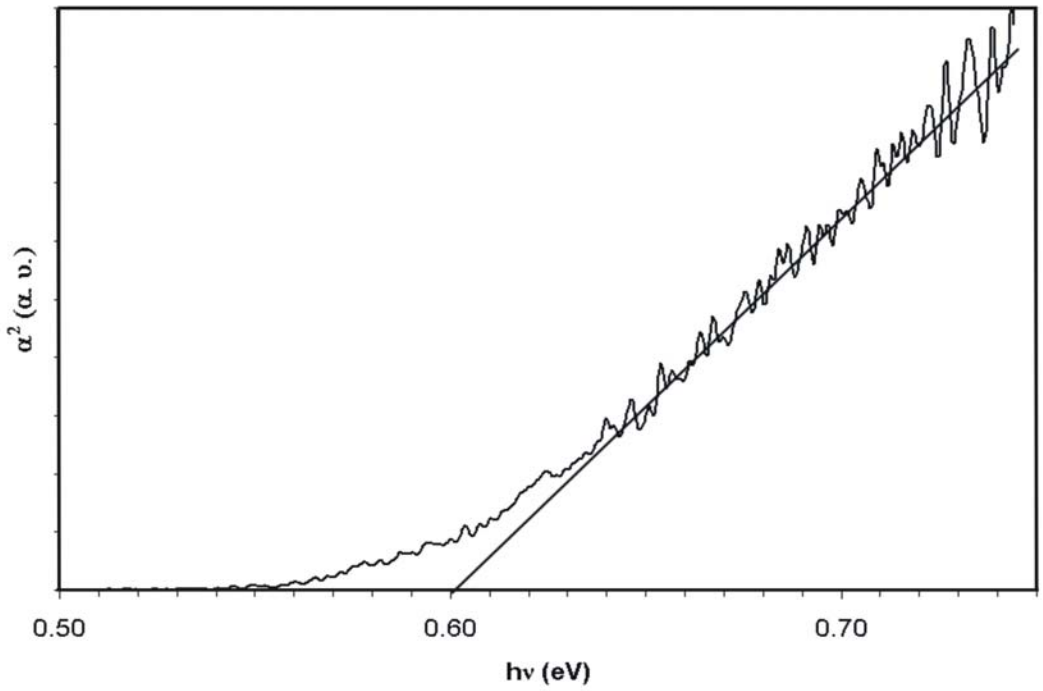

CHAPTER 3

OPTIMIZATION OF CDTE NANOFILM FORMATION BY ELECTROCHEMICAL ATOMIC LAYER EPITAXY (EC-ALE)[1]

[1] Venkatasamy, V., et al., Journal of Applied Electrochemistry, 2006. **36**(11): p. 1223-1229 (Used by permission).

Abstract

This paper concerns optimization studies of the growth of cadmium telluride, an important II-VI compound semiconductor, using electrochemical atomic layer epitaxy (EC-ALE). The importance of the potentials used to deposit atomic layers of Cd and Te, as well as the potential used to strip excess Te, were investigated. These potentials were used in a cycle, an EC-ALE cycle, to form deposits one atomic layer at a time, using a sequence of surface limited reactions. The optimal potentials for the CdTe EC-ALE cycle included Cd deposition at -0.65 V, Te deposition at -0.35 V and bulk Te stripping at -0.70 V. The deposits obtained were stoichiometric, with a Te/Cd atomic ratio of 1.01 from electron probe microanalysis (EPMA). Electrochemical quartz crystal microbalance (EQCM) studies of the optimal condition indicated that about a third of the deposited Cd was oxidatively stripped at the potential used to deposit Te. Glancing angle X-ray diffraction studies showed a (111) preferred orientation for the deposit, while room temperature near infrared absorption measurements indicated a direct band gap of 1.5 eV.

Keywords: CdTe; EC-ALE; EQCM; EPMA; Ellipsometry; Photo voltaics; XRD

Introduction

Cadmium telluride, CdTe, is a II-VI compound semiconductor that has found application in the field of photovoltaics [1-5]. Reasons for its use as a photovoltaic include that it possesses a direct bandgap, 1.5 eV, very close to that theoretically calculated to be optimal for solar cells, based on a single absorber, single bandgap configuration. In addition, because of its direct bandgap, it has a very high absorption coefficient.

High quality thin films of CdTe have been achieved with excellent control over stoichiometry and thickness by using high temperature techniques like molecular beam epitaxy (MBE) [6] and metal organic vapor phase epitaxy (MOVPE) [7]. Cadmium telluride has also been obtained by other low temperature techniques like chemical bath deposition (CBD) and electrodeposition [8-13]. Currently, electrodeposition is employed for the fabrication of CdTe films for high efficiency photovoltaic devices [14].

Electrodeposition has advantages such as low or even room temperature deposition, low cost of production and high deposit quality. Cost is the most important factor in making viable photovoltaics for large scale energy conversion. Compound electrodeposition techniques like precipitation [15], co-deposition [16], and EC-ALE [5] have been reviewed in the literature. In general, to achieve the low cost need for general use photovoltaics, co-deposition is probably the only viable electrodeposition methodology.

EC-ALE is a technique for electrodepositing nanofilms, and has been used most extensively to form compound semiconductors. EC-ALE is the electrochemical analog of ALE [17-19] and ALD [20-23], all methods based on the use of surface limited reactions to form deposits with atomic layer control. The advantages of these methodologies are that they can be used to control deposition at the atomic level. The method breaks the deposition process into a

sequence of individually controllable steps, thus greatly improving the ability to optimize a process. In some scenarios, they promote epitaxy, as has been found in the case of EC-ALE. However, such processes tend to increase the complexity of the deposition hardware.

In electrochemical studies, surface limited reactions are generally referred to as under potential deposition (UPD) [24-28]. UPD is a phenomenon where in one element electrodeposits on another, at a potential prior to (under) the potential at which the first element deposits on to itself. EC-ALE involves the sequential electrodeposition of atomic layers of elements, to form nanofilms of materials using underpotentials.

Most previous work with EC-ALE has involved electrodeposition of nanofilms of compound semiconductors, including: II-VI compounds such as CdTe, CdS and ZnSe [29-32] as well as some III-V compounds such as GaAs, InAs, and InSb [31-34]. PbSe [35], PbTe and Bi_2Te_3 have also been grown using EC-ALE. Recently, this work has been extended to the formation of metal nanofilms, such as Cu and Pt.

In the author's group, the formation of CdTe thin films by EC-ALE has been well studied, using a variety of electrochemical cell configurations and geometries, as well as using a variety of cycle programs and solution chemistries [29, 36-38]. The quality of the deposits has improved dramatically from the first studies using a thin layer electrochemical cell (TLE) [39], to the present flow cell design [30]. Early studies were fraught with problems such as poor reproducibility and deposit inhomogeneity. There were also problems with the design of the EC-ALE cycle, and problems deciding on solution composition. Such questions have made it hard to develop and optimize the EC-ALE cycle program. Answers to such questions have become clearer as more studies have been performed on the deposition of CdTe, and other compounds.

The cycle program described here has been well optimized by our present standards, for use with the thin layer flow cells used in this study.

As noted above, using EC-ALE to form simple photovoltaics is not economically a wise choice. The quality of a photovoltaic formed using the cycle described here may very well be better then those presently produced using the codeposition method, but the simplicity of codeposition makes it the right choice. This raises the question of what materials are worth depositing via EC-ALE. There are bound to be materials that can only be formed using EC-ALE. However it is more likely that there are structures that can be formed using this method that cannot be formed using another electrodeposition method, or any other method period. For example, when a nanofilm of defined thickness is needed, or the formation of a superlattice, EC-ALE should be considered.

The work presented here has been performed to develop an optimized CdTe cycle, to be combined with one developed for HgTe (to be reported separately) so that superlattices of HgTe and CdTe can be formed and studied. Mer Cad Tel (MCT) is a very important IR detector material ($Hg_XCd_{(1-X)}Te$). It is felt by this group that given EC-ALE programs for both CdTe and HgTe, control over the composition of electrodeposited MCT may be achievable.

This paper presents optimization studies of CdTe deposition by EC-ALE using an automated flow deposition system. The influence of changes in the Cd and Te deposition potentials and the Te stripping potential were varied with the intent of designing a cycle which produces homogeneous and stoichiometric deposits of CdTe, an atomic layer at a time.

Experimental

Depositions were performed using a thin layer flow electrodeposition system [5, 40, 41], consisting of pumps, valves, a flow cell and a potentiostat. All components were computer

controlled using a LABVIEW program. The flow cell has been described previously [30], with minor design changes to the reference compartment. A Teflon compression fitting was changed to a simple O-ring to hold the reference electrode, providing a better seal. The auxiliary electrode was an ITO glass slide, and the reference was Ag/AgCl (3 M NaCl) (Bioanalytical Systems, Inc., West Lafayette, IN). Substrates consisted of 300 nm thick gold films on glass. The substrates were annealed at 400^{o}C for 12 hours under a vacuum of 10^{-6} Torr, after Au vapor deposition, resulting in a (111) habit.

The solutions used were 0.5 mM $CdSO_4$, pH 5 and 0.2 mM TeO_2, pH 4, and both contained 0.5 M Na_2SO_4. The blank solution contained only the 0.5 M Na_2SO_4, at pH 4. Solution pH was adjusted using H_2SO_4. The water used to make solutions was supplied from a Nanopure water filtration system (Barnstead, Dubuque, IA) attached to the house DI water system. Chemicals were reagent grade or better.

The EC-ALE cycle used to deposit CdTe was as follows: the Cd solution was flushed into the cell for 2 s (40 ml min^{-1}), and then held quiescent for 15 s, all at the chosen Cd deposition potential. Blank solution was then flushed through the cell for 3 s. This was followed by filling the cell with the Te solution for 2 s, and holding quiescent for 15 s for deposition. The cycle was then completed by flushing with blank solution for 3 s. This cycle was repeated 100 times for each experiment.

Deposit thickness was monitored using a single wavelength ellipsometer (Sentech SE 400). A Scintag PAD-V diffractometer with CuKα radiation (λ= 1.5418 A), was used to obtain glancing angle X-ray diffraction patterns. Electron probe microanalysis (EPMA) was run on a Joel 8600 wavelength dispersive scanning electron microprobe. Glancing angle absorption

measurements were performed, using pi-polarized radiation at a glancing angle of 85 degrees using a 300 W, ozone-free Xe lamp and a monochromator (1/4 M Cornerstone, Spectra Physics).

Optimal deposition conditions were studied using a flow cell electrochemical quartz crystal microbalance (EQCM). A 9 MHz AT-cut quartz crystal (Seiko EG&G) was used, where both sides were coated with circular Au electrodes (ca. 0.2 cm^2, 5 mm in diameter). The electrodes were formed with 50 nm of Ti, followed by 300 nm of sputtered Au. Calibration of the EQCM was carried out using Ag electrodeposition combined with cyclic voltammetry.

Results and Discussions

The deposition potentials for Cd and Te used in the initial EC-ALE cycle were obtained from cyclic voltammetry, however, these were simple approximations, given that the deposits were formed on Au, not a CdTe surface. The voltammetric behavior of the gold on glass substrates in the blank solution is shown in Figure 1. The Te scan (Figure 2) was started at 0.95 V in the cathodic direction. Three distinct reduction peaks were observed at -0.35 V, -0.10 V and 0.28 V, corresponding to the bulk, upd (I) and upd (II) respectively. Further scanning in the cathodic direction resulted in hydrogen evolution below -0.80 V, as well as the reduction of some bulk Te to a telluride species such as HTe^-. During subsequent anodic scans, peaks at -0.75 V, 0.42 V and 0.55 V were evident, corresponding to oxidation of HTe^- to Te, and stripping of bulk and upd Te, to $HTeO_2^+$, respectively.

Figure 3 is the cyclic voltammogram for gold on glass in 0.5 mM Cd^{+2}, pH 5 solution. The scan started at 0.55 V in the cathodic direction, showed a reduction shoulder around -0.05 V, corresponding to Cd^{2+} upd on gold. Bulk Cd deposition occurred at potentials negative of -0.80 V, and its stripping can be seen in the subsequent oxidative scan, in a peak at -0.55 V. Besides upd, it is well known that Cd forms an alloy with Au, and the extra current evident in both the

reductive and oxidative scans can be ascribed to alloy formation and its subsequent stripping. Cd upd stripped near -0.15 V.

Potentials of -0.55 V for Cd and -0.40 V for Te were chosen, based on the voltammetry. The cycle included a 2 s Cd^{2+} solution rinse followed by 15 s deposition under static conditions (no flow) at -0.55 V. The cell was then rinsed with blank solution for 3 s at the same potential, followed by a 3 s $HTeO_2^+$ solution rinse and 15 s deposition under static condition at -0.40 V. The blank solution was again used to flush the $HTeO_2^+$ solution from the cell, for 3 s, at the same potential used for Te deposition.

Previous studies of Te deposition and CdTe formation, using EC-ALE [42], suggested that Te electrodeposition is kinetically slow. In the cyclic voltammetry (Figure 2), no Te deposits were formed at an underpotential, only at overpotentials. However, from the voltammetry for Te deposition (Figure 2), the initial deposition peaks are clearly not the result of a diffusion limited process, but appear to be surface limited reactions. It has been concluded by this group that surface limited deposits of Te are stable on Au, but the kinetics for their deposition are so slow that they do not occur at underpotentials on the experimental time scale, appearing only at overpotentials in the voltammetry. If they are formed at an overpotential, then by definition, bulk Te is stable as well. Hence, formation of just the surface limited amounts of Te becomes problematic. However, the surfaces limited reactions are significantly faster than the bulk deposition reactions. Thus by using short deposition times, the surface limited reactions predominate, but will contain some minimal amount of bulk Te.

A solution to this problem has been to electrochemically reduce the Te deposit in a blank solution, at a fairly negative potential. Under these conditions, bulk Te has been found to be reduced to a telluride species, probably HTe^-, which then diffuses away. Te stabilized by

bonding to the substrate remains, while the bulk is removed [30]. Thus, to circumvent the problem of traces of bulk Te, a reduction step in blank has been inserted, after the Te deposition step. Blank solution was rinsed for 3 seconds at a potential of -0.88 V, after the previous blank rinse step.

These steps constituted the initial EC-ALE cycle for CdTe deposition used in the present studies. The resulting CdTe deposit was patchy, inhomogeneous and showed a gradient across the surface. Visual inspection, optical microscopy, and ellipsometric measurements, evidenced a thicker deposit towards the outlet, with increased roughness there.

At present, deposit quality is gauged by the homogeneity over the deposit surface by optical microscopy, the thickness from ellipsometry, the stoichiometry from EPMA, and the structure from the XRD pattern. As these films are so thin, less then 100 nm, and of a direct band gap material, the color of a deposit is a direct indication of how thick a deposit is, and variations in color indicate variations in thickness. In addition, significant deposit roughening can be identified by microscopy, and diffuse scattering, scattering of some reflected light. Color changes, as well as scattering can be observed with the eye in many cases.

The need to modify this initial cycle was evident by the variation in color across the deposit. In general, if the deposit shows a gradient in color from the inlet to the outlet, the cycle is not completely controlled by surface limited deposition, as expected. That is, some step(s) in the process is probably results in transport controlled deposition. The cycle must be modified to better optimize the process.

From previous work on the EC-ALE formation of CdTe, it appears that the reduction of excess bulk Te, the Te stripping step, requires a significant amount of time to complete [42]. Hence, the first change was to increase the time for stripping to 10 s and performing it without

solution flow, static mode. This was then followed by a blank rinse at the same potential for 1 s, to flush resulting HTe^- species from the cell. The result was greatly improved homogeneity in the deposit. It appears that when the stripping step was performed for a short time with solution flowing, the products of the reduction step, telluride species, may have redeposited further down the substrate, resulting in less at the entrance, where blank entered the cell, and more at the outlet.

With the above change to the stripping step, studies of the potential dependence of the cycle were pursued. First, to determine the optimal deposition potential for Te, a series of experiments were performed where the Te deposition potential was varied from -0.25 V to -0.55 V, while maintaining the Cd deposition potential at -0.65 V and the Te stripping potential at -0.70V (Figure 4). Optical microscopy and EPMA were performed on each of the deposits to determine the homogeneity and stoichiometry respectively. Based on the homogeneity of the deposits and the stoichiometry, it was inferred that the ideal deposition potential for Te was -0.35 V. The potential of -0.35 V was well below the first surface limited peak in Figure 2, but close to the potential observed for the second peak. Figure 4 shows a 50 mV plateau near -0.35 V, consistent with surface limited deposition as opposed to potential controlled deposition, consistent with the improved homogeneity and stoichiometry observed in the deposits. To more negative potentials, the coverage for Te increased rapidly, as bulk deposition becomes more important, while above -0.35 V the coverage dropped, as it was insufficient to deposit a Te atomic layer.

As noted above, the stripping step was required as Te deposition took place negative of the formal potential for the reduction of $HTeO_2^+$ (0.65 V negative of the formal potential), and some bulk was deposit along with the Te atomic layer. A series of experiments were thus

performed where the deposition potentials of Cd and Te were held constant at -0.65 V and -0.35 V, respectively, and the Te stripping potential was varied from -0.55 V to -0.80 V (Figure 5). Deposit homogeneity and thickness were again monitored. Deposit thickness was observed to decrease as the potential was shifted negatively, as expected, since more Te would be reduced from the surface. In addition, deposit homogeneity decreased at the more negative potentials. Figure 5 suggests that the all Te was stripped at sufficiently negative potentials. Similar studies with stripping of Se in the formation of CdSe have shown that all Se can be stripped at sufficiently negative potentials [42]. Based on the deposit stoichiometry data from EPMA, and ellipsometric observations of the deposit thickness and homogeneity, -0.70 V was picked as the reductive stripping potential for the cycle.

To optimize Cd deposition, experiments were performed where the Cd deposition potential was varied between -0.30 V and -0.85 V, keeping all other parameters constant (Figure 6). The best Cd deposition potential appeared to be -0.65 V, where a plateau was evident in the graph. EPMA results indicated potentials below -0.75 V resulted in Cd rich deposits, while those above -0.60 V were Te rich (Figure 7). The Cd coverage took off at potentials below the formal potential for Cd, -0.8V, resulting in excess of 6 ML per cycle, consistent with deposition of bulk Cd.

After the studies described above of the potentials for Cd and Te deposition and the Te stripping potential, the following cycle was devised (Figure 9): Cd^{2+} solution was rinsed for 2 s at -0.65 V, and held for 15 s for deposition. The cell was then flushed with blank for 3 s at -0.65 V. Te solution was then flushed through the cell for 2 s, and held for 15 s at -0.35 V, followed by a blank rinse at -0.35 V for 3 s. The potential was then shifted to -0.70 V for 10 s under static

conditions. Finally, the cell was flushed with blank solution at the same potential for 1 s, to remove all HTe^- species form the cell.

The coverages of Cd and Te, from coulometry, for deposits formed with the above cycle were 0.69 ML and 0.21 ML respectively, where a monolayer (ML) is defined as one adsorbate atom for every gold surface atom. From previous studies on CdSe, it was found that the formation of one CdSe bi-layer from the (111) plane of zinc blende CdSe would require 0.44 ML of Cd and 0.44 ML of Se [43]. Thus, as a first approximation, similar coverages are expected of Cd and Te in a (111) layer of CdTe. As will be shown below, the predominant orientation for the CdTe deposit, from XRD, was (111). Clearly, the coverages measured here from coulometry are far from those expected a stoichiometric CdTe deposit, however, EPMA suggests that these deposits are stoichiometric.

In order to better understand the deposition process, and this disparity between charge and stoichiometry, an EQCM (Electrochemical quartz crystal microbalance) study was performed using a similar deposition program. The program did, however, differ as experience has shown that the EQCM flow cell works best if solution is continuously flowed through the cell, but at a much slower flow rate (6 ml min^{-1}). From Figure 8, it is evident, from coulometry, that the Cd coverage was significantly greater than that for Te. It is also clear, however, that some Cd was oxidatively stripped when the potential was switched from the -0.65 V used to deposit the Cd, to -0.35V, used to deposit Te. This was evident from both the presence of oxidative current after the potential shift, and the mass loss. This is understandable, given the reversibility of Cd deposition, the large positive step in potential, and loss of the activity of Cd^{2+} from the solution. The Cd loss was around 0.24 ML, based on coulometry, suggesting a net Cd coverage of around 0.45 ML, about what was expected.

However, measurements from ellipsometry, suggest that the deposit was only 24.4 nm thick, while a 100 cycle deposit of CdTe is expected to be 37.4 nm, based on staking (111) planes of zinc blende. As the deposit was only 24.4 nm thick, instead of 37.4 nm, it is expected that each atomic layer should correspond to a coverage of 0.29 ML in stead of the model of 0.44 ML, as previously suggested. So even taking into account the loss of Cd by oxidation, resulting in a coverage of 0.45 ML, as discussed above, this is still too much Cd to account for a 24.4 nm thick stoichiometric layer of CdTe. In addition, the thickness of the Te layers from coulometry was only 0.21 ML, instead of the 0.29 ML suggested from ellipsometry.

One of the problems with coulometry is that it measures the net current, not the absolute current for a given reaction. From Figure 8 it is evident that the initial deposition current for Te is lower than expected, and it may very well be that some Cd was oxidized while Te was initially deposited. If the difference in coverage is taken between what was measured for Cd deposition from coulometry, 0.45 ML, and what was actually realized, 0.29 ML, based on a stoichiometric layer only 24.4 nm thick, 0.16 ML of Cd is missing each cycle. In the case of Te, a coverage of 0.21 ML was measured from coulometry, and a coverage of 0.29 ML was realized based on stoichiometry and ellipsometry, or a difference of 0.08 ML. Cd oxidation is a two electron process, while that for Te deposition from a tellurite species is a four electron process, so the coverage of Te that would result from the electrons from 0.16 ML of Cd oxidation would be half, or would result in the deposition of an extra 0.08 ML of Te. These numbers suggest that the extra Cd was oxidized by reducing tellurite to Te, resulting in the observed 24.4 nm thick stoichiometric CdTe deposit.

Glancing angle X ray diffraction was run with an incident angle of 1^{o} from the sample plane, in order to maximize thin film sensitivity (Figure 10). Figure 10 shows the diffraction

pattern of a 200 cycle deposit of CdTe, which displays peaks consistent with a zinc blende deposit of CdTe. The relative sizes of the peak indicated a strong (111) preferred orientation. Room temperature absorption measurements of the ideal deposit indicated a direct bandgap of 1.50 eV (Figure 11), consistent with literature values for CdTe.

Conclusion

The dependence of nanofilms of CdTe grown using EC-ALE on the deposition potentials used for Cd and Te, as well as that used for a reductive Te stripping step, has been reported. The optimal deposition cycle devised included deposition of Cd at -0.65 V, deposition of Te at -0.35 V and, stripping of excess Te at -0.70 V. The resulting 100 cycle deposit was only 24.4 nm thick, less than that expected from the ideal model of one compound monolayer for each cycle, but the deposit was stoichometric, and showed a strong preferential (111) orientation. The absorption spectrum for this deposit suggested a direct band gap of 1.50 eV, consistent with the literature. Studies using an EQCM flow cell helped in understanding disparities between measured coulometric coverages for Cd and Te, and the resulting stoichiometry and deposit thickness. It appears that some of the Cd each cycle was oxidatively stripped upon switching the potential from the Cd deposition potential of -0.65V to that for Te deposition, -0.35V. In addition, it appears that some Cd was exchanged for Te. However, the net result was a high quality nanodeposit of stoichiometric CdTe.

Acknowledgements

The authors acknowledge the support of NSF divisions of Material Science and Chemistry.

References

1. Gamboa, S.A., et al., Solar Energy Materials and Solar Cells, 1998. **55**(1-2): p. 95-104.
2. Duffy, N.W., et al., Electrochimica Acta, 2000. **45**(20): p. 3355-3365.
3. Peter, L.M. and R.L. Wang, Electrochemistry Communications, 1999. **1**(11): p. 554-558.
4. Touskova, J., D. Kindl, and J. Tousek, Thin Solid Films, 1997. **293**(1-2): p. 272-276.
5. Stickney, J.L., *Electrochemical atomic layer epitaxy*, in *Electroanalytical Chemistry*, A.J. Bard and I. Rubenstein, Editors. 1999, Marcel Dekker: New York. p. 75-211.
6. A.T.S. Wee, et al., J. Phys. Chem.: Condens. Matter, 1995. **7**: p. 4359.
7. Maruyama, K., et al., Journal Of Electronic Materials, 1996. **25**(8): p. 1353-1357.
8. Elwell, D., JCG, 1981. **52**: p. 741.
9. Fulop, G.F. and R.M. Taylor, Ann. Rev. Mater. Sci., 1985. **15**: p. 197.
10. Gregory, B.W. and J.L. Stickney, Journal of Electroanalytical Chemistry, 1991. **300**(1-2): p. 543-561.
11. Rajeshwar, K., Adv. Mater., 1992. **4**: p. 23.
12. Fulop, G., et al., Appl. Phys. Lett., 1982. **40**: p. 327.
13. Pandey, R.K., G. Razzini, and L.P. Bicelli, Solar Energy Mater., 1992. **26**: p. 285.
14. Woodcock, J.M., et al. *Thin film solar cells based on electrodeposited CdTe*. in *IEEE Photovoltaic specialists*. 1991: IEEE.
15. D. Ham, et al., Chem. Mater., 1989. **1**: p. 619.
16. Kroger, F.A., J. Electrochem. Soc., 1978. **125**: p. 2028.
17. Bedair, S., *Atomic Layer Epitaxy*. 1993, Amsterdam: Elsevier. 304.
18. Kuech, T.F., P.D. Dapkus, and Y. Aoyagi, eds. *Atomic Layer Growth and Processing*. Vol. 222. 1991, Materials Research Society: Pittsburgh. 360.

19. Goodman, C.H.L. and M.V. Pessa, JAP, 1986. **60**: p. R65.

20. Leskela, M. and M. Ritala, Thin Solid Films, 2002. **409**(1): p. 138-146.

21. Yousfi, E.B., et al., Thin Solid Films, 2001. **387**(1-2): p. 29-32.

22. Sammelselg, V., et al., Applied Surface Science, 1998. **134**(1-4): p. 78-86.

23. Ylilammi, M., Thin Solid Films, 1996. **279**(1-2): p. 124-130.

24. Kolb, D.M., M. Przasnyski, and H. Gerisher, JEC, 1974. **54**: p. 25-38.

25. Kolb, D.M., *Physical and Electrochemcial Properties of Metal Monolayers on Metallic Substrates*, in *Advances in Electrochemistry and Electrochemical Engineering*, H. Gerischer and C.W. Tobias, Editors. 1978, John Wiley: New York. p. 125.

26. Juttner, K. and W.J. Lorenz, Z. Phys. Chem. N. F., 1980. **122**: p. 163.

27. Hubbard, A.T., et al., *Electrochemical surface characterization*, in *New Dimensions in Chemical Analysis*, B.L. Shapiro, Editor. 1985, Texas A & M University Press: College Station, Texas. p. 135.

28. Gewirth, A.A. and B.K. Niece, Chem. Rev., 1997. **97**: p. 1129-1162.

29. Colletti, L.P. and J.L. Stickney, Journal of the Electrochemical Society, 1998. **145**(10): p. 3594.

30. Flowers, J., Billy H., et al., Journal of Electroanalytical Chemistry, 2002. **524-525**: p. 273-285.

31. Wade, T.L., et al. *Formation of II-VI and III-V compound semiconductors by electrochemical ALE*. in *National Meeting of the Electrochemical Society, Spring*. 1999. Seattle, Washington: The Electrochemical Society.

32. Wade, T.L., et al. *Electrochemical Atomic Layer Eptitaxy: Electrodeposition of III-V and II-VI Compounds,*. in *Materials Research Society*. 2000: Materials Research Society.

33. Wade, T.L., et al., JEC, 2001. **500**: p. 322-332.

34. Wade, T.L., L.C. Ward, and J.L. Stickney, Chemistry of Materials, 1999.

35. Vaidyanathan, R., U. Happek, and J.L. Stickney, J. Appl. Phys., 2003. **in prep.**

36. Gregory, B.W., M.L. Norton, and J.L. Stickney, J. Electroanal. Chem., 1990. **293**: p. 85.

37. Gregory, B.W., D.W. Suggs, and J.L. Stickney, J. Electrochem. Soc., 1991. **138**: p. 1279.

38. Suggs, D.W., et al., Mat. Res. Soc. Symp. Proc., 1991. **222**: p. 283.

39. B.W. Gregory, D.W.S., J.L. Stickney, J. Electrochem. Soc., 1991. **138**: p. 1279.

40. Wade, T.L., T. Sorenson, A., and J.L. Stickney, *Epitaxial Compound Electrodeposition*, in *Interfacial Electrochemistry*, A. Wieckowski, Editor. 1999, Marcel Dekker: New York. p. 757-768.

41. Wade, T.L., et al. *Morphology control in the formation of compound semiconductors using electrochemical atomic layer epitaxy (EC-ALE)*. in *Electrochemical Society National Meeting*. 2001. Washington D.C.: Electrochemcial Society.

42. Colletti, L.P., B.H. Flowers, and J.L. Stickney, JECS, 1997.

43. JCG, 1998. **186**: p. 354 and 543.

43. T. E. Lister, and J. L. Stickney, *Appl. Surf. Sci*. **107** (1996) 153.

Figure 3.1: Cyclic voltammogram of Au electrode in 0.5 M Na_2SO_4, pH 4.

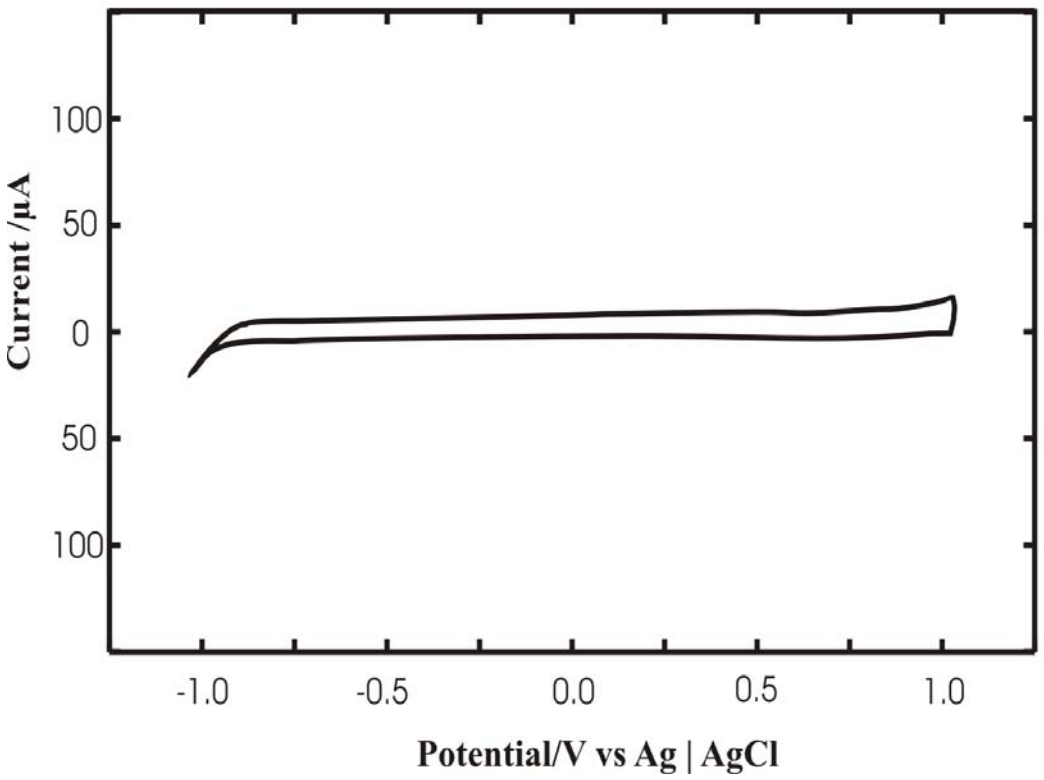

Figure 3.2 : Cyclic voltammogram of Au electrode in 0.2 mM $HTeO_2^+$, pH 4.

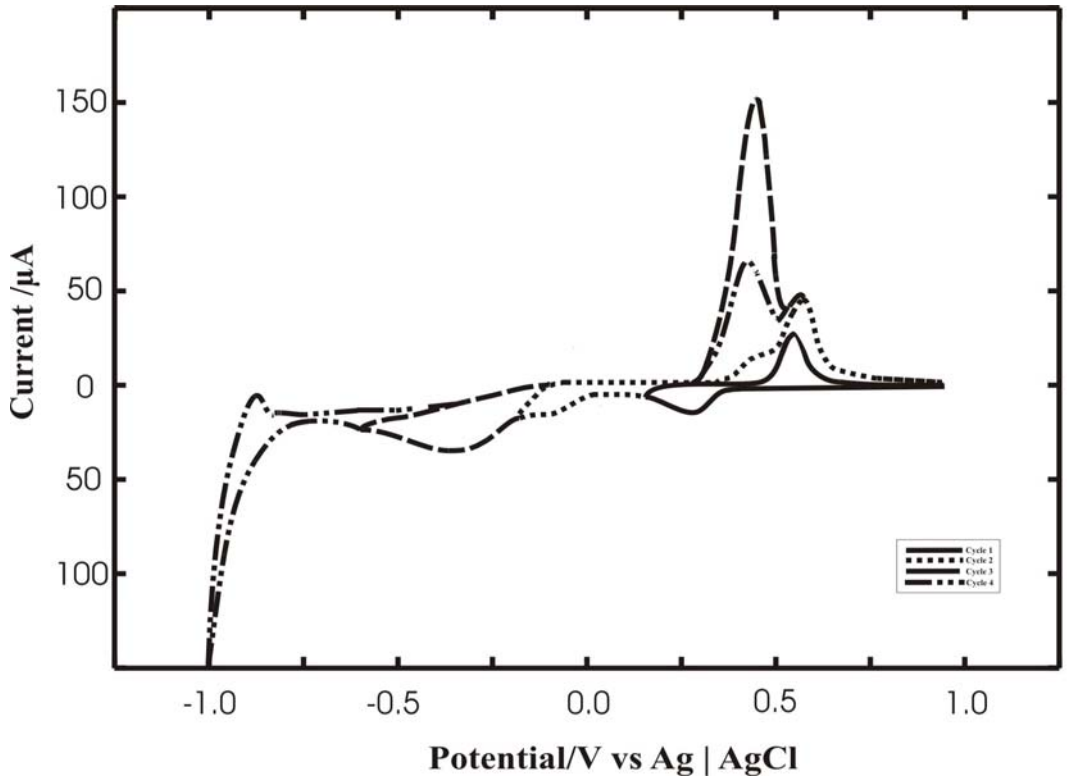

Figure 3.3 : Cyclic voltammogram of Au electrode in 0.5 mM Cd^{2+}, pH 5.

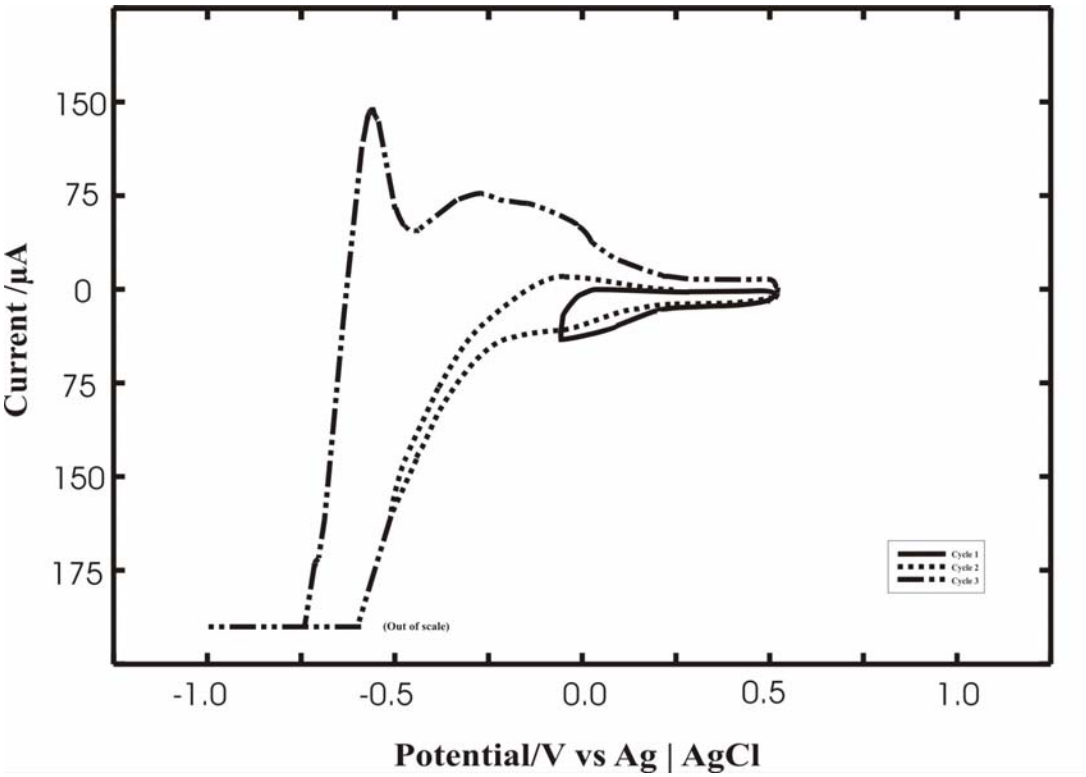

Figure 3.4 : Effect of Te deposition potential.

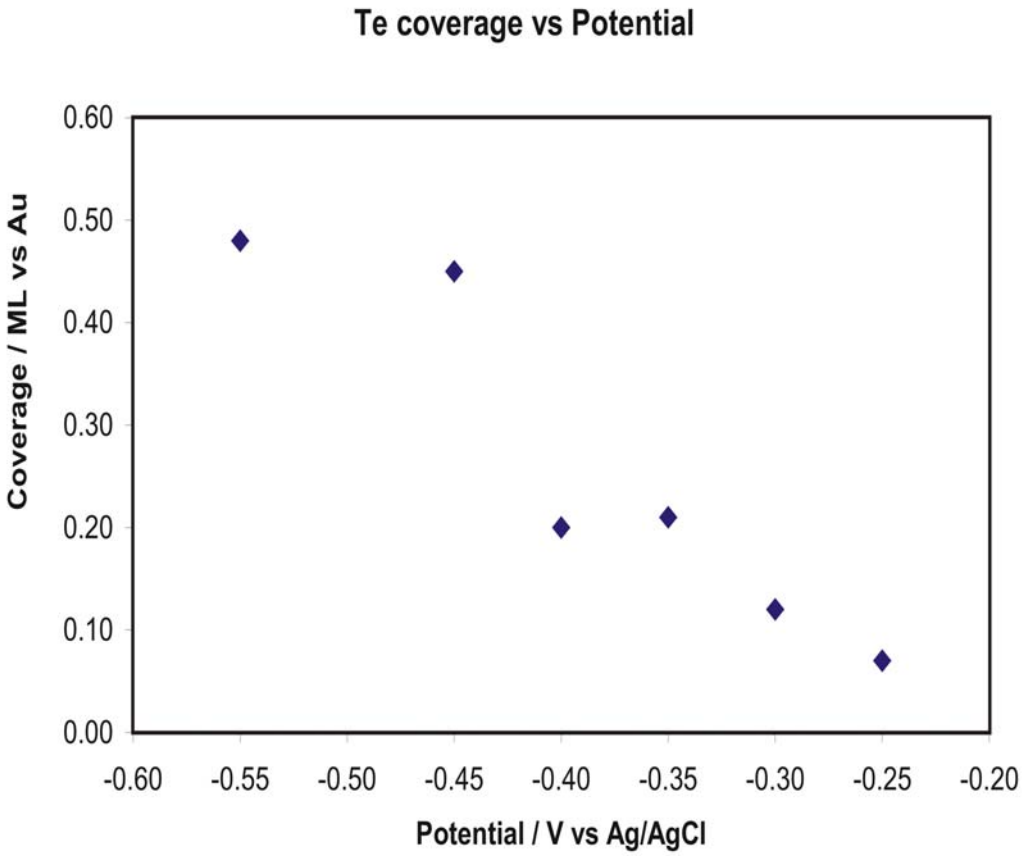

Figure 3.5 : Effect of Te stripping potential.

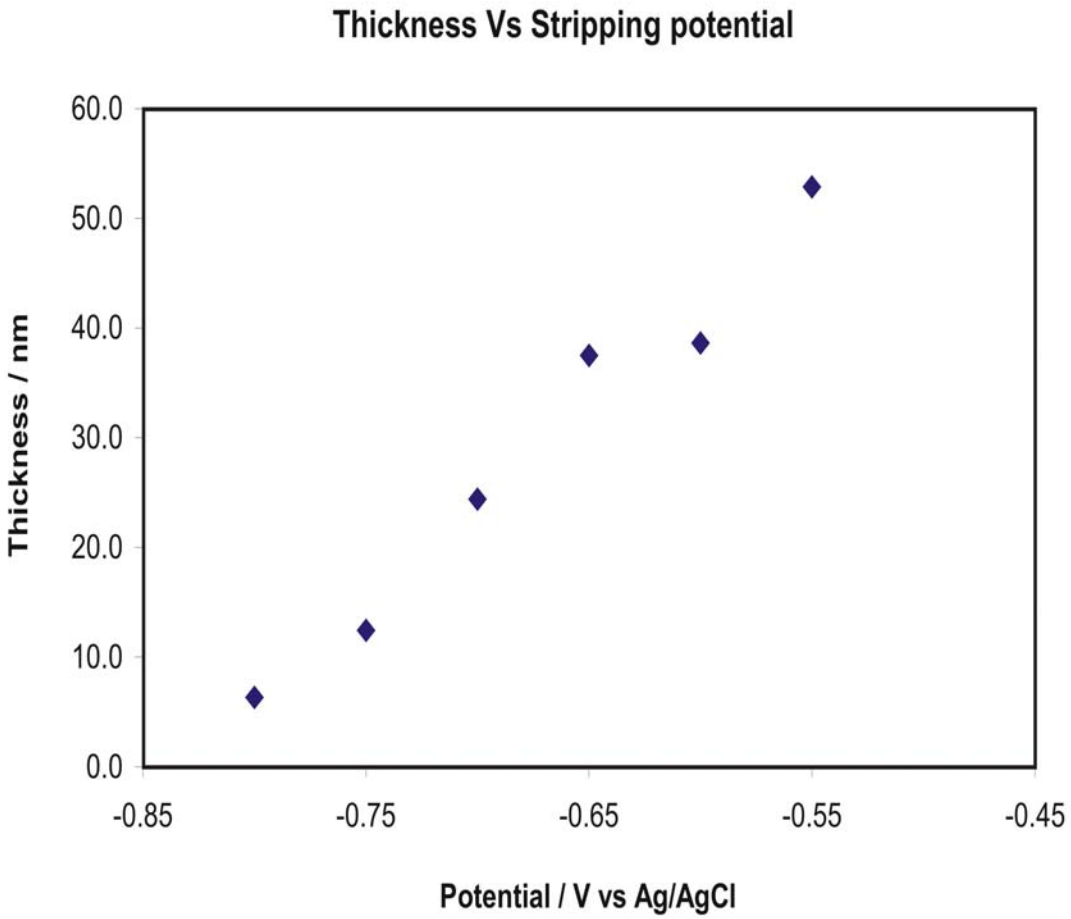

Figure 3.6 : Effect of Cd deposition potential.

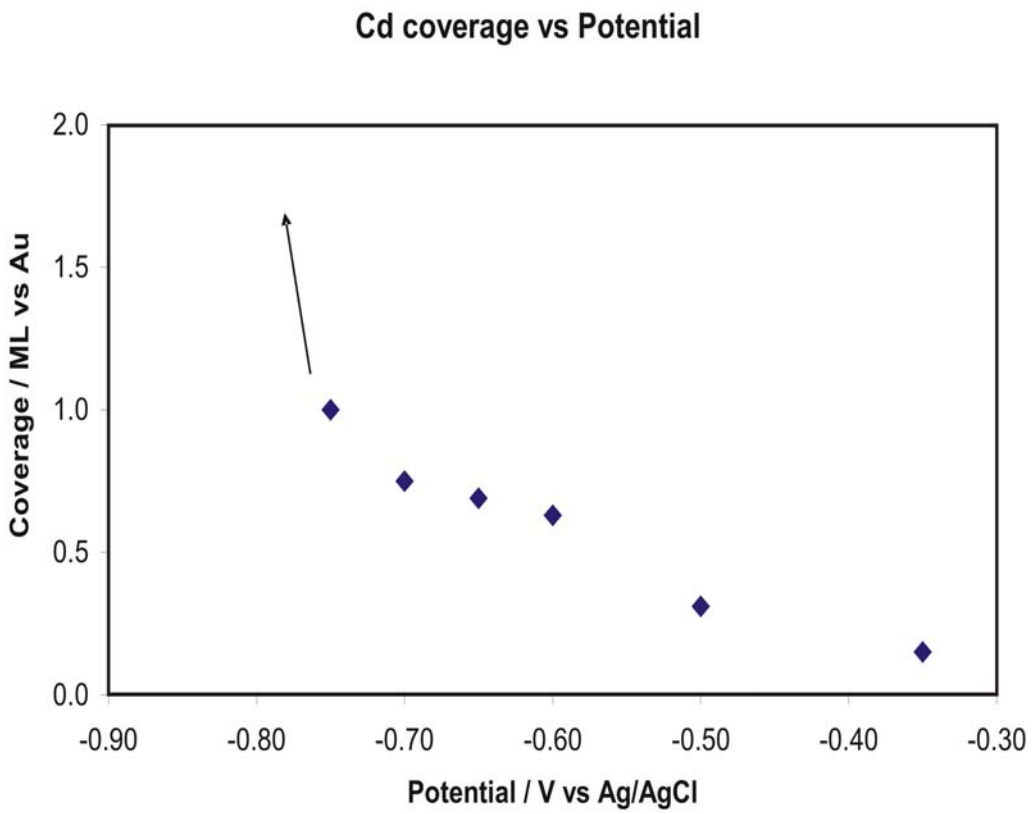

Figure 3.7 : Effect of Cd deposition potential on the deposit stoichiometry.

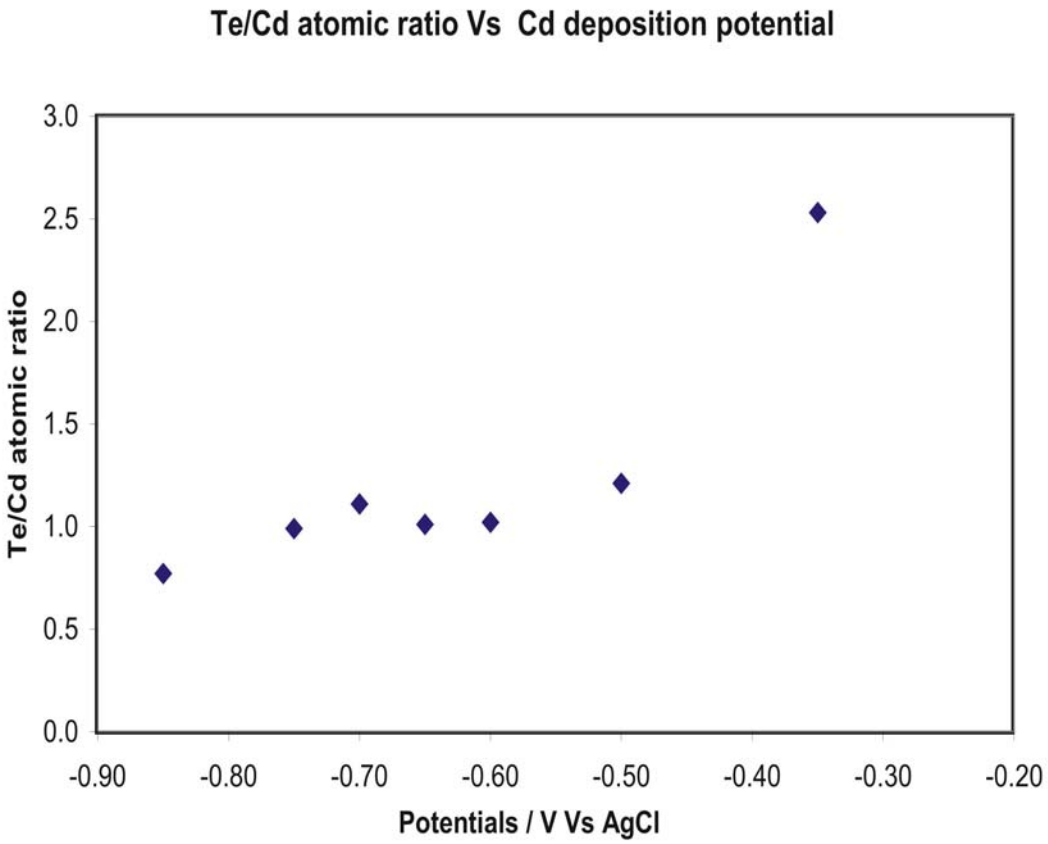

Figure 3.8 : Current-time profile during CdTe deposition using optimal deposition program.

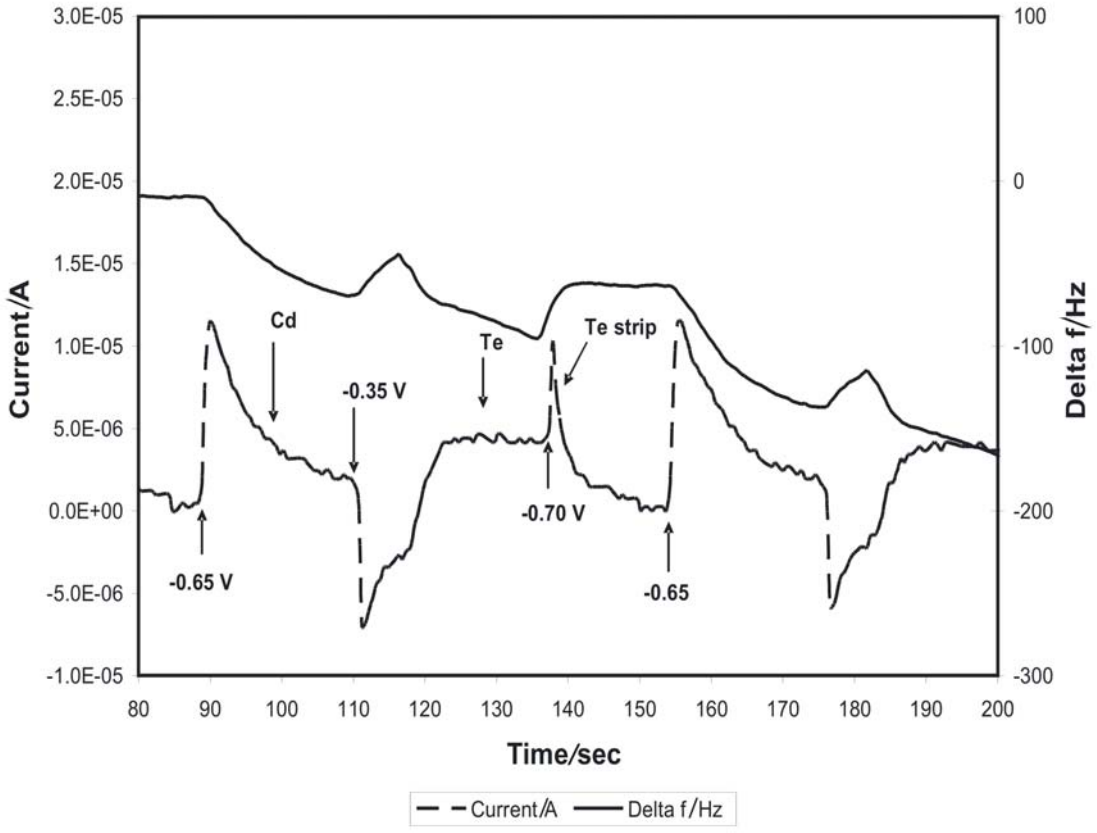

Figure 3.9 : Optimal deposition program

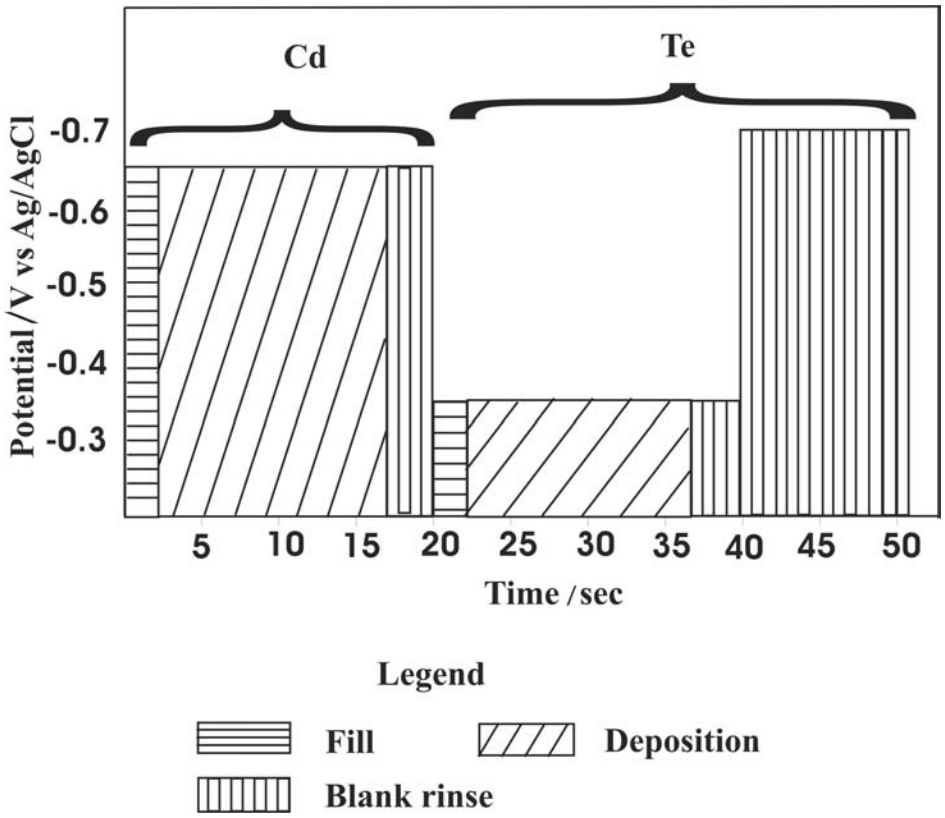

Figure 3.10 : XRD diffraction pattern of 200 cycle CdTe thin film.

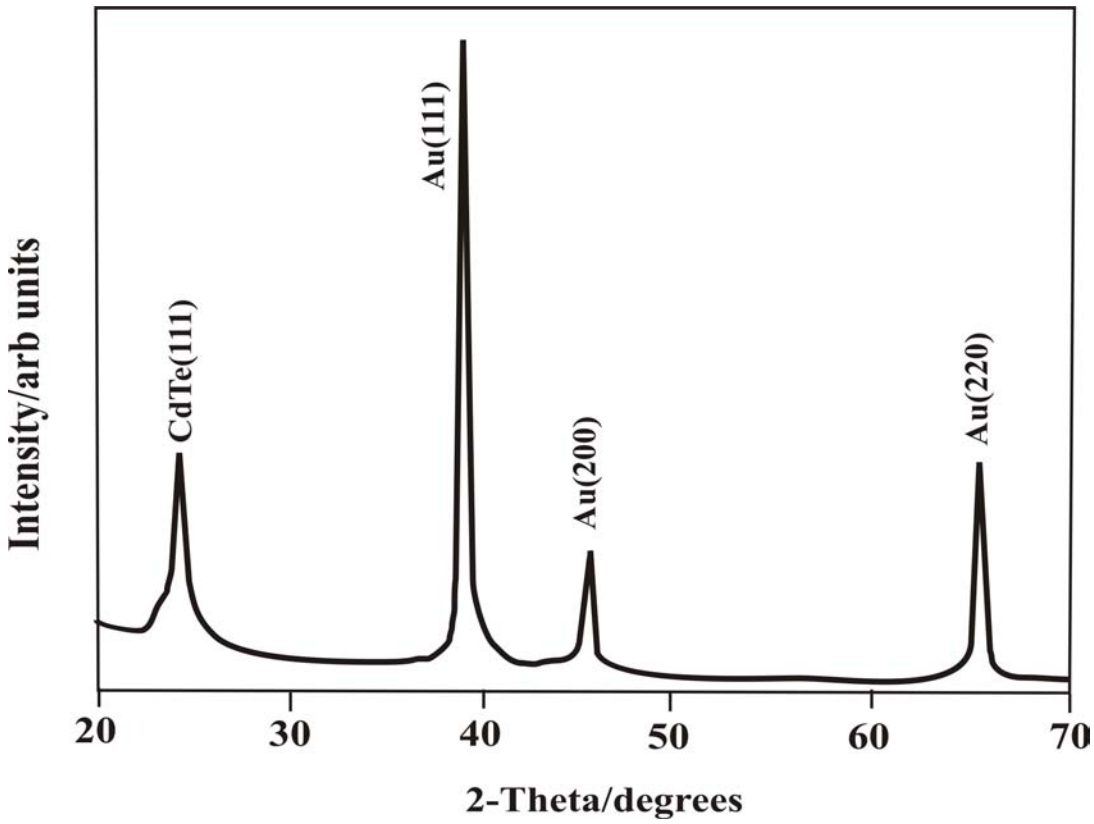

Figure 3.11: Absorption spectrum of 200 cycle CdTe thin film.

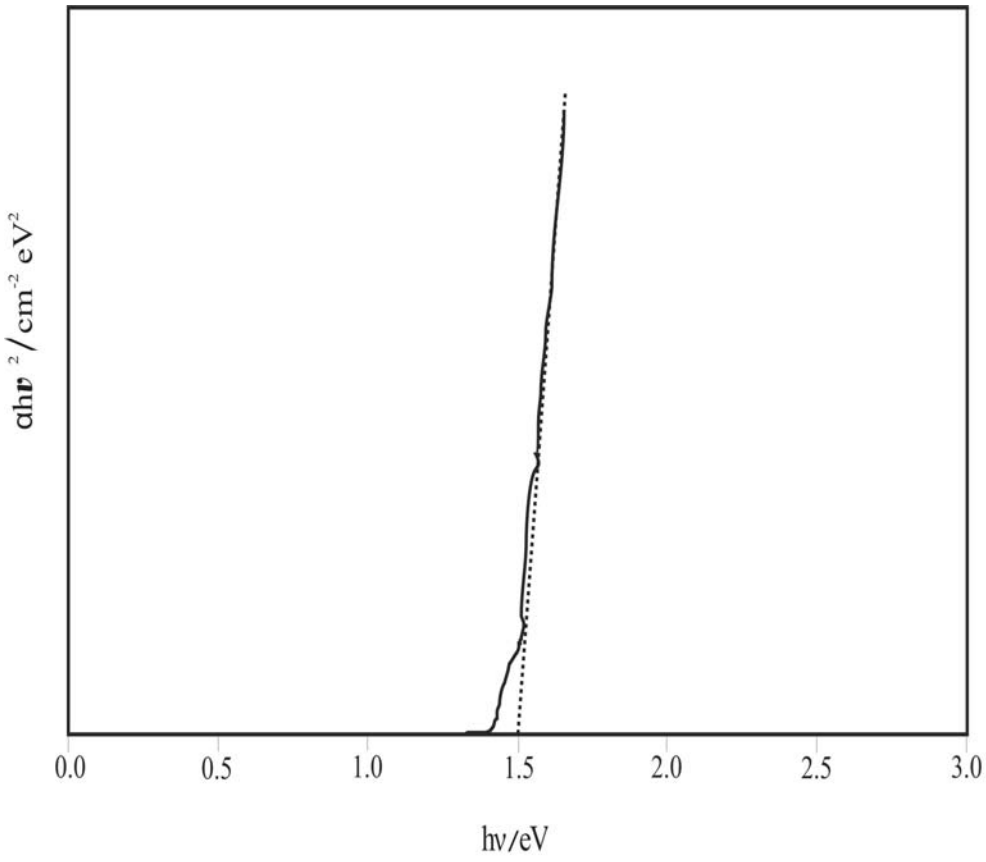

CHAPTER 4

DEPOSITION OF HGTE BY ELECTROCHEMICAL ATOMIC LAYER EPITAXY (EC-ALE)[1]

[1] Venkatasamy, V., et al., Journal of Electroanalytical chemistry, 2006. **589**(2): p. 195-202 (Used by permission).

Abstract

This paper describes the first instance of HgTe growth by electrochemical atomic layer epitaxy (EC-ALE). EC-ALE is the electrochemical analog of atomic layer epitaxy (ALE) and atomic layer deposition (ALD), all of which are based on the growth of materials a monolayer at a time, using surface limited reactions. The number of such cycles then determines the thickness of the resulting deposit. This study describes attempts to optimize an EC-ALE cycle for the growth of HgTe. The effect of changes in the deposition potentials for Hg and Te are studied, as well as that used to strip excess Te. All depositions took place in an automated electrochemical flow cell deposition system, so that potentials and solutions could be repeatedly changed on the fly. Based on these studies, the best deposits were formed using Hg and Te deposition potentials of 0.40 V and -0.35 V, respectively, and using a Te stripping potential of -0.70 V. Ellipsometric measurements of 100 cycle deposits formed using these conditions showed a film thickness of 71.9 nm, about twice that expected, based on the view that each cycle should result in one HgTe compound monolayer. Electron probe microanalysis (EPMA) of the deposit indicated a Te/Hg atomic ratio of 1.02, the expected stoichiometry for the deposit. Electrochemical quartz crystal microbalance (EQCM) studies of this cycle, also using an automated flow cell, indicated that some deposited Te was stripped at the potential used to deposit Hg. X-ray diffraction studies showed the deposits to grow in a strongly (111) orientation. Room temperature IR absorption studies of HgTe indicated a negative bandgap, -0.20 eV.

Keywords: HgTe; EC-ALE; EQCM; EPMA; Ellipsometry; IR detectors; XRD

Introduction

Mercury telluride, HgTe, is a II-VI compound, which has gained importance for its use in the development of Mer Cad Tel ($Hg_{(1-x)}Cd_xTe$) IR detector material [1-5]. HgTe is a semi metal with a negative band gap, -0.14 eV at 300 K [6]. Incorporation of Cd into this matrix results in a bandgap anywhere between -0.15 eV to 1.6 eV, bandgap engineering, making it a very desirable detector material. HgTe has been formed by ALE [7], flash evaporation [8] and electrodeposition [34]. Seyam and Elfalaky synthesized p-type HgTe with a bandgap between 0.02-0.3 eV [8]. Optical properties of HgTe, formed by MBE, have been the subject of several papers [9, 10].

Electrochemical atomic layer epitaxy (EC-ALE) is the electrochemical analog of atomic layer epitaxy (ALE) [11-13] and atomic layer deposition (ALD) [14-17], both of which are gas or vacuum phase thin film formation techniques based on deposition one atomic layer at a time, using surface limited reactions. Underpotential deposition (UPD), is used in EC-ALE to achieve atomic layer by atomic layer growth [18-22]. UPD is the deposition of one element on a second at a potential prior to that needed to deposit the element on itself, the result of the free energy of compound formation between the depositing element and the terminating element of the deposit surface.

A number of II-VI [23-25] and III-V [26-28] compound semiconductors have been successfully deposited by EC-ALE. The use of separately optimized precursor solutions for each of the depositing elements, as well as separate deposition potentials, times etc., has proven to be very important for the successful deposition of a wide variety of materials. EC-ALE has recently been applied to the deposition of metals, layer by layer, using redox replacement of an atomic (UPD) layer of a more reactive metal by a more noble metal.

This paper is the first report of the deposition of HgTe by EC-ALE. All depositions were performed in an automated flow deposition system [29-31]. The dependence of the HgTe deposit structure and composition on the potentials for Hg and Te, as well as the Te reductive stripping potential, was investigated. Studies were performed using ellipsometry, optical microscopy, X-ray diffraction (XRD), electron probe micro analysis (EPMA) and Fourier transform infrared spectroscopy (FTIR). Optimal conditions obtained were further studied using an electrochemical quartz crystal microbalance (EQCM) flow cell to better understand the deposition process.

Experimental

The electrochemical flow deposition system used for these studies has been previously described [29-31]. Pump heads, valves and tubing were confined inside a nitrogen purged Plexiglas box to limit oxygen, which affects deposit quality. The electrochemical cell consists of a thin-layer design to promote laminar flow. The auxiliary electrode was an ITO glass slide (Delta Technologies, Ltd., Stillwater MN), and the reference electrode was Ag/AgCl (3 M NaCl) (Bioanalytical Systems, Inc., West Lafayette, IN). Substrates consisted of 300 nm thick gold films on glass. The substrates were annealed at 400^{o}C for 12 hours under a vacuum of 10^{-6} Torr, after Au vapor deposition, resulting in a (111) habit. The working and auxiliary electrodes were held apart by a 2 mm thick silicon rubber gasket, which defined a 1x3 cm^2 rectangular opening where deposition took place. The ITO auxiliary was transparent, allowing deposition to be followed visually. The reference electrode, Ag/AgCl (3M NaCl) was positioned at the cavity outlet.

The solutions used were 0.2 mM HgO, pH 2 and 0.2 mM TeO_2, pH 4, and both contained 0.5 M Na_2SO_4. The blank solution contained only the 0.5 M Na_2SO_4, at pH 4. Solution pH was adjusted using H_2SO_4. Water used for solutions was supplied from a Nanopure water filtration

system (Barnstead, Dubuque, IA) attached to the house DI water system. Chemicals were reagent grade or better.

The basic EC-ALE cycle used to deposit HgTe was as follows: the Te solution was flushed into the cell for 2 s (40 mL/min), and held quiescent for 15 s, all at the potential chosen for Te deposition. Blank solution was then flushed through the cell for 3 s. This was followed by filling the cell with the Hg solution for 2 s, and holding quiescent for 15 s for deposition. The cycle was then completed by flushing with blank for 3 s. For the majority of the deposits discussed here, this cycle was repeated 100 times.

Deposit thickness was monitored using a single wavelength ellipsometer (Sentech SE 400). A Scintag PAD-V diffractometer with CuKα radiation (λ= 1.5418 A), was used to obtain glancing angle X-ray diffraction patterns. Electron probe microanalysis (EPMA) was run on a Joel 8600 wavelength dispersive scanning electron microprobe. Glancing angle absorption measurements were performed, using an FTIR spectrophotometer (Bruker FTS-66v, Bruker optics, Inc.).

Optimal deposition conditions were studied using a flow cell based electrochemical quartz crystal microbalance (EQCM). A 9 MHz AT-cut quartz crystal (Seiko EG&G) was used, where both sides were coated with circular Au electrodes (ca. 0.2 cm^2, 5 mm in diameter). The electrodes were formed with 50 nm of Ti, followed by 300 nm of sputtered Au. Calibration of the EQCM was carried out using Ag electrodeposition coulometry.

Results and Discussions

The deposition potentials initially chosen for Hg and Te, and used in the first EC-ALE cycle, were obtained from cyclic voltammetric data for Au electrodes in the Hg and Te solutions. The use of upd potentials obtained from cyclic voltammetry on Au must be considered a first

approximation, as the potential needed to form atomic layer on the growing deposit generally differ from those on the substrate. However, values for UPD on Au provide a set of potentials for an initial cycle.

The voltammetric behavior of Hg^{2+} on gold on glass electrodes is shown in Figure 1. The Hg scan was started at 0.95 V in the cathodic direction. Two distinct reduction peaks were observed at potentials of 0.45 V and 0.30 V. These correspond to upd and bulk reduction features of Hg^{2+}, respectively. Corresponding stripping features for bulk and UPD Hg occurred at 0.42 V and 0.55 V, respectively (dotted curve in Figure 1). It is interesting to note, that as the potential was scanned negative of 0.30 V, no further increase in the bulk Hg oxidation feature (0.42 V) was observed. However, a new peak between 0.70 and 0.75 V did appear, and grew as the negative limit for the scan decreased. It is well known that Hg forms amalgams with Au, and present results (Figure1) suggest that most of the additional Hg, deposited below 0.30 V, went subsurface, forming a surface amalgam. Stripping this surface amalgam then required a more positive potential than that for Hg UPD stripping, accounting for the most positive oxidation peak and its growth.

The voltammetry of a gold on glass substrate in the 0.2 mM $HTeO_2^+$, pH 4, solution is shown in Figure 2. The cathodic Te scan was started at 0.95 V and displayed $HTeO_2^+$ reduction peaks at -0.35 V, -0.10 V and 0.28 V, corresponding to the bulk, upd (I) and upd (II) peaks respectively. Further scanning in the cathodic direction resulted in hydrogen evolution below -0.80 V, as well as the reduction of some bulk Te to a telluride species such as HTe^-. During subsequent anodic scans, peaks at -0.75 V, 0.42 V and 0.55 V were evident, which correspond respectively to HTe^- oxidation, bulk and upd stripping.

The preliminary EC-ALE cycle, designed to deposit HgTe, was constructed as follows: the Te solution was rinsed into the cell for 2 s at 0.20 V, at which point the solution was held without flowing, quiescent, for 15 sec to deposit the Te atomic layer. In order to avoid co-deposition of HgTe by mixing Hg^{2+} and $HTeO_2^+$ ions in the cell, a blank rinse step, at 0.20 V, was used to flush the Te solution before introduction of the Hg solution. This was followed by a 2 s rinse with the Hg solution and 15 sec quiescent deposition at 0.48 V. The cycle was completed by rinsing again with the blank solution, to conclude one EC-ALE cycle. In general, in this study, deposits were formed using 100 cycles.

The above cycle, however, resulted in no observable deposit. From plots of the current vs. time during the 100 cycles, a lack of Te deposited was evident, which is understandable given the slow kinetics for Te deposition, evident by the overpotential needed to deposit Te (Figure 3) [32]. If an overpotential was used for Te deposition, the Te formed usually consisted of both bulk and UPD components, resulting in more Te than desired. The problems associated with deposition of both bulk and UPD can be minimized by using a short deposition time, as the surface limited reaction (UPD) is significantly faster than bulk deposition, and bulk deposition must, by definition, commence only on top of UPD. In the present study after the first deposits did not work, the deposition potential and time were optimized to achieve Te deposition and minimize bulk Te formation. However, some bulk Te was still present, motivating the inclusion of an extra step in which excess, or bulk, Te was reductively stripped at a more negative potential in a blank solution, leaving only an atomic layer of Te [32].

Changes to the existing EC-ALE cycle involved use of a more negative Te deposition potential, and use of the above mentioned Te stripping step to remove any bulk Te remaining. The stripping step involved rinsing the deposit at -0.70 V for 3 s in the blank solution, after the

Te deposition step. Bulk Te was reduced to HTe^-, a soluble species that was rinsed away with the blank.

To optimize the deposition of Te, a series of experiments were performed where the deposition potential of Te was varied from -0.25 V to -0.60 V while maintaining the deposition potential for Hg at 0.40 V and the Te stripping potential at -0.70 V. The resulting deposits were analyzed by coulometry, optical microscopy and EPMA. The coulomteric results (Figure 3) indicated that the deposition of Te did not start until a potential of -0.30 V was used, which again points out the slow kinetics for Te deposition (0.6 V negative of the formal potential for $HTeO_2^+$ reduction). The graph shows a plateau region between -0.35 V and -0.55 V, where the ML coverage for Te deposition was nearly constant while the potential was shifted negative. A monolayer (ML) is a unit of coverage defined in surface science as one adsorbate atom for every surface atom. Annealed gold on glass was used as substrate, which generally shows a strongly preferred (111) oriented growth habit. Thus for the present study, a monolayer was defined assuming the surface to be (111), with a roughness factor of 1. The actual surface will not be completely (111) or atomically flat, however, the errors associated with these factors are in opposite directions, minimizing problems. Based on EPMA, optical microscopy and coulometry, -0.35 V was chosen as the best deposition potential for Te.

A similar approach was taken for finding the best Te stripping potential. So the Hg and Te deposition potentials were maintained at 0.40 V and -0.35 V respectively and the Te stripping potential was varied from -0.35 to -0.95 V. As the deposit thickness was an indirect measure of the amount of Te deposited, and thus an indication of the amount of Te being stripped, the resulting deposits were analyzed by a single wavelength ellipsometer to follow the effect of the stripping step. EPMA and optical microscopy were also performed to determine deposit

stoichiometry and morphology, respectively. Figure 4 shows the dependence of deposit thickness on the Te stripping potential. At the more negative potentials, such as -0.95 V, essentially no deposit was observed, as all the Te (including UPD Te) was stripped. Correspondingly, potentials positive of the telluride reduction potential had little effect on the deposit thickness. Based on optical microscopy and EPMA data for the deposit stoichiometry, -0.70 V was chosen as the stripping potential, even though the deposit thickness was considerably higher than the ideal deposit thickness (71.9 nm vs. 37.4 nm). The optimal thickness for a 100 cycle deposit is based on the assumption of one Hg-Te bi-layer growing each cycle with the (111) orientation of a zinc blende crystal structure, which should be 37.4 nm.

A possible reason for the excess thickness could be the redox replacement of the deposited Te by Hg ions. It is well known that more active species are oxidized by and exchanged for more noble species, in a redox replacement reaction. Since Hg is nobler than Te, it is possible that some Te was exchanged for Hg. The extra Hg would then react with more Te. Another possibility is that the extra thickness is inherent in the growth of HgTe, and the simple model of one Hg-Te bilayer is faulty. To address this question, an electrochemical quartz crystal microbalance (EQCM) flow cell system was used, and the results will be discussed below.

To obtain the ideal deposition potential for Hg, a potential dependence study was performed by keeping the Te deposition and stripping potentials constant at -0.35 V and -0.70 V, respectively (Figure 5). The nature of the deposition of Hg is intriguing, as a typical S shaped curve is evident in Figure 5. The figure is based on coulometry for the deposition of Hg, as a function of the potential used for Hg deposition. What is intriguing is that at more positive potentials, oxidative currents were observed, not reductions. The negative coverages observed for Hg could probably be due to the simultaneous oxidation of Te at Hg deposition potentials.

Further discussions on this topic are given below. There is a plateau in the graph, between 0.40 and 0.52 V, but the coverage relating to the plateau corresponds to a coverage of essentially 0 ML. However, based on EPMA results and optical microscopy observations of the deposits, 0.40 V was chosen for Hg deposition.

The following EC-ALE cycle was then chosen (Figure 6) based on the above mentioned studies: Te solution was rinsed into the cell for 2 s at -0.35 V, and the solution then held static for 15 s, for deposition. The cell was then flushed with blank solution for 3 s at -0.35 V, at which point, the potential was then changed to -0.70 V for 3 s. After which, Hg solution was flushed through the cell for 2 s, and held static for 15 s at 0.40, to deposit. This was followed by another blank rinse at 0.40 V for 3 s.

As noted above, questions concerning this cycle and the deposition mechanism were investigated using an EQCM (Electrochemical quartz crystal microbalance) flow cell. Some aspects of the deposition process in the EQCM flow cell differed from those in the standard flow cell hardware used for the majority of the studies here. For instance, experience showed that the EQCM flow cell worked best if solution was continuously flowed through the cell, no static deposition was used, however a much lower flow rate was used (6 mL/min). Overall, use of continuous flow in the EQCM did not appear to significantly change the resulting deposit. The optimal EC-ALE program was repeated for 5 cycles, with the fifth cycle shown in Figure 7. The cycle to cycle variations were minimal and predictable, allowing conclusions to be drawn concerning the changes in mass between cycles. However, within a cycle, variations in frequency were function of a number of variables besides the masses of electrodeposited atomic layers. For instance, reversibly adsorbed electrolyte may increase, upon adsorption, or decrease, upon desorption, the observed mass changes in a given solution. This forces statements

concerning mass changes observed within a cycle to be educated guesses. On the other hand, mass changes from the same points in one cycle to the next are an accurate measure of the mass change for a cycle.

The results shown in Figure 7 indicate a Te coverage of 2.62 ML from mass and 1.79 ML from coulometry. The Hg coverage was 2.18 ML and -0.39 ML from mass and charge respectively. The negative Hg coverage, based on charge (Figure 5), indicates that a net oxidative charge was passed during Hg deposition. The question is then what is being oxidized if Hg^{2+} ions are being reduced? Given the voltammetry for Te (Figure 2), it is clear that Te may be vulnerable to oxidation at such a positive potential. This then leads to the question of a redox replacement reaction, where deposited Te is traded for Hg at this potential. An experiment devised to investigate this question involved first deposition of three cycles of HgTe, followed by a blank rinse for 17 s at the Hg deposition potential (0.40 V). An oxidation current was observed (Figure 8), which appears to indicate that Te was being oxidized in the absences of Hg^{2+} ions, as there was nothing else in the solution to oxidize. It was also important to determine the length of time required to oxidize all of the excess Te at Hg deposition potential. So, again the same experiment was performed, but instead of flowing blank for 17 s, a 10 minute rinse was performed (Figure 9), which suggests that it takes about 3 minutes to strip excess Te from the deposit surface. The net Te coverage was 0.42 ML, on top of the previously deposited Hg layer, very close to the ideal Te coverage of 0.44 ML. From previous studies on CdSe it was found that the formation of one CdSe bi-layer from the (111) plane of zinc blende CdSe would require 0.44 ML of Cd and 0.44 ML of Se [33]. This is a good approximation of the CdTe, and HgTe in the present case.

The next question is whether Hg^{2+} was replacing Te by a redox replacement reaction. In order to study this problem, three cycles of HgTe were deposited using the deposition program, followed by rinsing with the Hg^{2+} solution for 1 minute at open circuit (Figure 10). The mass of the electrode appeared to have increased but not enough to suggest a redox replacement of Te taking place. If there was an actual replacement taking place then the deposited Te would be oxidizing into $HTeO_2^+$, giving out four electrons to Hg^{2+} ions to deposit. So for every Te atom being oxidized, two Hg atoms would be reducing. The mass change in terms of frequency change of the quartz crystal for this reaction would be around 537.8 Hz. This kind of mass change was not observed by the EQCM experiment (137.0 Hz). Moreover, a 3 s blank rinse after the open circuit Hg solution rinse resulted in a corresponding decrease in electrode mass, suggesting desorption of adsorbed Hg ions. These results suggest that Te was not replaced by Hg at open circuit.

Presently, it is proposed that as Hg is electrochemically reduced on the excess of Te, some Te is simultaneously oxidized. The net current, essentially zero, is thus the sum of that for the reduction of Hg^{2+} ions and for the oxidation of excess Te. Given the above results with the EQCM, where no net replacement of Te was observed at open circuit in the presences of the Hg^{2+} ions, it appears that the deposition of Hg catalyzes the oxidation of Te. If it is assumed that Hg is mobile, and will penetrate into the Te layer, extending the HgTe crystal, this should change the bonding of the adjacent layer of Te, possibly making it more reactive, and promoting its oxidation.

Ellipsometric measurements of 100 cycle deposits formed using this program indicate that the film was 71.9 nm thick. EPMA of the deposit indicated a Te/Hg atomic ratio of 1.02. Figure 11, shows the X-ray diffraction pattern for the deposit. Peaks corresponding to (111),

(220) and (311) planes of HgTe (JCPDS 8-469) were evident, and no elemental peaks for Hg and Te were observed. The deposit, however, showed a strongly predominant (111) orientation. Room temperature IR absorption studies of HgTe were performed using a glancing angle of 85^{o} from the surface normal. Figure 12 displays a plot of the square of the absorption data vs. energy for the 100 cycle HgTe deposit. An absorption edge was found around -0.20 eV. Much like HgSe, HgTe is also a semimetal, with a negative energy gap. Theoretically, the value of the fundamental energy gap for HgTe is -0.14 eV at 300 K [6].

Conclusion

The dependence of nanofilms of HgTe grown using EC-ALE on the deposition potentials used for Hg and Te, as well as that used for a reductive Te stripping step, has been reported. The optimal deposition cycle devised included deposition of Hg at 0.40 V, deposition of Te at -0.35 V and, stripping of excess Te at -0.70 V. The resulting 100 cycle deposit was 71.9 nm thick, more than that expected from the ideal model of one compound monolayer for each cycle, but the deposit was stoichometric, and showed a strong preferential (111) orientation. The absorption spectrum for this deposit suggested a negative band gap of 0.20 eV, consistent with the literature. Studies using an EQCM flow cell helped in understanding the deposition process. It was observed that some of the Te each cycle was oxidatively stripped upon switching the potential from the Te deposition potential of -0.35V to that for Hg deposition, 0.40V. In addition, it also appeared that Te was not exchanged for Hg. However, the net result was a high quality nanodeposit of stoichiometric HgTe.

Acknowledgements

The authors acknowledge the support of NSF divisions of Material Science and Chemistry.

References

1. Hetzler, S.R., et al., Appl. Phys. Lett., 1985. **47**: p. 260.
2. Guldner, Y., et al., Phys. Rev. Lett., 1983. **51**: p. 907.
3. Meyer, J.R., et al., Journal of Crystal Growth, 1994. **138**(1-4): p. 981-987.
4. Schulman, J.N., Journal of Crystal Growth, 1990. **86**(1-4): p. 25-27.
5. Voos, M., Surface Science Reports, 1987. **7**(5): p. 189-209.
6. Hansen.G.L and Schmit.J.L, J. Appl. Phys, 1983. **54**(3).
7. Karam, N.H., et al., Thin Solid Films, 1993. **225**(1-2): p. 261.
8. Seyam, M.A.M. and A. Elfalaky, Vacuum, 2000. **57**: p. 31 - 41.
9. Janowitz, C., et al., Journal of Alloys and Compounds, 2001. **328**(1-2): p. 84-89.
10. Banouni, M., M. Nasser, and G. Leveque, Journal of Crystal Growth, 1996. **159**(1-4): p. 736-740.
11. Bedair, S., ed. *Atomic Layer Epitaxy*. 1993, Elsevier: Amsterdam. 304.
12. Kuech, T.F., P.D. Dapkus, and Y. Aoyagi, *Atomic Layer Growth and Processing*. Vol. 222. 1991, Pittsburgh: Materials Research Society. 360.
13. Goodman, C.H.L. and M.V. Pessa, JAP, 1986. **60**: p. R65.
14. Yousfi, E.B., et al., Thin Solid Films, 2001. **387**(1-2): p. 29-32.
15. Sammelselg, V., et al., Applied Surface Science, 1998. **134**(1-4): p. 78-86.
16. Ylilammi, M., Thin Solid Films, 1996. **279**(1-2): p. 124-130.
17. Leskela, M. and M. Ritala, Thin Solid Films, 2002. **409**(1): p. 138-146.
18. Kolb, D.M., M. Przasnyski, and H. Gerisher, JEC, 1974. **54**: p. 25-38.

19. Kolb, D.M., *Physical and Electrochemcial Properties of Metal Monolayers on Metallic Substrates*, in *Advances in Electrochemistry and Electrochemical Engineering*, H. Gerischer and C.W. Tobias, Editors. 1978, John Wiley: New York. p. 125.

20. Juttner, K. and W.J. Lorenz, Z. Phys. Chem. N. F., 1980. **122**: p. 163.

21. Hubbard, A.T., et al., *Electrochemical surface characterization*, in *New Dimensions in Chemical Analysis*, B.L. Shapiro, Editor. 1985, Texas A & M University Press: College Station, Texas. p. 135.

22. Gewirth, A.A. and B.K. Niece, Chem. Rev., 1997. **97**: p. 1129-1162.

23. Colletti, L.P. and J.L. Stickney, Journal of the Electrochemical Society, 1998. **145**(10): p. 3594.

24. Flowers, J., Billy H., et al., Journal of Electroanalytical Chemistry, 2002. **524-525**: p. 273-285.

25. Wade, T.L., et al. *Formation of II-VI and III-V compound semiconductors by electrochemical ALE*. in *National Meeting of the Electrochemical Society, Spring*. 1999. Seattle, Washington: The Electrochemical Society.

26. Wade, T.L., et al., Electrochemical and Solid State Letters, 1999. **2**(12): p. 616.

27. Wade, T.L., et al. *Electrochemical Atomic Layer Eptitaxy: Electrodeposition of III-V and II-VI Compounds,*. in *Materials Research Society*. 2000: Materials Research Society.

28. Wade, T.L., et al., JEC, 2001. **500**: p. 322-332.

29. Stickney, J.L., *Electrochemical atomic layer epitaxy*, in *Electroanalytical Chemistry*, A.J. Bard and I. Rubenstein, Editors. 1999, Marcel Dekker: New York. p. 75-211.

30. Wade, T.L., T. Sorenson, A., and J.L. Stickney, *Epitaxial Compound Electrodeposition*, in *Interfacial Electrochemistry*, A. Wieckowski, Editor. 1999, Marcel Dekker: New York. p. 757-768.

31. Wade, T.L., et al. *Morphology control in the formation of compound semiconductors using electrochemical atomic layer epitaxy (EC-ALE)*. in *Electrochemical Society National Meeting*. 2001. Washington D.C.: Electrochemcial Society.

32. Colletti, L.P., B.H. Flowers, and J.L. Stickney, JECS, 1997.

33. Lister, T.E. and J.L. Stickney, Applied Surface Science, 1996. **107**: p. 153.

Figure 4.1 : Cyclic voltammogram of Au electrode in 0.5 mM Hg^{2+}, pH 2.

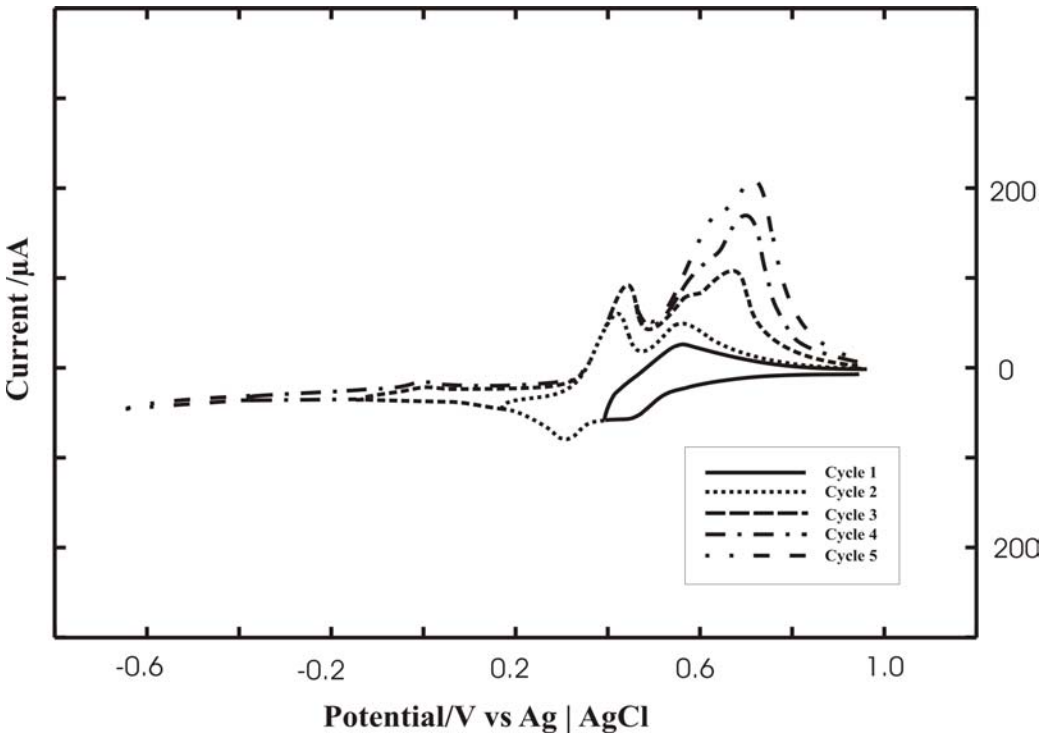

Figure 4.2 : Cyclic voltammogram of Au electrode in 0.2 mM $HTeO_2^+$, pH 4.

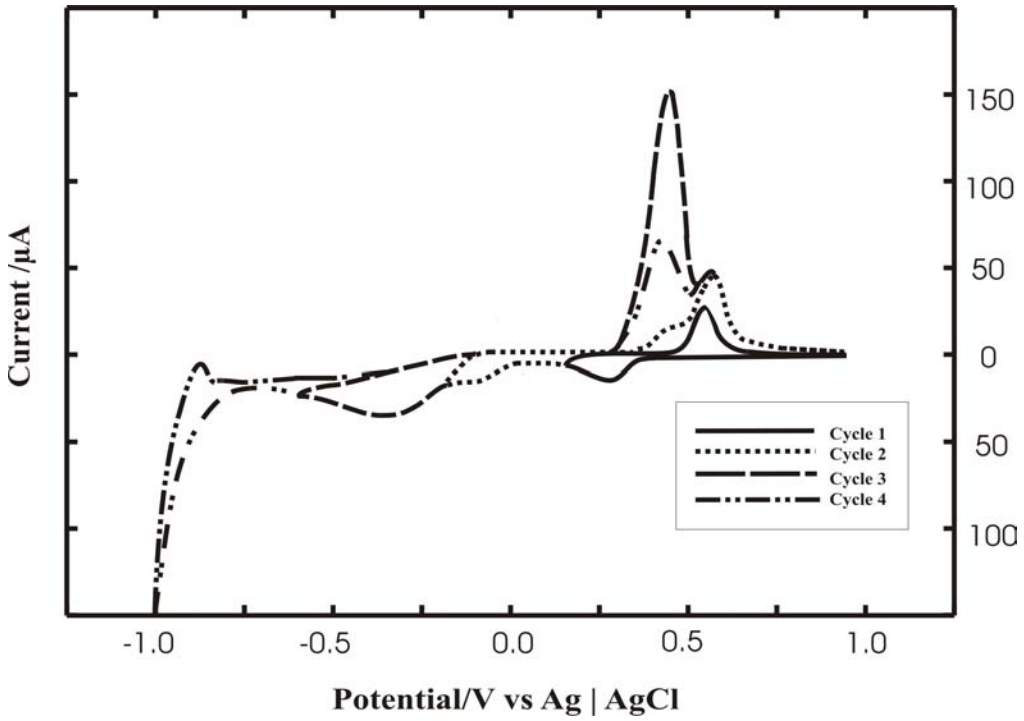

Figure 4.3 : Effect of Te deposition potential on 100 cycle deposits.

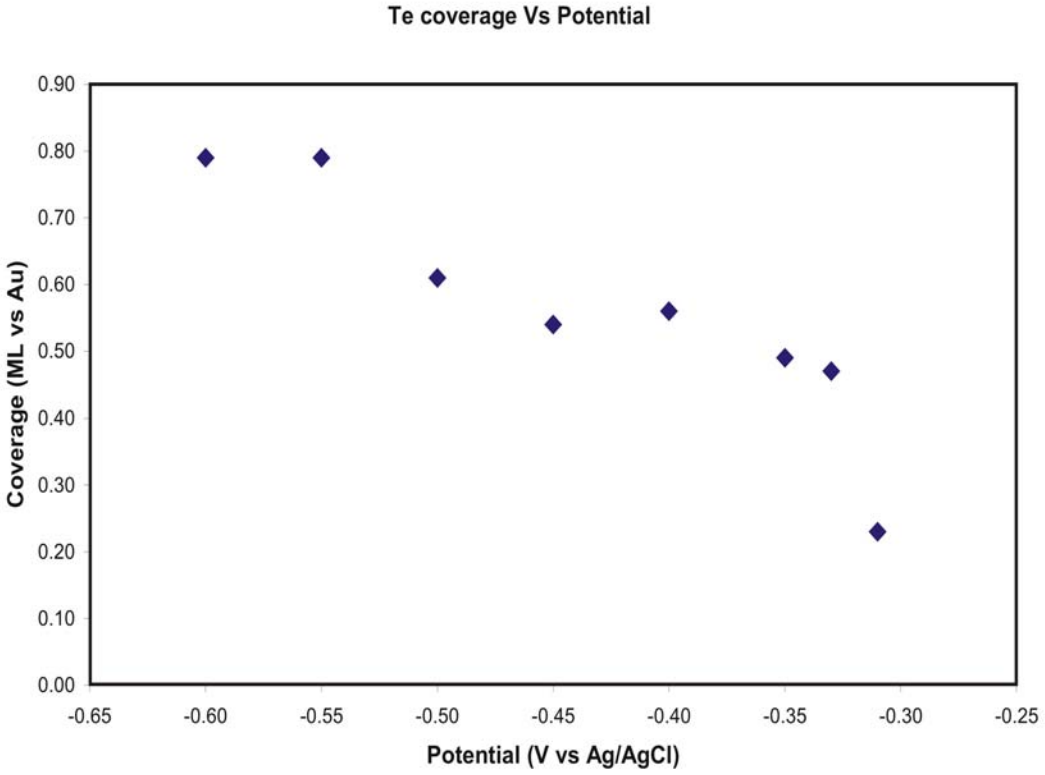

Figure 4.4 : Effect of Te stripping potential on the thickness of 100 cycle deposits.

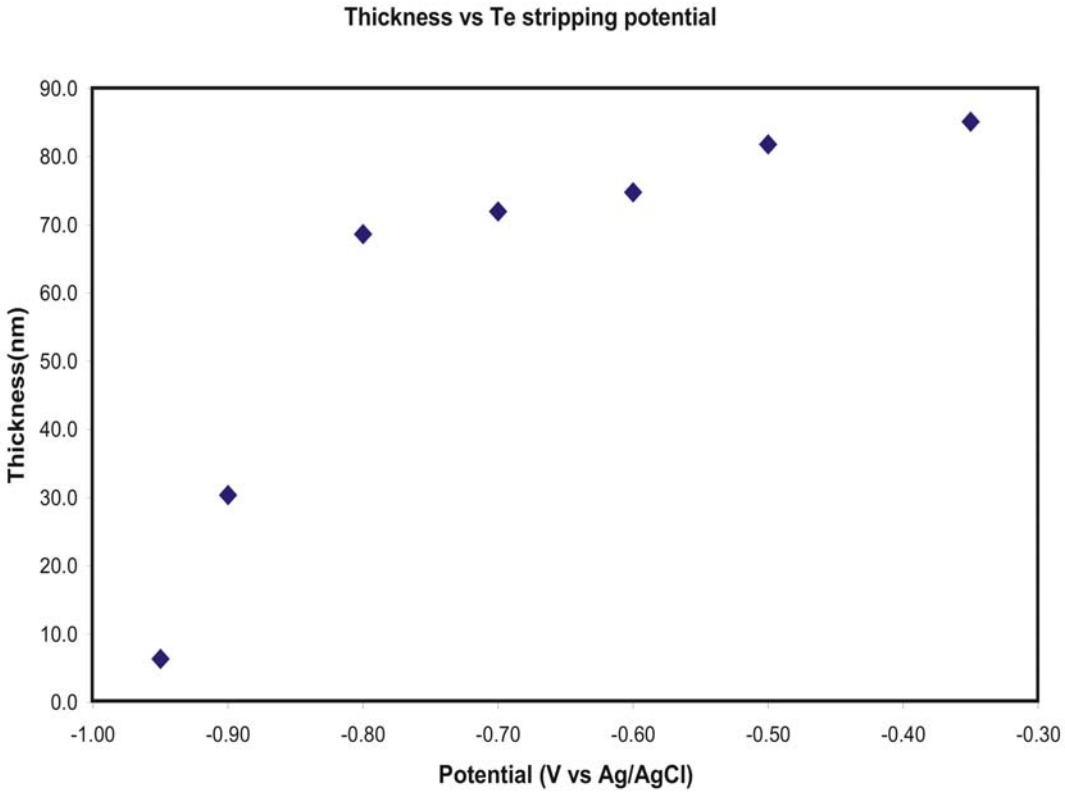

Figure 4.5 : Effect of Hg deposition potential on 100 cycle deposits.

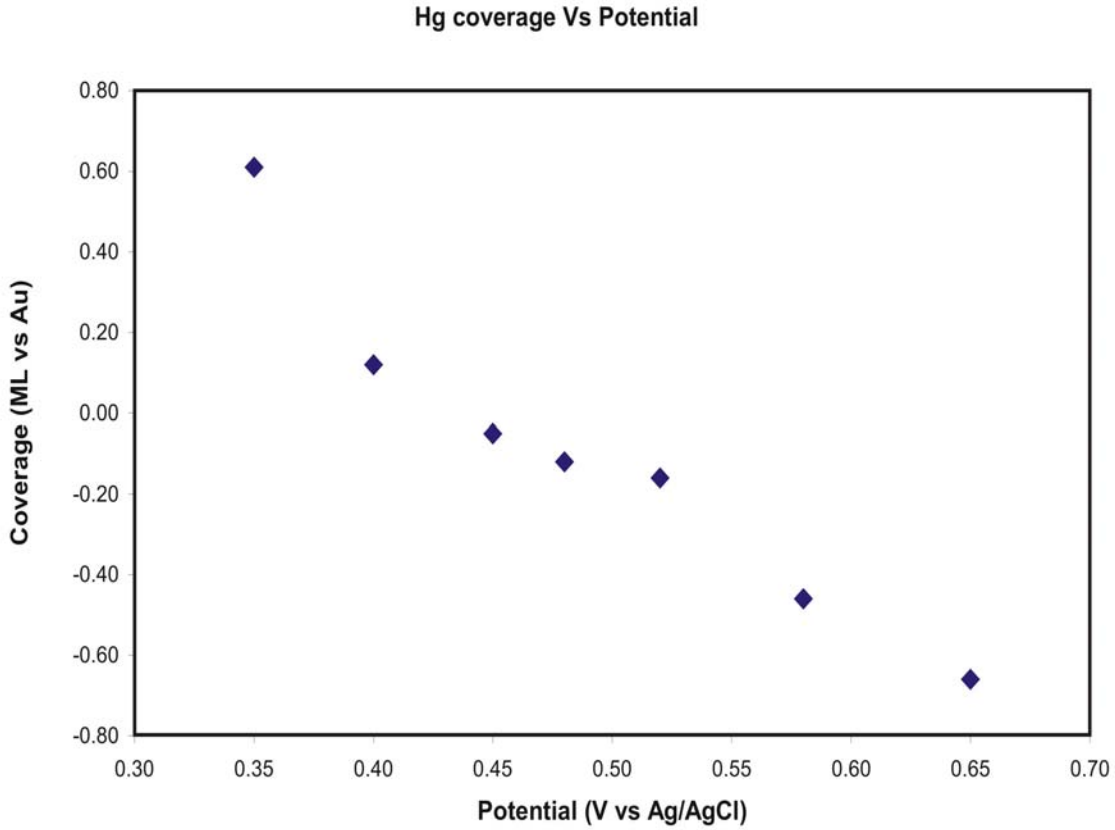

Figure 4.6 : Optimal deposition program for HgTe deposition.

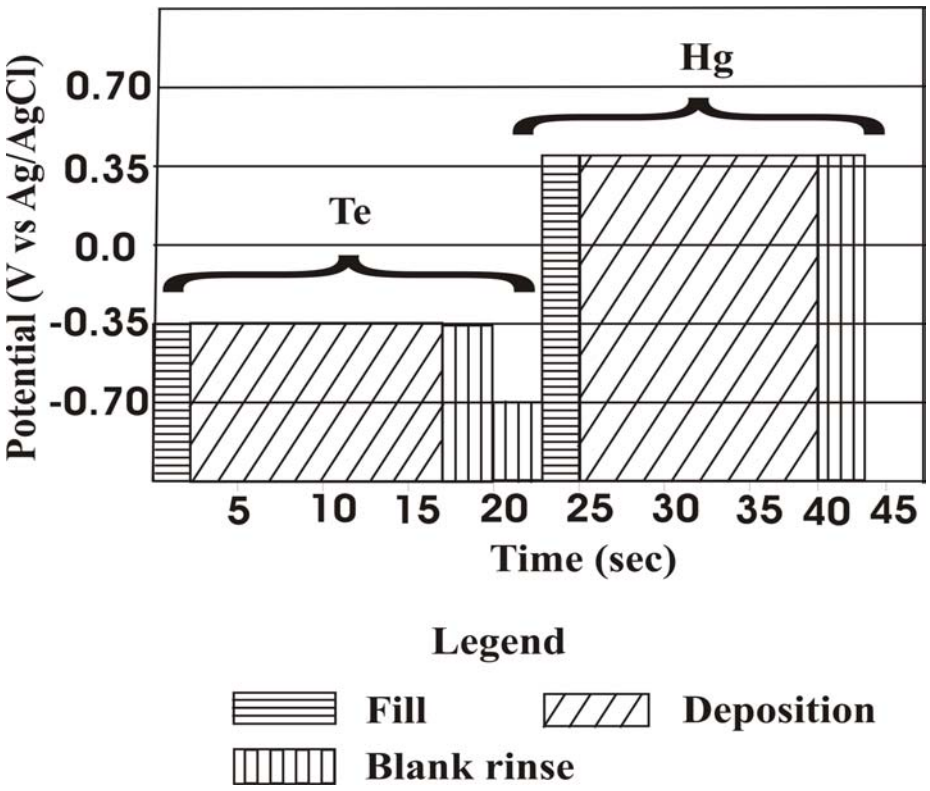

Figure 4.7 : Current-time profile during HgTe deposition using optimal deposition program.

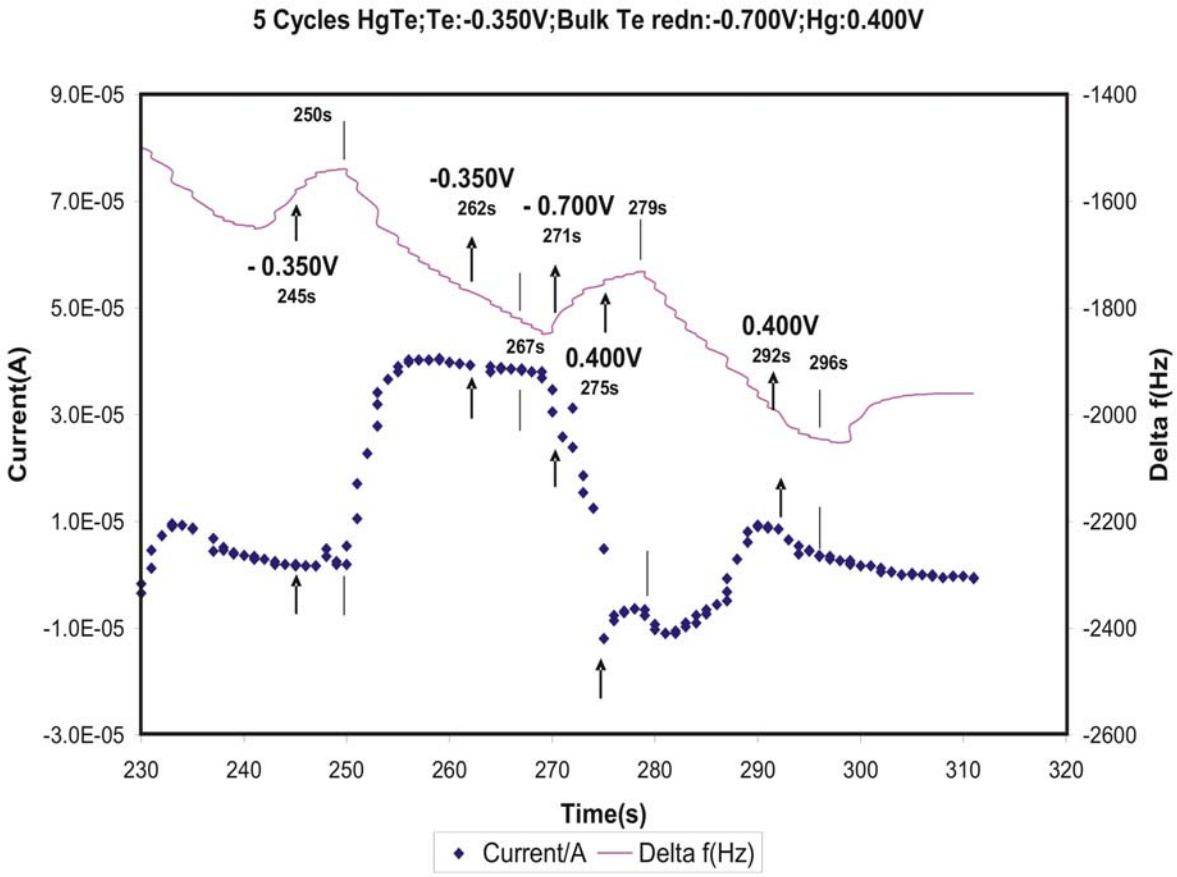

Figure 4.8 : EQCM experiment showing oxidation of Te at Hg deposition potential.

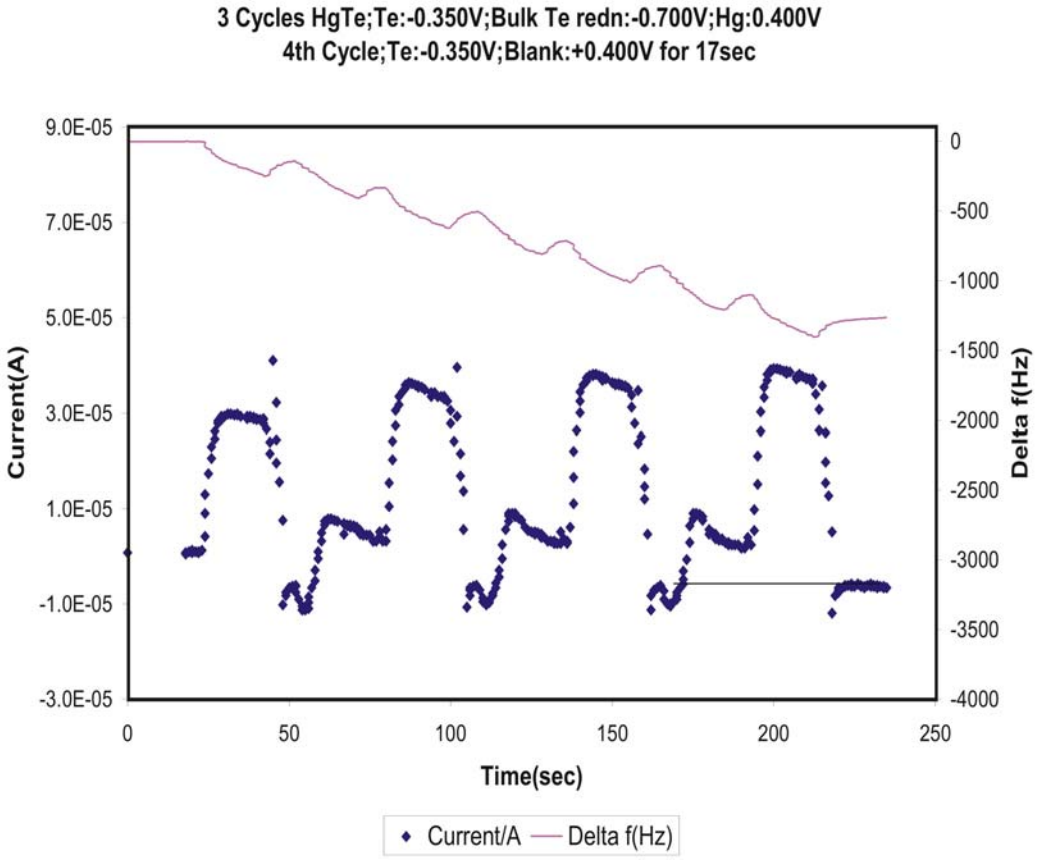

Figure 4.9 : EQCM experiment showing the time dependence of Te oxidation at Hg deposition potential.

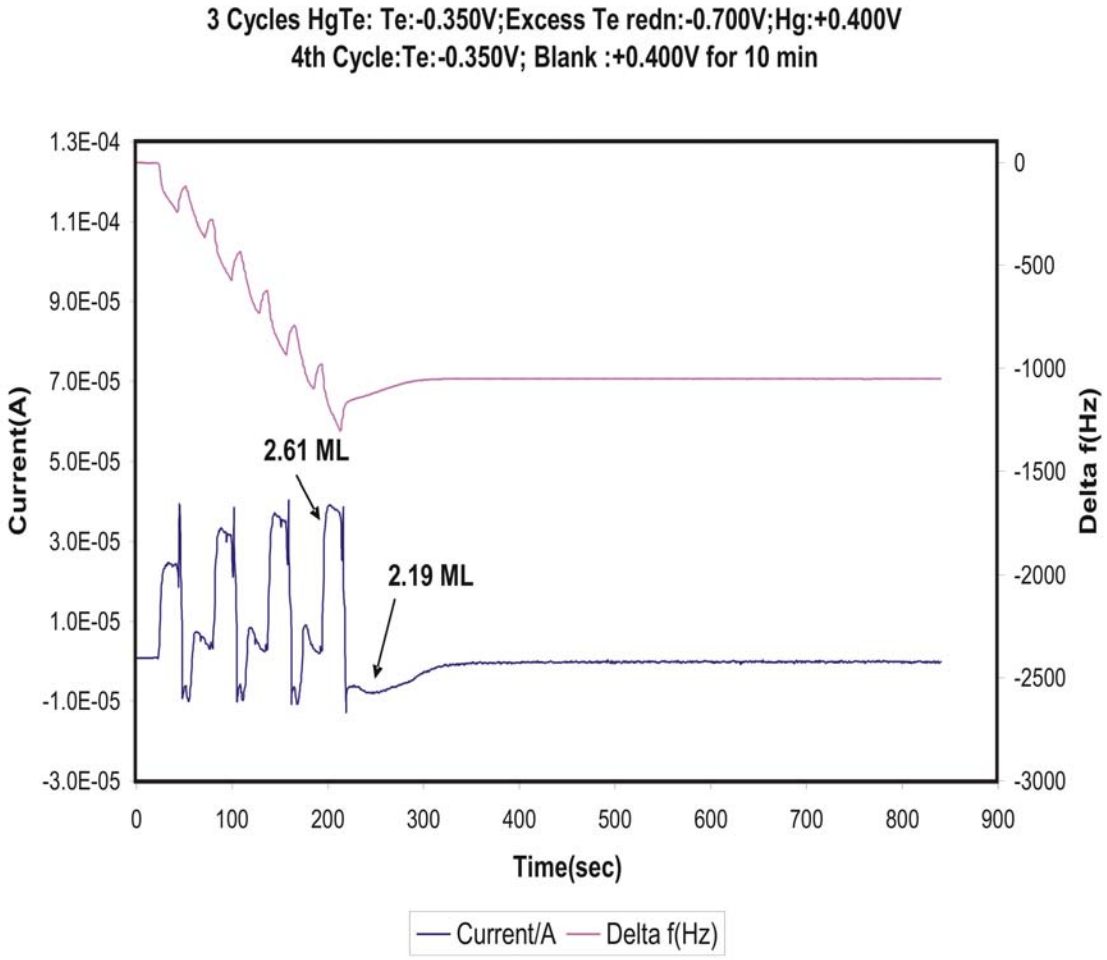

Figure 4.10 : EQCM experiment to determine redox exchange of Te with Hg at open circuit.

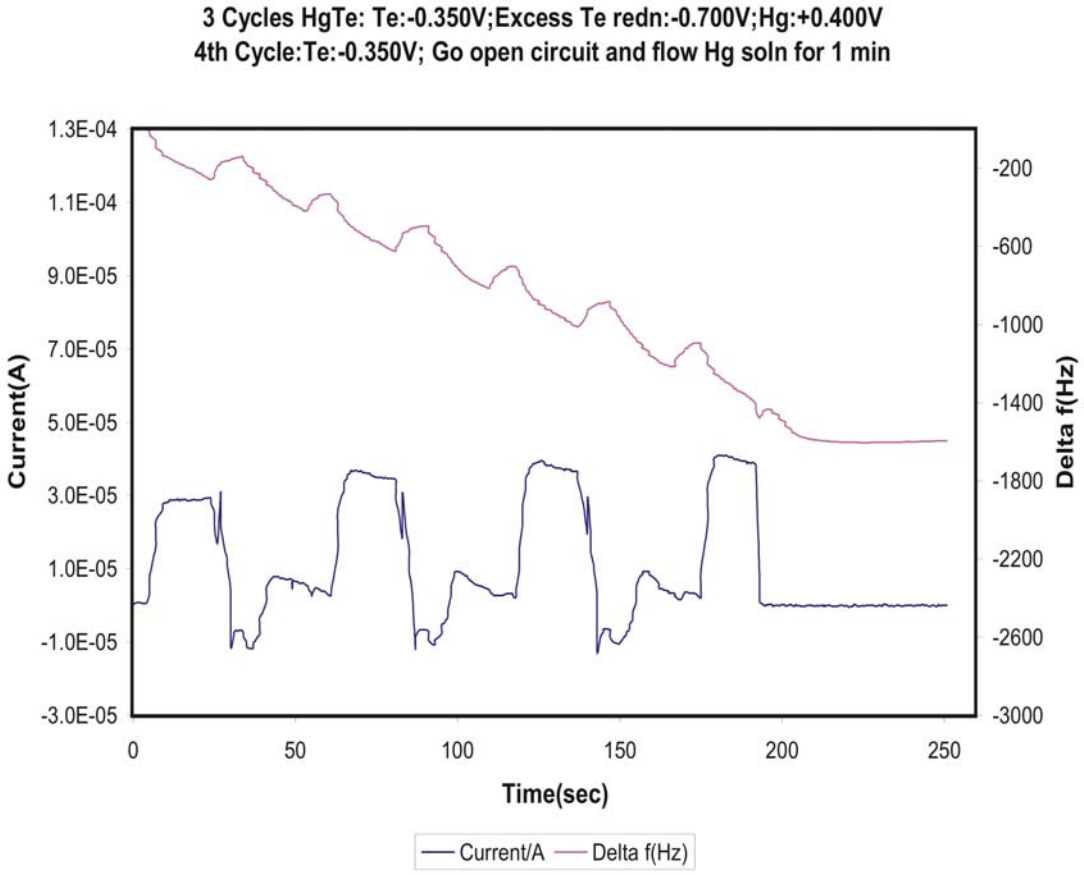

Figure 4.11: XRD diffraction pattern of 100 cycle HgTe thin film.

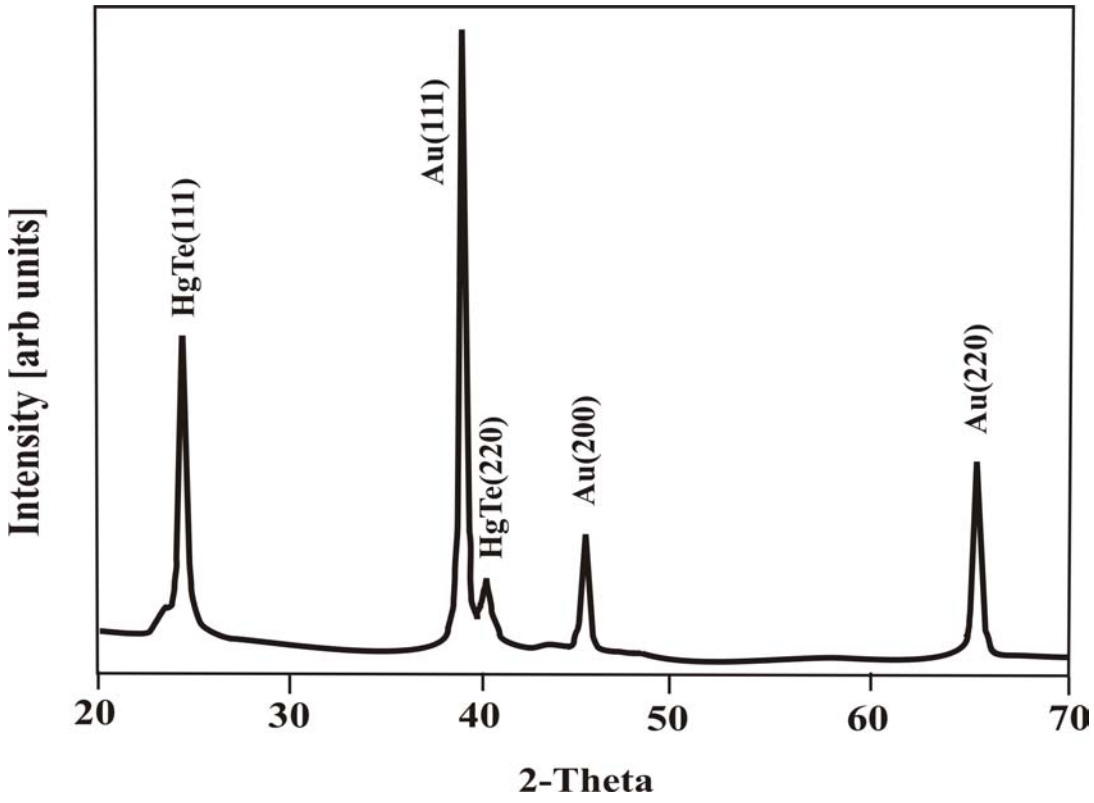

Figure 4.12: IR absorption spectrum of 100 cycle HgTe thin film.

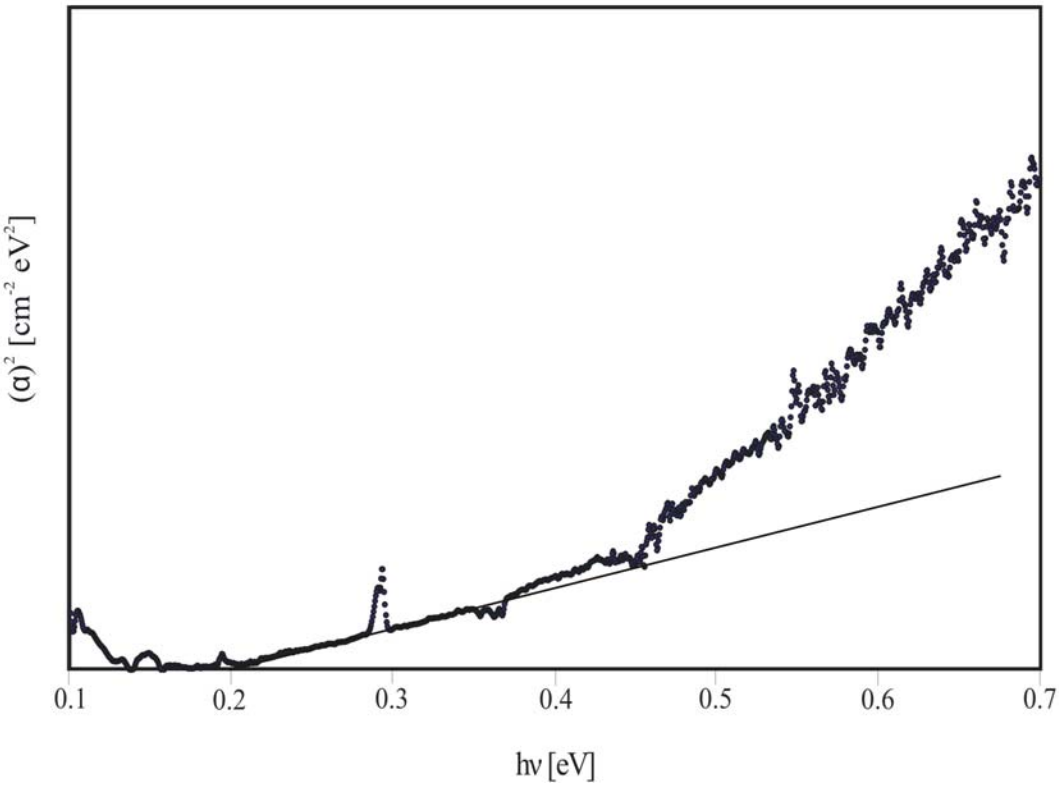

CHAPTER 5

STUDIES OF $HG_{(1-x)}CD_xTE$ FORMATION BY ELECTROCHEMICAL ATOMIC LAYER DEPOSITION (ALD) AND INVESTIGATIONS INTO BANDGAP ENGINEERING [1]

[1] Venkatasamy, V., et al., Journal of Electrochemical Society, 2007. **Submitted**.

Abstract

Films of $Hg_{(1-x)}Cd_xTe$ (MCT) were grown using electrochemical atomic layer deposition (ALD), the electrochemical analog of atomic layer epitaxy (ALE) and atomic layer deposition (ALD). The present study describes the growth of MCT via electrochemical ALD, using an automated electrochemical flow cell deposition system. The system allows potential control and solution exchange as desired. Deposits were characterized using X-ray diffraction (XRD), electron probe microanalysis (EPMA) and reflection absorption Fourier transform Infrared spectroscopy (FTIR). The as deposited films showed strong (111) preferred orientation. No post deposition annealing was required. Changes in deposit composition showed the expected trend in band gaps: the more Hg the lower the band gap, but with some significant deviations. Deposit composition was controlled using a superlattice deposition program. $Hg_{0.5}Cd_{0.5}Te$ and $Hg_{0.8}Cd_{0.2}Te$ deposits resulted in band gaps of 0.70 eV and 0.36 eV, respectively. Electrochemical quartz crystal microbalance (EQCM) studies, using an automated flow cell, indicated that some deposited Cd was stripping at potentials used to deposit Hg. In addition, redox replacement of Cd for Hg was evident, a function of the greater stability of Hg than Cd.

Keywords: MCT, Bandgap engineering, ALD, EC-ALE, upd, Electrodeposition, XRD, FTIR, EPMA

Introduction

$Hg_{(1-x)}Cd_xTe$ (MCT) is an important ternary compound semiconductor, belonging to the II-VI family [1], with a direct bandgap anywhere between -0.15 eV to 1.6 eV, determined by the Hg/Cd ratio. Because of its optical and electronic properties, and its tunable bandgap, there has been extensive interest in MCT for a number of applications [2], such as IR detector materials, when it is Hg rich, and photovoltaics, for the Cd rich alloys [3, 4]. Traditionally MCT has been prepared by various vapor phase techniques like MBE [5-7], MOCVD [8, 9], MOVPE [10, 11], or by liquid phase epitaxy [12-15]. There have also been reports of MCT formation using pulse laser deposition (PLD) [16, 17] and laser evaporation [18]. High quality Hg rich films have been prepared by most of the above techniques, but at a relatively high cost. Thus such methods are questionable for the deposition of Cd rich MCT films for photovoltaic applications, where cost is of central importance. Electrodeposition tends to be a cost effective methodology. Some work on MCT electrodeposition has been performed, mostly using the co-deposition methodology, where a single solution contains precursors for all constituent elements, and a single potential or current density is used to form the deposit [3, 19-24]. Most such studies were performed in aqueous solutions, though some non aqueous solutions have also been studied [25, 26]. Only moderate success has been obtained in the electrodeposition of MCT. In nearly all cases low crystallinity was observed for as formed deposits, requiring post deposition annealing to display a reasonable XRD pattern.

Electrochemical ALD is the electrochemical analog of atomic layer epitaxy (ALE) [27, 28] and atomic layer deposition (ALD) [29-32]. All three methods are based on the use of surface limited reactions to form nanofilm deposits with atomic layer control. These methods break the deposition process into a sequence of individually controllable steps, which are then

used in a cycle, to form deposits of a thickness determined by the number of cycles performed. Use of such cycles greatly improves the ability to optimize a deposition process, though it tends to increases the complexity of the deposition hardware, and can increase the deposition time. In the formation of nanofilms, however, deposition time is seldom the primary concern, as the number of cycle needed is limited.

In electrochemistry, underpotential deposition (UPD) is the prominent surface limited reaction [33-37]. UPD refers to a phenomenon where an atomic layer of one element electrodeposits on another at a potential prior to (under) the potential at which the element deposits on to itself, limiting UPD to the formation of an atomic layer. Electrochemical ALD is the application of UPD, or other electrochemical surface limited reactions, to the sequential deposition of atomic layers of elements for the growth of nanofilms of materials [38-40]. In some systems ALD can promote epitaxy, in which case the method has been referred to at times as atomic layer epitaxy (ALE). There are a number of such electrochemical cases, and they have previously been referred to as electrochemical atomic layer epitaxy (EC-ALE) [38-40].

Most previous work with electrochemical ALD has involved formation of nanofilms of compound semiconductors, including: II-VI compounds such as CdTe, CdS, ZnSe and HgSe [41-44] as well as some III-V compounds such as GaAs, InAs, and InSb [43, 45-47]. PbSe [48], PbTe, Bi_2Te_3 [49-51] and Sb_2Te_3 [52] have also been grown using electrochemical ALD. Recently, this work has been extended to the formation of metal nanofilms, such as Cu, Ag [53, 54] and Pt [53, 55-57].

We report here the first instance of MCT formation by electrochemical ALD. These deposits were formed using an automated flow deposition system [42, 58]. The resulting films were characterized using X-ray diffraction (XRD), Electron Probe Microscope Analysis (EPMA) and

Fourier Transform Infrared spectroscopy (FTIR). The deposition conditions were further studied using an electrochemical quartz crystal microbalance (EQCM) flow cell to help with questions concerning Hg deposition after CdTe formation.

Experimental

The flow deposition system [46, 59, 60], used for the formation these MCT films consisted of peristaltic pumps, a solenoid selection valve and a flow cell. The tubing was kept inside a nitrogen purged Plexiglas box, to cut down on oxygen issues. The electrochemical flow cell was of a laminar flow over design. The Auxiliary electrode (ITO) and the working electrode (Au on glass thin film) were held apart by a silicon rubber gasket, which defined a rectangular opening where deposition took place, 3 cm X 1 cm. The ITO auxiliary was transparent, allowing the deposition process to be followed visually. The reference electrode, Ag/AgCl (3M NaCl) (Bioanalytical Systems, Inc., West Lafayette, IN) was positioned at the cavity outlet.

The solutions used consisted of 0.2 mM HgO (pH 2), 0.5 mM $CdSO_4$ (pH 5) and 0.2 mM TeO_2 (pH 4), all of which contained 0.5 M Na_2SO_4 supporting electrolyte. The blank solution contained only the 0.5 M Na_2SO_4 (pH 4). Solution pH was adjusted using H_2SO_4. The water used to make solutions was supplied from a Nanopure water filtration system (Barnstead, Dubuque, IA) attached to the house DI water system. Chemicals were reagent grade or better.

The ALD program used to deposit MCT involved the separate deposition of HgTe and CdTe monolayers. The cycle used for depositing HgTe monolayers was as follows: the Te solution was flushed into the cell for 2 s (40 mL/min), and held quiescent for 15 s at the potential chosen for Te deposition. Blank solution was then flushed through the cell for 3 s, followed by filling the cell with the Hg solution for 2 s, and holding quiescent for 15 s, for deposition. The cycle was completed by flushing with blank for 3 s [58].

CdTe ML depositions were performed using the following cycle: Cd solution was flushed into the cell for 2 s (40 mL/min) and held quiescent for 15 s, at the chosen Cd deposition potential. Blank solution was then flushed through the cell for 3 s, followed by filling the cell with the Te solution for 2 s, and holding quiescent for 15 s for deposition, at the selected Te deposition potential. Any excess Te was then removed by flushing the cell with the blank, and holding at -0.7 V, which served to reduce any bulk Te to telluride ions, which were then flushed from the cell with a three second blank rinse [58]. The number of cycles of CdTe deposition together with those for HgTe deposition constituted one period. The period could be repeated as many times as desired for a deposit.

A Scintag PAD-V diffractometer with CuKα radiation (λ= 1.5418 A), was used to obtain glancing angle X-ray diffraction patterns. Electron probe microanalysis (EPMA) was run on a Joel 8600 wavelength dispersive scanning electron microprobe. Glancing angle absorption measurements were performed using an FTIR spectrophotometer (Bruker FTS-66v, Bruker optics, Inc.).

Deposition studies using an electrochemical flow cell quartz crystal microbalance (EQCM), employed a 9 MHz AT-cut quartz crystal (Seiko EG&G), where both sides were coated with circular Au electrodes (ca. 0.2 cm^2, 5 mm in diameter). The electrodes were formed with 50 nm of Ti, followed by 300 nm of sputtered Au. Calibration of the EQCM was carried out using Ag coulometry.

Results and Discussions

The starting potential set for development of an electrochemical ALD cycle have usually been obtained from cyclic voltammetry on a Au electrode, in solutions of precursors to the constituent elements (Hg^{2+}, Cd^{2+} and $HTeO_2^+$). The initial potentials used in this study were

-0.35 V and -0.70 V for Te deposition and its subsequent reductive stripping, while -0.65 V and 0.40 V were used for Cd and Hg deposition, respectively, as previously reported by this group for the deposition of HgTe [61] and CdTe [58] nanofilms.

A LABVIEW program was used to control the flow cell deposition system. The program controlled pumps, valves and potentials for each of the steps, cycles and periods in the formation of a superlattice. Initial studies were designed to form a superlattice, by alternating the deposition of several cycles of HgTe with several cycles of CdTe, one period. Repeating this period should have created a HgTe/CdTe, as in the case where electrochemical ALD was used for the growth of PbSe/PbTe superlattices [62]. The size and symmetry of the superlattice period could then be adjusted, in order to engineer the band gap and deposit thickness.

That Hg forms an amalgam with Au is well known, and previous experience with HgTe deposition [61] showed that Hg did alloy with the Au substrate. In an attempt to prevent formation of the amalgam, a 100 cycle layer of CdTe (pre-layer) was first deposited on the Au, before starting the superlattice program. All the deposits mentioned in this paper have this CdTe pre-layer. On this CdTe layer, 20 periods were performed. For example, one period involved 5 cycles of HgTe followed by 5 cycles of CdTe deposition, repeated 20 times.

The deposition program, as describe in the experimental section, was Te solution rinsed for 2 s at -0.35 V, and held for 15 s. Blank was flushed for 3 s, at -0.35 V, and the potential switched to -0.70 V, for 3 s, reducing extra Te to telluride. Hg was pumped for 2 s, held for 15 s at 0.40, followed 3 s of blank 0.40 V. Ideally, this cycle should have resulted in deposition of one ML of HgTe. A ML of HgTe is defined as one bilayer of the Zinc blende structure of HgTe with the (111) orientation, or 6.18×10^{14} atoms/cm^2 of Hg and 6.18×10^{14} atoms/cm^2 of Te, essentially formation of a single (111) layer of HgTe. The program for CdTe was similar: Cd^{2+}

solution pumped for 2 s at -0.65 V, held for 15 s, then flushed with blank for 3 s at -0.65 V. Te deposition was the same as for the formation of HgTe, with the net result being a CdTe ML.

The X-ray diffraction pattern for the resulting deposit (Figure 1) shows only a very small peak, and no evidence of the satellite peaks expected for a superlattice. In fact no satellite peaks were observed for any of the deposits formed in this study, suggesting no strong modulation corresponding to the deposition period. MCT superlattices have been formed using MBE at a substrate temperature of 186 C [63-65]. However, in this case, it appears that no superlattice was formed, only an alloy ($Hg_{(1-x)}Cd_xTe$). As will be discussed below, there were issues during Hg deposition, after CdTe formation, which may account for the absences of superlattice formation.

As noted, the (111) peak for MCT in the XRD pattern in Figure 1 is small compared to the Au (111) substrate peak. There are several possible reasons for this, including low crystallinity in the deposit. One is the minimal thickness of the MCT nanofilm, composed of only 20 (5:5) periods. To increase the sensitivity, a glancing incidence XRD geometry was used, with an angle very close to 1 degree from the surface plane. In this geometry, very small variations in the incident angle, even small variation how the sample is mounted, can result in large variation in the ratio of substrate to deposit peaks.

Figure 2 displays the XRD pattern for a 20 (5:15) period superlattice (5 cycles of HgTe and 15 cycles of CdTe). The MCT (111) peak, relative to substrate, was much larger than that observed in Figure 1. The deposit shown in Figure 2 should be twice as thick as that shown in Figure 1, however, the deposit to substrate peak ratio was significantly more than twice that in Figure 1, again suggesting small variations in incident angle. Other MCT peaks are evident in Figure 2, as well, such as the (220) and (311), indicating some polycrystallinity, but overall, the pattern suggests a strong (111) growth habit: preferred orientation.

Electron probe microanalysis (EPMA) of these two deposits indicated compositions of $Hg_{0.8}Cd_{0.2}Te$ and $Hg_{0.5}Cd_{0.5}Te$, respectively. Furthermore, room temperature IR reflection absorption studies performed on the samples, using a glancing angle of 85^{o} from the surface normal, indicated bandgaps around 0.36 eV and 0.70 eV for the $Hg_{0.8}Cd_{0.2}Te$ and $Hg_{0.5}Cd_{0.5}Te$ deposits respectively (Figure 3 and 4).

To investigate the XRD peak intensities for MCT relative to deposit thickness, a set of deposits were formed using 5 HgTe cycles in the period and the number of periods was kept to 20, while the number of CdTe cycles per period was varied from 2-20. Figure 5 displays XRD intensity, for the MCT (111) peak, vs. the number of CdTe cycles in the period. The peak intensities did increase with the number of CdTe cycles in the period, though not quite in the linear fashion as expected. If it is assumed, in Figure 5, that 8000 units was correct for 10 cycles of CdTe (and 5 cycles of HgTe for 20 periods on a pre-layer of 100 cycles of CdTe), then the y-intercept would be 4000 units, given that 0 in Figure 5 corresponds to zero cycles of CdTe (and 5 cycles of HgTe for 20 periods on a pre-layer of 100 cycle CdTe). The resulting line (Figure 5) is reasonable until the point corresponding to 20 CdTe cycles, where it is much lower then expected. Reasons for this could involve variation in the incident angle. Alternatively, something may have gone wrong with the deposition.

Although no evidence of a superlattice is present in Figure 2, EPMA results for the two deposits were encouraging, showing that the alloy composition could be varied by changing the relative ratio of cycles in the period of the ALD program. To investigate control over the deposit composition using the electrochemical ALD superlattice program, a series of experiments were performed by varying the number of HgTe cycles in a period from 2 to 20, while keeping the number of CdTe cycles (5), and the number of periods (20) constant. The resulting deposits were

then analyzed using EPMA for their elemental compositions. Table 1 lists the number of cycles run for CdTe and HgTe in a period, along with the relative atomic proportions for Cd and Hg, calculated from EPMA, excluding the Au contribution. In addition, theoretical compositions are listed, based on the assumption that each cycle resulted in deposition of one monolayer of the respective compound: HgTe or CdTe.

The Hg composition (1-x) in an alloy should increase with an increase in the number of HgTe cycles per period. The experimental results are consistent with this trend, as the Hg component in the alloy increased from 0.53 to 0.84 when the number of HgTe cycles in a period was increased from 2 to 20. The complementary Cd composition (x) decreased, as expected, with the Hg increase. The band gaps of the MCT deposits were also studied as a function of deposit compositions by varying the relative number of CdTe and HgTe cycles in the period. In each case, 20 periods were formed. The deposits were then analyzed by room temperature reflection absorption spectroscopy to determine their band gaps. Figure 6 shows the relationship between band gaps for the MCT films and values of x, or the relative fraction of CdTe in the alloy. From Figure 6 it is clear that the band gaps have the desired trend as a function of composition, but deviated from the theoretical line, derived by Hansen et.al., [66] at both high and low values of x. The band gaps were too high at low values of x and too low at high values of x.

The high band gaps at low values of x may reflect that some Hg does appear to form an alloy with the Au substrate, an amalgam. Alloying was clearly observed when the deposits were etched away with concentrated nitric acid, leaving behind only a white patch of the Au-Hg amalgam on the Au substrates. The extent of amalgam formation increased the higher the fraction of Hg, (1-x). The more amalgam, the lower the amount of Hg that was actually present in the MCT deposit, and thus the higher band gap. This suggests that Hg is fairly mobile within

the deposit, as well in the Au. Discussions of the problem of Hg deposition on pre-deposited CdTe, discussed below, could also explain the high band gaps. It might be that concentration of Hg was even higher than expected in the deposited alloy, shifting the band gap below zero, so it might not have been noticed [67]. In which case the band gap measured would be that of the CdTe pre-layer, and reflects diffusion of Hg in to this film.

As for the low band gaps at high values of x, the deposits are really composed of two layers. As noted, each deposit starts with 100 cycles of CdTe, and the MCT is then grown on top. In the case of growing MCT with 5 cycles of CdTe, and 2 cycles of HgTe per period, for 20 periods, the MCT layer consists of 140 cycles, on 100 cycles of CdTe. Because of this 100 cycle pre-layer, the overall fraction of CdTe looks larger by EPMA. The MCT determines the measured band gap, as the CdTe does not start to absorb until closer to 1.5 eV.

MCT has proven to be significantly more difficult to form using electrochemical ALD than either CdTe or HgTe, because of the large difference in stability between Hg and Cd, nearly a volt. To better understand the deposition program, an electrochemical quartz crystal microbalance (EQCM) flow cell system was employed. The program used with the EQCM differed slightly from that used to form the deposits previously discussed. The main difference was that experience has shown that stopping flow with the EQCM resulted in dramatic changes in the frequency, while continuous flow through the cell does not show this effect, at reasonable flow rates. No problems of this type were observed using 6 mL/min. Figure 7 shows the current-time response and the frequency change during the deposition of 3 cycles of CdTe followed by 3 cycles of HgTe. Of particular note is the fact that no reduction was evident during the Hg^{2+} reduction steps. In fact, an oxidative current was actually present. However, from EPMA, it was clear that Hg was deposited.

The problem is that at the potentials needed to deposit Hg UPD, Cd in CdTe is not very stable. Apparently, some of the Cd deposited in previous CdTe cycles was oxidatively stripped when the potential was switched to 0.40 V, to deposit Hg. To substantiate this conclusion, 3 cycles of CdTe were deposited, followed by a blank rinse at 0.40 V. Oxidation current was observed (Figure 8) as well as a mass decrease, indicating loss of Cd from the surface, while the potential was maintained at 0.40 V.

In addition, redox replacement of Cd by Hg^{2+} was likely under these conditions, where some charge for Hg^{2+} reduction came directly from oxidation of Cd to Cd^{2+}, a fairly probable event given the difference in the potentials used in the present study for Hg and Cd deposition, 0.40 V and -0.65 V respectively. To better understand this process, five cycles of CdTe were formed using the same deposition program (Figure 9), but instead of flowing the Hg^{2+} solution at 0.40 V, it was introduced at open circuit for 1 minute (Figure 9). The mass of the electrode increased, even in the absence of potential control, as heavy Hg atoms replaced lighter Cd atoms. The mass loss, evident at the end (Figure 9), resulted from a blank rinse. Anytime the solution flowing over the EQCM electrode changes, some mass change is expected, given the substitution of reversibly adsorbed species in equilibrium with the old solution are exchanged for those in equilibrium with new solution. This makes assignment of mass changes from step to step difficult, but allows mass changes from equivalent points in different cycles to be assigned. If all the Cd deposited in the five cycles of CdTe were replaced by Hg, a mass change of 450 Hz would be expected. The measured mass change was 480 Hz. That is, given sufficient time, all the Cd was exchanged at open circuit in the Hg^{2+}solution, for Hg. This raises the question of why there was any Cd present in the deposits formed in this study? There were two significant differences between the program and instrumentation used for the EQCM experiment shown in

Figure 9 and those used to form the deposits in this study: longer times and continuous flow were used for the EQCM study. It is thus proposed here that all the Cd was not replaced because only 15 second was allowed for exchange, and there was no flow during the deposition, limiting the redox replacement of Cd for Hg. The effect of holding the potential at 0.40 V is not clear. Obviously, 0.40 V must have been positive of the OCP, given that oxidative current was observed. It would then be expected that Cd oxidation would accelerate, while Hg deposition might slow down. The net result over the 15 seconds used for Hg deposition was that some Cd was replaced or oxidized but not all, and Hg did deposit.

There are three main issues in the present investigation that require further study. The first is the issue of amalgam formation. By use of Ni as a substrate, the importance of amalgam formation should be minimized. However, Ni is significantly more reactive than Au, and will oxidized at the potentials needed to deposit Hg, unless passivated via a pre-layer. Another issue, however, is the use of a pre-layer. Stoichiometry determination would be improved in the absence of a pre-layer. Finally, that a superlattice was not formed is of concern. Superlattices have been formed of PbSe/PbTe [62] , which suggest given reasonable cycles for HgTe [61], and CdTe [58], a superlattice is likely. Most of the problems forming a superlattice appear related to the need to deposit Hg at 0.40 V, where the Cd in CdTe is unstable. One solution would be to shift the potential for Hg deposition negatively using a complexing agent, to a potential where the Cd would remain stable.

Conclusion

Initial studies of the formation of MCT by electrochemical ALD have been reported. XRD patterns of the deposits indicated the formation of $Hg_{(1-x)}Cd_xTe$ (MCT) alloys, with a preferred (111) growth habit. The deposit composition showed a strong dependence on the ALD

period program, suggesting that the MCT composition can be controlled over a broad range of x. Room temperature IR reflection absorption studies indicated that the band gap for the MCT deposits could be engineered using the electrochemical ALD program. EQCM flow cell studies were used to investigate the Hg deposition step, where it was confirmed that some Cd, in previously deposited CdTe, was oxidatively stripped upon switching to 0.40 V for Hg deposition. In addition, some Cd was exchanged for Hg by a redox replacement reaction. There was no indication from XRD of satellite peaks, or the formation of a superlattice. At present, it appears that the absences of satellite peaks may be the result of the instability of Cd at the potentials needed for Hg deposition.

Acknowledgements

The authors would like to acknowledge the support of NSF divisions of Material Science and Chemistry.

References

1. McMillan, B.G., et al., Electrochimica Acta, 2004. **49**: p. 1339–1347.
2. Kumaresan, R., S.M. Babu, and P. Ramasamy, Materials Chemistry and Physics, 1999. **59**(2): p. 107-113.
3. Basol, B.M., Solar Cells, 1988. **23**: p. 69-88.
4. Kumaresan, R., S. Moorthy Babu, and P. Ramasamy, Journal of Crystal Growth, 1999. **198-199**(2): p. 1165-1169.
5. Wu, O.K. and G.S. Kamath, Semicond. Sci. Technol., 1991. **6**: p. C6-C9.
6. Wijewarnasuriya, P.S., Journal of Crystal Growth, 1997. **175-176**: p. 647-652.
7. He, L., et al., Journal of Crystal Growth, 2001. **227–228**: p. 677–682.
8. Matsushita, K. and A. Kamata, Journal of Crystal Growth, 1998. **184-185**: p. 1228-1231.
9. Shigenaka, K., et al., Journal of Crystal Growth, 1992. **117**(1-4): p. 37-43.
10. Maruyama, K., et al., Journal Of Electronic Materials 1996. **25**(8): p. 1353-1357.
11. Mitra, P., et al., Journal of Crystal Growth, 1997. **170**: p. 542-548.
12. Li, B., et al., J. Crystal Growth, 1995. **148**: p. 41-48.
13. Gawron, W. and A. Rogalski, Infrared Physics & Technology, 2002. **43**: p. 157-163.
14. Radhakrishnan, J.K., S. Sitharaman, and S.C. Gupta, J. Crystal Growth, 2003. **252**: p. 79-86.
15. Radhakrishnan, J.K., S. Seetharaman, and S.C. Gupta, Appl. Surf. Sci. , 2003. **207**: p. 33-39.
16. Rudyj, I.O., et al., Applied Surface Science, 2000. **154–155**: p. 206–210.
17. Wisz, G., I. Virtb, and M. Kuzma, Thin Solid Films, 1998. **336**: p. 188-190.
18. Gorbach, T.Y., et al., Applied Surface Science, 1996. **96-98**: p. 881-886.

19. Rakhshani, Appl.Electrochem., 2002.

20. Sahu, S.N., M.J. Antonio, and C. Sanchez, Solar Energy Materials and Solar Cells, 1996. **43**(3): p. 223-235.

21. Jun, L., T. Zheng, and M. Tian-Ying, Sci. China (series B), 1990. **33**: p. 1153.

22. Ramiro, J., E. Garcia, and E.G. Camarero, JMS, 1996. **31**: p. 2047.

23. Sahu, S.N. and C. Sanchez, Solid State Communications, 1990. **73**(9): p. 597-600.

24. Basol, B.M., et al. *Cd(1-x)ZnxTe thin films prepared by a two-stage process utilizing electrodeposition*. in *IEEE Photovoltaic specialists conference*. 1988: IEEE.

25. Colyer, C.L. and M. Cocivera, J. Electrochem. Soc., 1992. **139**: p. 406-409.

26. Nair, J.P., et al., Journal of Physics and Chemistry of Solids, 1999. **60**(10): p. 1693-1703.

27. Bedair, S., *Atomic Layer Epitaxy*. 1993, Amsterdam: Elsevier. 304.

28. Kuech, T.F., P.D. Dapkus, and Y. Aoyagi, *Atomic Layer Growth and Processing*. Vol. 222. 1991, Pittsburgh: Materials Research Society. 360.

29. Leskela, M. and M. Ritala, Thin Solid Films, 2002. **409**(1): p. 138-146.

30. Yousfi, E.B., et al., Thin Solid Films, 2001. **387**(1-2): p. 29-32.

31. Sammelselg, V., et al., Applied Surface Science, 1998. **134**(1-4): p. 78-86.

32. Ylilammi, M., Thin Solid Films, 1996. **279**(1-2): p. 124-130.

33. Kolb, D.M., Przasnys.M, and Gerische.H, Journal of Electroanalytical Chemistry, 1974. **54**(1): p. 25-38.

34. Kolb, D.M., *Physical and Electrochemical Properties of Metal Monolayers on Metallic Substrates*, in *Advances in Electrochemistry and Electrochemical Engineering*, H. Gerischer and C.W. Tobias, Editors. 1978, John Wiley: New York. p. 125.

35. Juttner, K. and W.J. Lorenz, Z. Phys. Chem. N. F., 1980. **122**: p. 163.

36. Hubbard, A.T., et al., *Electrochemical surface characterization*, in *New Dimensions in Chemical Analysis*, B.L. Shapiro, Editor. 1985, Texas A & M University Press: College Station, Texas. p. 135.

37. Gewirth, A.A. and B.K. Niece, Chem. Rev., 1997. **97**: p. 1129-1162.

38. B.W. Gregory, D.W.S., J.L. Stickney, J. Electrochem. Soc., 1991. **138**: p. 1279.

39. Stickney, J.L., *Electrochemical Atomic Layer Epitaxy*, in *Electroanalytical Chemistry*, A.J. Bard and I. Rubenstein, Editors. 1997, Marcel Dekker: New York. p. in press.

40. Stickney, J.L., et al., *Compound semiconductor formation by electrochemical atomic layer eptiaxy (EC-ALE): Surface Chemistry*, in *Encyclopedia of Surface and Colloid Science*, A.T. Hubbard, Editor. 2002, Marcel Dekker, Inc.: New York.

41. Colletti, L.P., B.H. Flowers Jr., and J.L. Stickney, Journal of the Electrochemical Society, 1998. **145**(5): p. 1442-1449.

42. Flowers, J., Billy H., et al., Journal of Electroanalytical Chemistry, 2002. **524-525**: p. 273-285.

43. Wade, T.L., et al. *Formation of II-VI and III-V compound semiconductors by electrochemical ALE*. in *National Meeting of the Electrochemical Society, Spring*. 1999. Seattle, Washington: The Electrochemical Society.

44. Venkatasamy, V., et al., Electrochimica Acta, 2006. **51**(21): p. 4347-4351.

45. Wade, T.L., et al., Electrochemical and Solid State Letters, 1999. **2**(12): p. 616.

46. Wade, T.L., et al. *Electrochemical Atomic Layer Eptitaxy: Electrodeposition of III-V and II-VI Compounds,*. in *Materials Research Society*. 2000: Materials Research Society.

47. Wade, T.L., et al., JEC, 2001. **500**: p. 322-332.

48. Vaidyanathan, R., J.L. Stickney, and U. Happek, Electrochimica Acta, 2004. **49**(8): p. 1321-1326.

49. Zhu, W., et al., Electrochimica Acta, 2005. **50**(20): p. 4041-4047.

50. Zhu, W., et al., J. Electroanal. Chem., 2005. **585**(1): p. 83-88.

51. Yang, J.Y., et al., J. Electroanal. Chem., 2005. **577**(1): p. 117-123.

52. Yang, J.Y., et al., J. Phys. Chem. B, 2006. **110**(10): p. 4599-4604.

53. Vasilic, R. and N. Dimitrov, Electrochem. Solid State Lett., 2005. **8**(11): p. C173-C176.

54. Vasilic, R., L. Viyannalage, and N. Dimitrov, J. Electrochem. Soc., 2006. **153**(9): p. C648-C655.

55. Brankovic, S.R., J.X. Wang, and R.R. Adzic, SS, 2001. **474**: p. L173-L179.

56. Mrozek, M.F., Y. Xie, and M.J. Weaver, Analytical Chemistry, 2001. **73**(24): p. 5953-5960.

57. Kim, J.Y., Y.G. Kim, and J.L. Stickney, ECS Transactions, 2006. **1**(30): p. 41-48.

58. Venkatasamy, V., et al., Journal of Applied Electrochemistry, 2006. **36**(11): p. 1223-1229

59. Stickney, J.L., *Electrochemical atomic layer epitaxy*, in *Electroanalytical Chemistry*, A.J. Bard and I. Rubenstein, Editors. 1999, Marcel Dekker: New York. p. 75-211.

60. Wade, T.L., T. Sorenson, A., and J.L. Stickney, *Epitaxial Compound Electrodeposition*, in *Interfacial Electrochemistry*, A. Wieckowski, Editor. 1999, Marcel Dekker: New York. p. 757-768.

61. Venkatasamy, V., et al., Journal of Electroanalytical Chemistry, 2006. **589**(2): p. 195-202.

62. Vaidyanathan, R., et al., Langmuir 2006. **22**(25): p. 10590-10595

63. Han, M.S., T.W. Kang, and T.W. Kim, Applied Surface Science, 1999. **153**(1): p. 35-39.

64. Han, M.S., T.W. Kang, and T.W. Kim, Applied Surface Science, 1999. **148**(1-2): p. 105-110.

65. Han, M.S., et al., Semicond. Sci. Technol., 1998. **13**: p. 915–920.

66. Hansen.G.L and Schmit.J.L, J. Appl. Phys, 1983. **54**(3).

67. Venkatasamy, V., et al., ECS Transactions, 2006. **3**: p. 95-110.

Table I : Dependence of MCT composition on the number of HgTe cycles in the period.

CdTe cycles	HgTe cycles	periods	Theoretical		Experimental	
			Hg (1-x)	Cd (x)	Hg (1-x)	Cd (x)
5	2	20	0.29	0.71	0.53	0.47
5	10	20	0.67	0.33	0.64	0.36
5	15	20	0.75	0.25	0.75	0.25
5	20	20	0.80	0.20	0.84	0.16

Figure 5.1 : XRD diffraction pattern of 5:5:20 period MCT thin film.

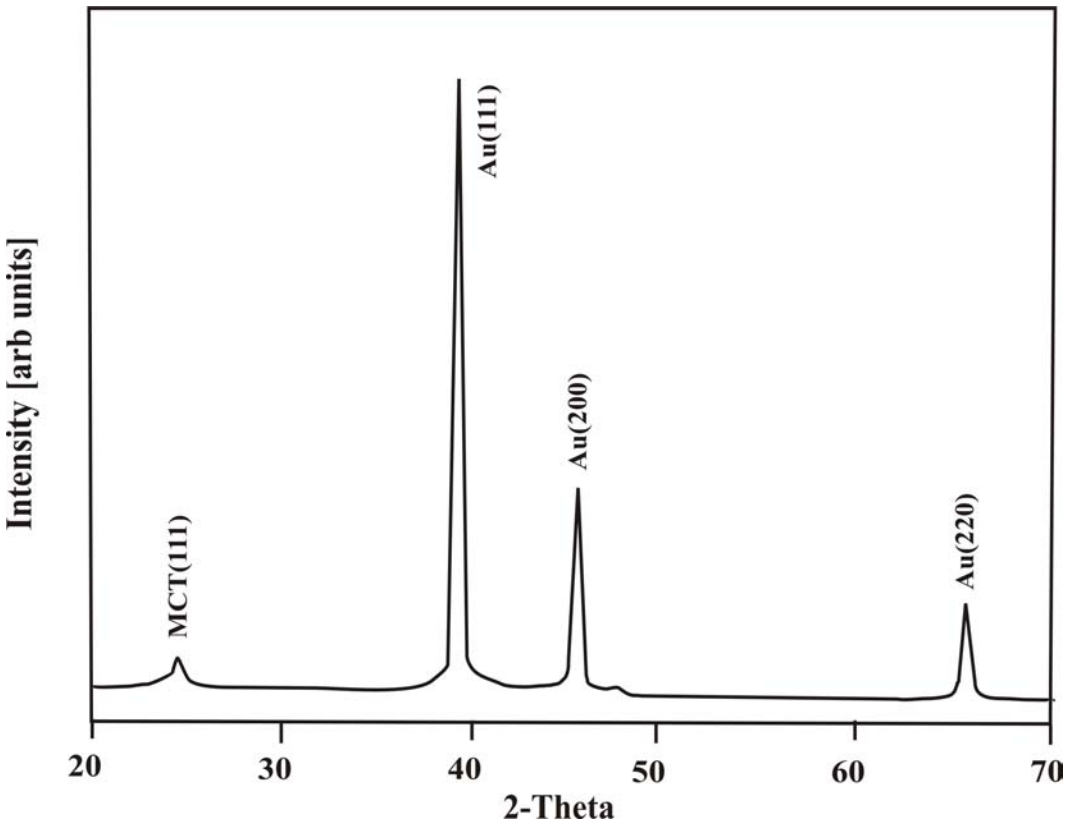

Figure 5.2 : XRD diffraction pattern of 5:15:20 period MCT thin film.

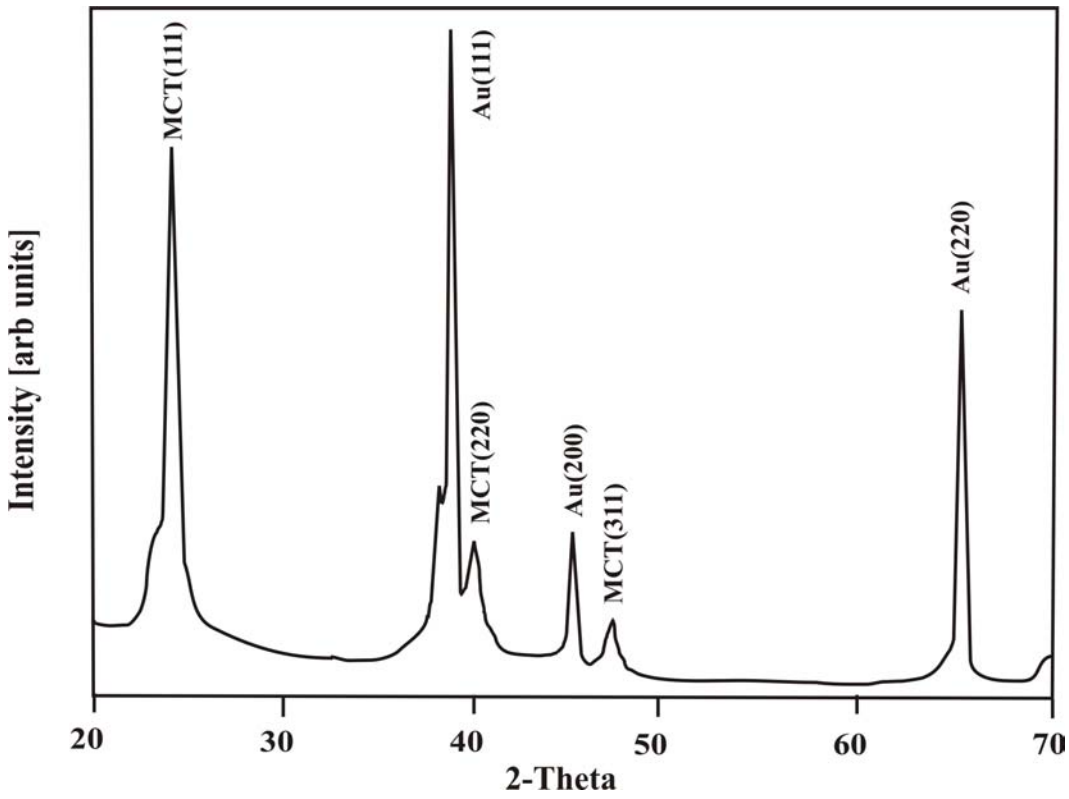

Figure 5.3 : IR absorption spectrum of 5:5:20 period MCT thin film.

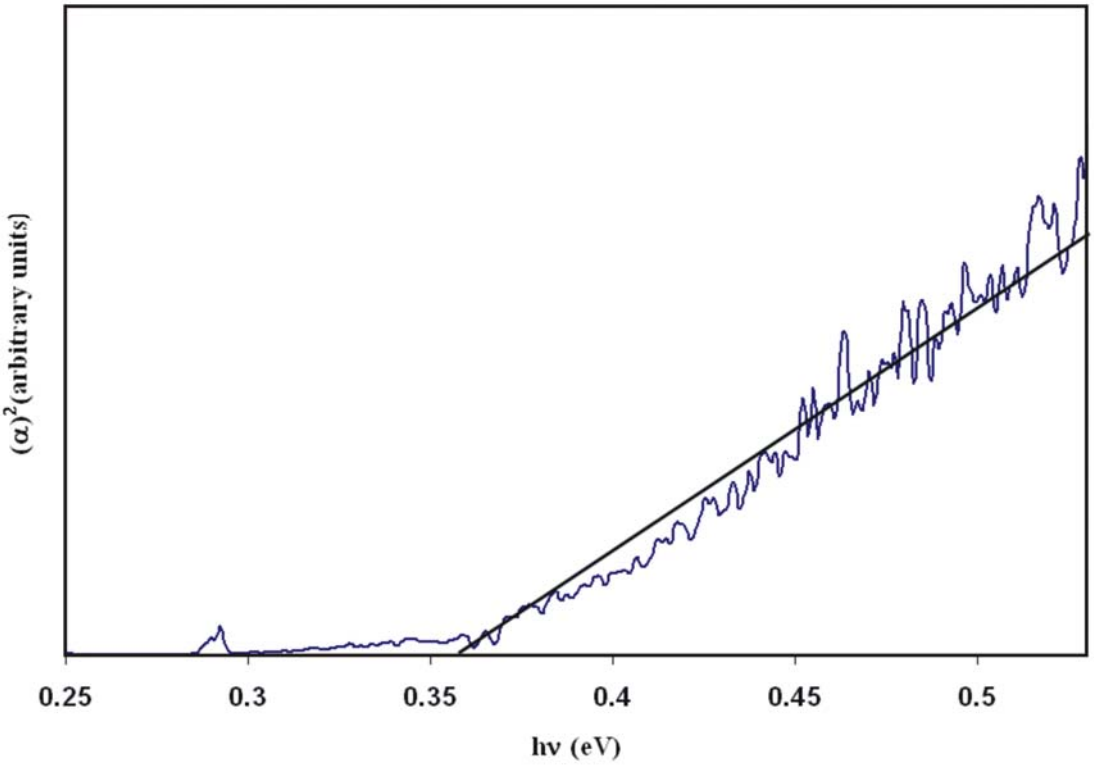

Figure 5.4 : IR absorption spectrum of 5:15:20 period MCT thin film.

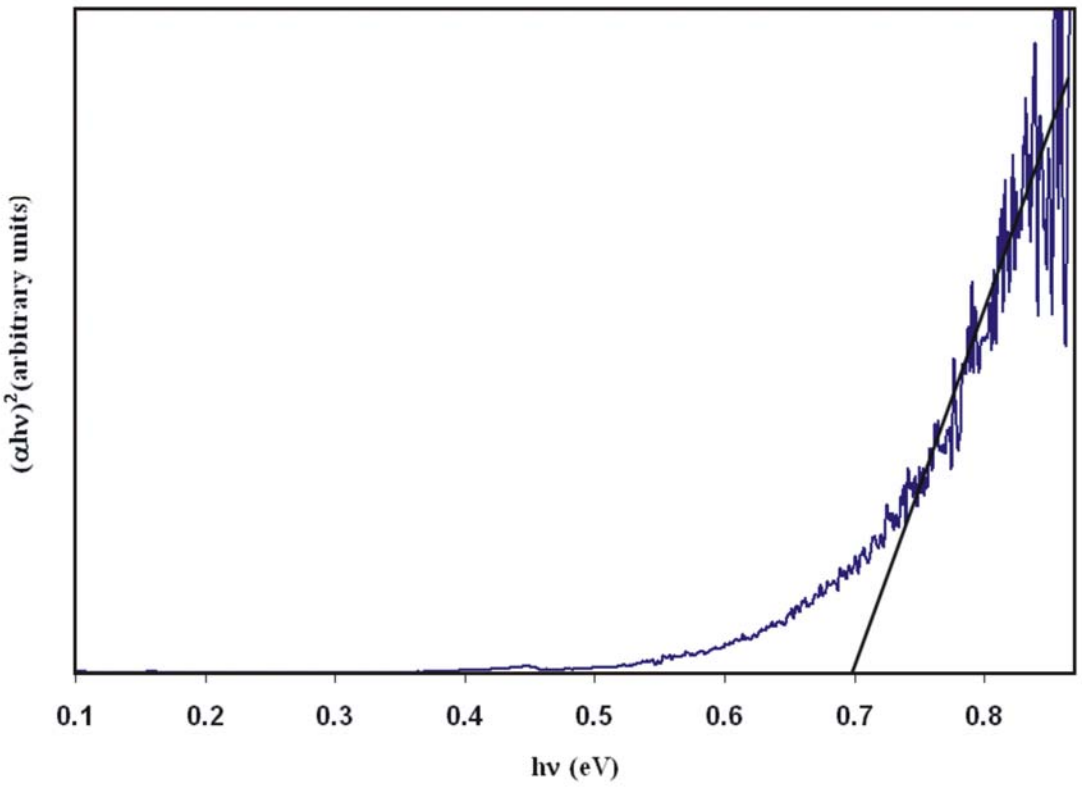

Figure 5.5 : Effect of CdTe deposition cycles on MCT (111) peak intensity.

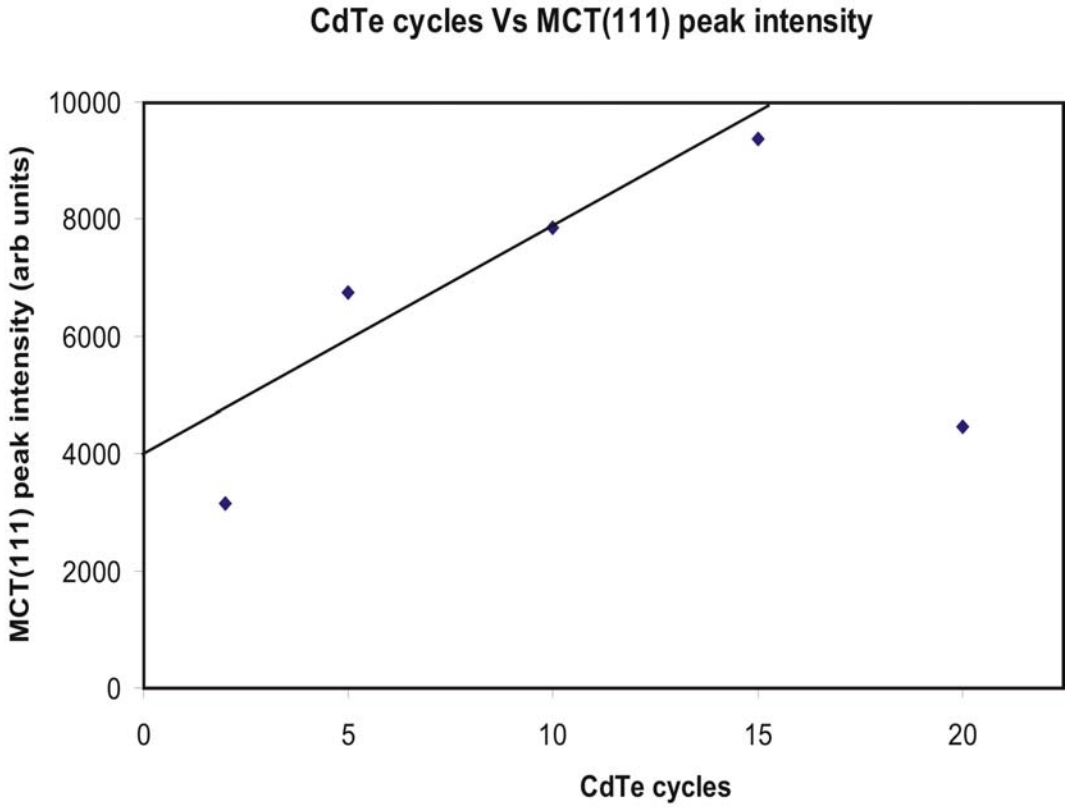

Figure 5.6 : Bandgap engineering experiment.

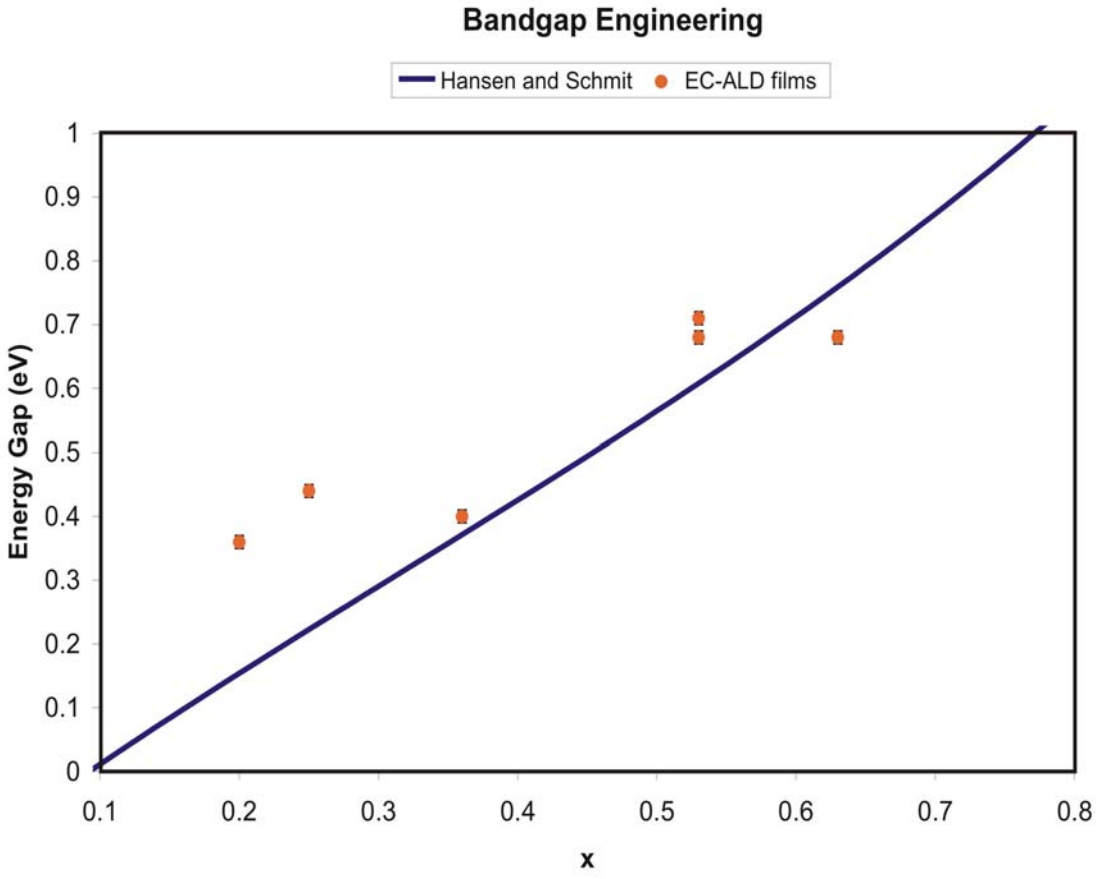

Figure 5.7 : Current-time profile during HgCdTe deposition.

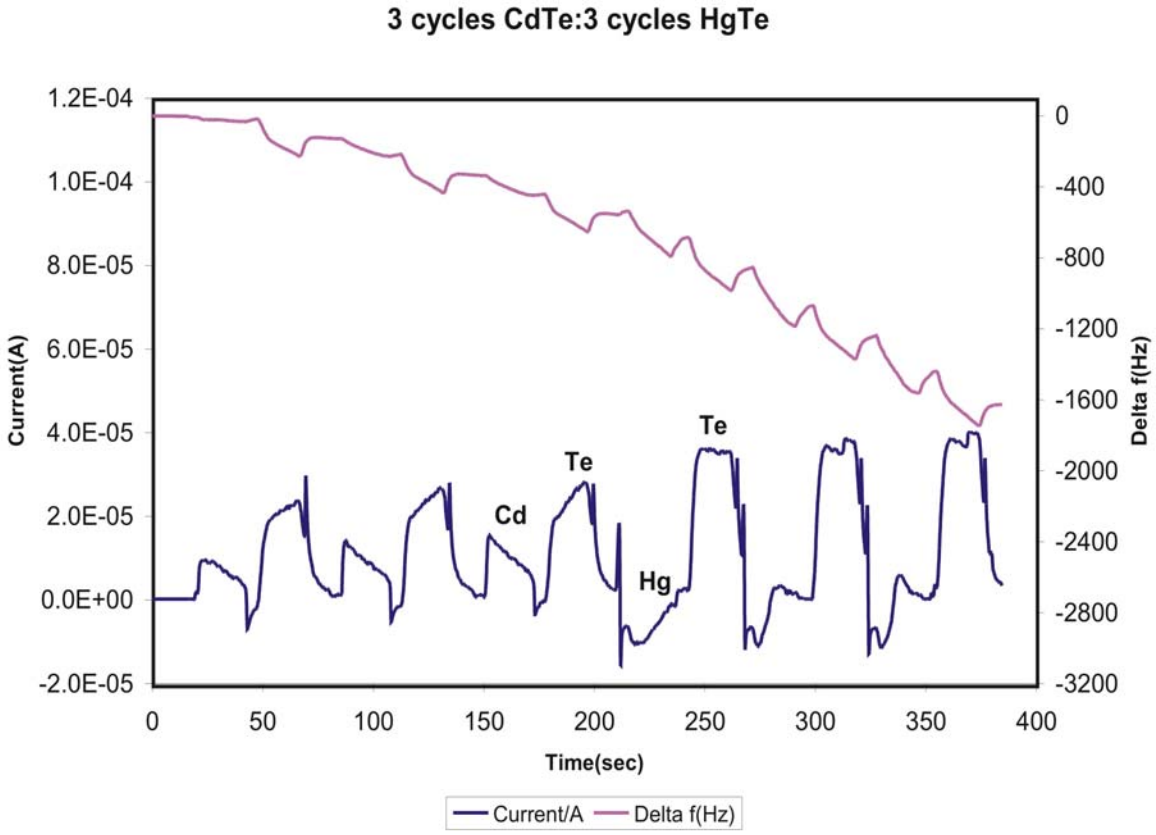

Figure 5.8 : EQCM experiment showing oxidation of Cd at Hg deposition potential.

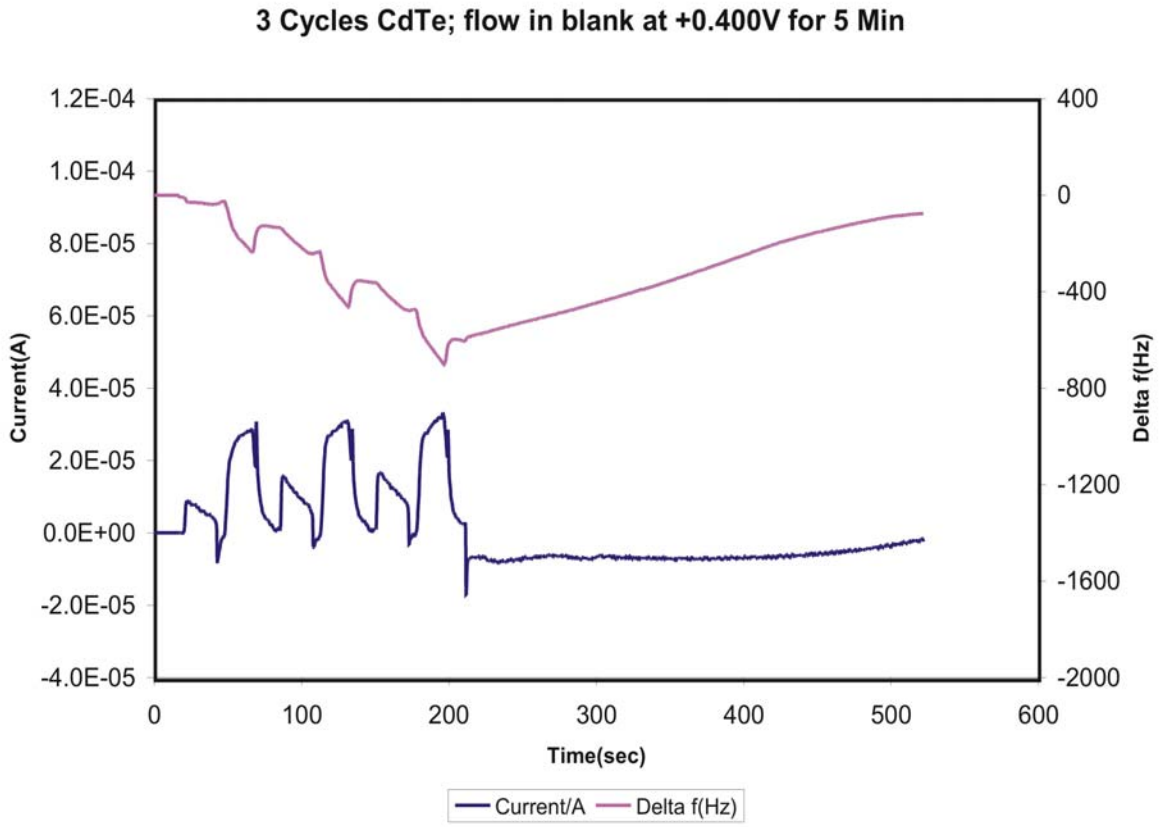

Figure 5.9 : EQCM experiment to determine redox exchange of Cd with Hg at open circuit.

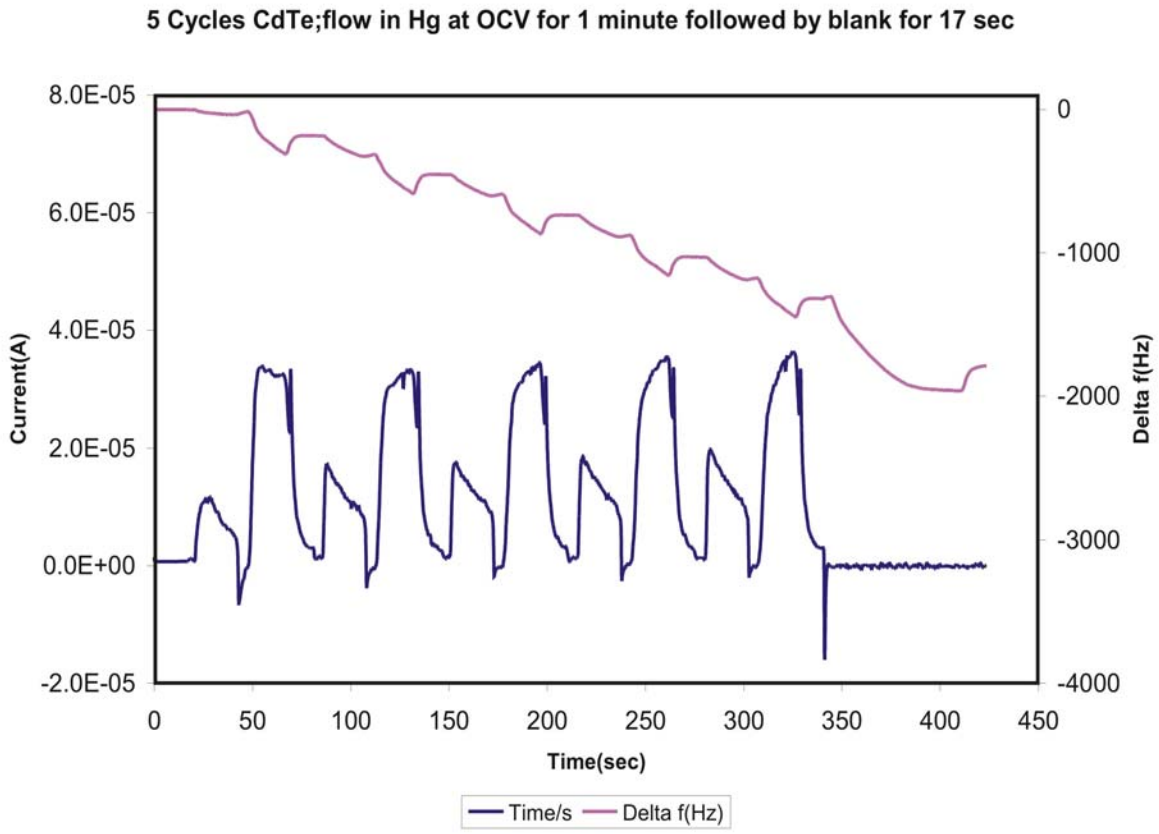

CHAPTER 6

CONCLUSION

The main objective of the research work undertaken was to develop an optimized deposition program to grow HgCdTe and demonstrate bandgap engineering by electrochemical ALD. The initial studies on the deposition of HgSe gave valuable insights concerning EC-ALE and EC-ALD as deposition techniques for the deposition of thin films. The dependence of the deposition potentials for Hg and Se, as well as the potential for reductive Se stripping on the deposit morphology, stoichometry and thickness were the focus of attention. The optimal deposition cycle, by the end of the study, included deposition of Se at -0.15 V, stripping of excess Se at -0.63 V, and deposition of Hg at 0.48 V. The resulting deposit was a little over half of that expected from the ideal model of one compound monolayer for each cycle, but the deposit was stoichometric, and showed strong preferential (111) deposition. The absorption spectrum for the deposit also appeared to be consistent with the literature value of -0.60 eV.

With some idea about the Hg deposition cycle, further work towards the development of an optimized deposition programs for CdTe and HgTe were undertaken. First of all, a study to optimize CdTe thin films deposition was performed. The optimal deposition cycle consisted of the following: deposition of Cd at -0.65 V, deposition of Te at -0.35 V and, stripping of excess Te at -0.70 V. The resulting 100 cycle deposits were only 24.4 nm thick, less than that expected from the ideal model of one compound monolayer for each cycle, but the deposit was stoichometric, and, again, showed a strong preferential (111) orientation. The absorption spectrum for such deposits suggested a direct band gap of 1.50 eV, consistent with the literature. Studies performed using an EQCM flow cell helped to elucidate disparities between measured coulometric coverages for Cd and Te, and the resulting stoichiometry and deposit thickness. It was understood that some of the Cd each cycle was oxidatively stripped upon switching the potential from the Cd deposition potential of -0.65V to that for Te deposition, -0.35V. In

addition, it also appeared that some Cd was exchanged for Te. However, the net result was a high quality nanofilm of CdTe.

Development of an ideal deposition program for HgTe was then pursued. The ideal program for HgTe had the deposition of Hg at 0.40 V, deposition of Te at -0.35 V and, stripping of excess Te at -0.70 V. The 100 cycle deposit, based on this ideal program, was 71.9 nm thick, more than that expected from the ideal model of one compound monolayer for each cycle. The deposit however, was stoichometric, and showed a strong preferential (111) orientation. The absorption spectrum for the deposit suggested a negative band gap, -0.20 eV, consistent with the literature. Studies performed on an EQCM flow cell showed that some of the Te each cycle was oxidatively stripped upon switching the potential from the Te deposition potential of -0.35V to that for Hg deposition, 0.40V. In addition, it was also understood that Te was not exchanged for Hg.

After developing the optimized programs for HgTe and CdTe deposition, studies were performed with the intention of forming superlattices of HgTe and CdTe and demonstrate bandgap engineering. XRD patterns of the initial deposits indicated the formation of an $Hg_{(1-x)}Cd_xTe$ (MCT) alloys, instead of a superlattice, with a preferred (111) growth habit. The deposit composition also showed a strong dependence on the ALD period program, suggesting that the MCT composition was controllable over a broad range of values of x. Room temperature IR reflection absorption studies indicated that the band gap for the MCT deposits changed using the electrochemical ALD program. The EQCM flow cell was further used to understand the deposition process, especially the Hg deposition step, where it was confirmed that some of the previously deposited Cd, in the CdTe layer, was oxidatively stripped upon switching to 0.40 V for Hg deposition. In addition, some Cd was also found to be exchanged for Hg by a redox

replacement reaction. There was no indication from XRD of satellite peaks, or the formation of a superlattice. It appears that the absences of satellite peaks and formation of a superlattice was the result of instability of the Cd at the potentials needed for Hg deposition.

Why the alloy was formed, instead of a superlattice, appears to be related to problems associated with the choice of the Hg deposition potential and the stability of more electronegative Cd atoms in presence of the Hg ions. The next logical move appears to be to bring down the ideal deposition potential of Hg from 0.40 V to some where close to the deposition potential of Cd, around -0.60 V, by either changing the solution pH or complexing the Hg solution with suitable complexing agents like EDTA. With the deposition potentials of Hg and Cd closeby, the possibility of stripping Cd oxidatively become a nonentity.

Once the oxidative stripping of Cd is prevented with the right choice of Hg deposition potential, redox replacement of Cd with Hg would be the next problem to overcome. The LABVIEW program used to deposit thin films and superlattices is very versatile. There are provisions in the LABVIEW program where potentials can be held at a particular value where the possibility of Cd being stripped with Hg can be prevented. With some slight modifications to the deposition program, the integrity of the CdTe layer could be maintained there by improving the chances of forming a superlattice.

From bandgap engineering experiments it appeared that the band gaps had the desired trend as a function of composition, but deviated from the theoretical line, derived by Hansen et.al., at both high and low values of x. The band gaps were too high at low values of x and too low at high values of x. The high band gaps at low values of x indicated that some Hg formed an alloy with the Au substrate. In order to overcome this problem, commercial substrates like

CdZnTe would be used in the future as they not only prevent the amalgam formation, but are also lattice matched and would probably result in high quality deposits.

The deposition program would also be modified such that no pre-layer of CdTe would be deposited before depositing MCT. This way, the chances of the pre-layer interfering with the bandgap measurements of a thin deposit of MCT, would be avoided.